

# The IceCube Neutrino Observatory Part I: Point Source Searches

THE ICECUBE COLLABORATION

## Contents

1	Model independent search for GRB neutrinos interacting inside IceCube (paper 0367)	5
2	Ultra-high energy neutrino online alert system for GRB and transient astronomical sources (paper 0409)	9
3	Searches for multiple neutrino sources in the Cygnus region and beyond with three years of IceCube data (paper 0471)	12
4	High-energy gamma-ray follow-up program using neutrino triggers from IceCube (paper 0537)	16
5	Search for multi-flares of high energy neutrinos from Active Galactic Nuclei with the IceCube detector (paper 0539)	20
6	Calculating energy-dependent limits on neutrino point source fluxes with stacking and unfolding techniques in IceCube (paper 0541)	24
7	IceCube : latest results on point and extended neutrino searches (paper 0550)	28
8	Probing cosmic ray production in massive open star clusters with three years of IceCube data (paper 0557)	32
9	Searches for flaring and periodic neutrinos emission with three years of IceCube data (paper 0649)	36
10	Optical and X-ray followup programs of IceCube (paper 0852)	40
11	Stacked searches for high-energy neutrinos from blazars with IceCube (paper 0942)	44
12	Search for prompt neutrino emission from Gamma Ray Burst with IceCube (paper 1180)	48

**Keywords:** IceCube, neutrino astronomy, neutrino telescopes, neutrino follow-up programs, neutrino point and extended sources, GRBs, AGNs, blazars, transient and periodic sources, Cygnus region, star clusters.

## IceCube Collaboration Member List

M. G. Aartsen<sup>2</sup>, R. Abbasi<sup>27</sup>, Y. Abdou<sup>22</sup>, M. Ackermann<sup>41</sup>, J. Adams<sup>15</sup>, J. A. Aguilar<sup>21</sup>, M. Ahlers<sup>27</sup>, D. Altmann<sup>9</sup>, J. Auffenberg<sup>27</sup>, X. Bai<sup>31,a</sup>, M. Baker<sup>27</sup>, S. W. Barwick<sup>23</sup>, V. Baum<sup>28</sup>, R. Bay<sup>7</sup>, J. J. Beatty<sup>17,18</sup>, S. Bechet<sup>12</sup>, J. Becker Tjus<sup>10</sup>, K.-H. Becker<sup>40</sup>, M. Bell<sup>38</sup>, M. L. Benabderrahmane<sup>41</sup>, S. BenZvi<sup>27</sup>, P. Berghaus<sup>41</sup>, D. Berley<sup>16</sup>, E. Bernardini<sup>41</sup>, A. Bernhard<sup>30</sup>, D. Bertrand<sup>12</sup>, D. Z. Besson<sup>25</sup>, G. Binder<sup>8,7</sup>, D. Bindig<sup>40</sup>, M. Bissok<sup>1</sup>, E. Blaufuss<sup>16</sup>, J. Blumenthal<sup>1</sup>, D. J. Boersma<sup>39</sup>, S. Bohaichuk<sup>20</sup>, C. Boehm<sup>34</sup>, D. Bose<sup>13</sup>, S. Böser<sup>11</sup>, O. Botner<sup>39</sup>, L. Brayeur<sup>13</sup>, H.-P. Bretz<sup>41</sup>, A. M. Brown<sup>15</sup>, R. Bruijn<sup>24</sup>, J. Brunner<sup>41</sup>, M. Carson<sup>22</sup>, J. Casey<sup>5</sup>, M. Casier<sup>13</sup>, D. Chirkin<sup>27</sup>, A. Christov<sup>21</sup>, B. Christy<sup>16</sup>, K. Clark<sup>38</sup>, F. Clevermann<sup>19</sup>, S. Coenders<sup>1</sup>, S. Cohen<sup>24</sup>, D. F. Cowen<sup>38,37</sup>, A. H. Cruz Silva<sup>41</sup>, M. Danninger<sup>34</sup>, J. Daughhetee<sup>5</sup>, J. C. Davis<sup>17</sup>, C. De Clercq<sup>13</sup>, S. De Ridder<sup>22</sup>, P. Desiati<sup>27</sup>, K. D. de Vries<sup>13</sup>, M. de With<sup>9</sup>, T. DeYoung<sup>38</sup>, J. C. Díaz-Vélez<sup>27</sup>, M. Dunkman<sup>38</sup>, R. Eagan<sup>38</sup>, B. Eberhardt<sup>28</sup>, J. Eisch<sup>27</sup>, R. W. Ellsworth<sup>16</sup>, S. Euler<sup>1</sup>, P. A. Evenson<sup>31</sup>, O. Fadiran<sup>27</sup>, A. R. Fazely<sup>6</sup>, A. Fedynitch<sup>10</sup>, J. Feintzeig<sup>27</sup>, T. Feusels<sup>22</sup>, K. Filimonov<sup>7</sup>, C. Finley<sup>34</sup>, T. Fischer-Wasels<sup>40</sup>, S. Flis<sup>34</sup>, A. Franckowiak<sup>11</sup>, K. Frantzen<sup>19</sup>, T. Fuchs<sup>19</sup>, T. K. Gaisser<sup>31</sup>, J. Gallagher<sup>26</sup>, L. Gerhardt<sup>8,7</sup>, L. Gladstone<sup>27</sup>, T. Glüsenkamp<sup>41</sup>, A. Goldschmidt<sup>8</sup>, G. Golup<sup>13</sup>, J. G. Gonzalez<sup>31</sup>, J. A. Goodman<sup>16</sup>, D. Góra<sup>41</sup>, D. T. Grandmont<sup>20</sup>, D. Grant<sup>20</sup>, A. Groß<sup>30</sup>, C. Ha<sup>8,7</sup>, A. Haj Ismail<sup>22</sup>, P. Hallen<sup>1</sup>, A. Hallgren<sup>39</sup>, F. Halzen<sup>27</sup>, K. Hanson<sup>12</sup>, D. Heereman<sup>12</sup>, D. Heinen<sup>1</sup>, K. Helbing<sup>40</sup>, R. Hellauer<sup>16</sup>, S. Hickford<sup>15</sup>, G. C. Hill<sup>2</sup>, K. D. Hoffman<sup>16</sup>, R. Hoffmann<sup>40</sup>, A. Homeier<sup>11</sup>, K. Hoshina<sup>27</sup>, W. Huelsnitz<sup>16,b</sup>, P. O. Hulth<sup>34</sup>, K. Hultqvist<sup>34</sup>, S. Hussain<sup>31</sup>, A. Ishihara<sup>14</sup>, E. Jacobi<sup>41</sup>, J. Jacobsen<sup>27</sup>, K. Jagielski<sup>1</sup>, G. S. Japaridze<sup>4</sup>, K. Jero<sup>27</sup>, O. Jlelati<sup>22</sup>, B. Kaminsky<sup>41</sup>, A. Kappes<sup>9</sup>, T. Karg<sup>41</sup>, A. Karle<sup>27</sup>, J. L. Kelley<sup>27</sup>, J. Kiryluk<sup>35</sup>, J. Kläs<sup>40</sup>, S. R. Klein<sup>8,7</sup>, J.-H. Köhne<sup>19</sup>, G. Kohnen<sup>29</sup>, H. Kolanoski<sup>9</sup>, L. Köpke<sup>28</sup>, C. Kopper<sup>27</sup>, S. Kopper<sup>40</sup>, D. J. Koskinen<sup>38</sup>, M. Kowalski<sup>11</sup>, M. Krasberg<sup>27</sup>, K. Krings<sup>1</sup>, G. Kroll<sup>28</sup>, J. Kunnen<sup>13</sup>, N. Kurahashi<sup>27</sup>, T. Kuwabara<sup>31</sup>, M. Labare<sup>22</sup>, H. Landsman<sup>27</sup>, M. J. Larson<sup>36</sup>, M. Lesiak-Bzdak<sup>35</sup>, M. Leuermann<sup>1</sup>, J. Leute<sup>30</sup>, J. Lünemann<sup>28</sup>, J. Madsen<sup>33</sup>, G. Maggi<sup>13</sup>, R. Maruyama<sup>27</sup>, K. Mase<sup>14</sup>, H. S. Matis<sup>8</sup>, F. McNally<sup>27</sup>, K. Meagher<sup>16</sup>, M. Merck<sup>27</sup>, P. Mészáros<sup>37,38</sup>, T. Meures<sup>12</sup>, S. Miarecki<sup>8,7</sup>, E. Middell<sup>41</sup>, N. Milke<sup>19</sup>, J. Miller<sup>13</sup>, L. Mohrmann<sup>41</sup>, T. Montaruli<sup>21,c</sup>, R. Morse<sup>27</sup>, R. Nahnhauser<sup>41</sup>, U. Naumann<sup>40</sup>, H. Niederhausen<sup>35</sup>, S. C. Nowicki<sup>20</sup>, D. R. Nygren<sup>8</sup>, A. Obertacke<sup>40</sup>, S. Odrowski<sup>20</sup>, A. Olivas<sup>16</sup>, M. Olivo<sup>10</sup>, A. O'Murchadha<sup>12</sup>, L. Paul<sup>1</sup>, J. A. Pepper<sup>36</sup>, C. Pérez de los Heros<sup>39</sup>, C. Pfendner<sup>17</sup>, D. Pieloth<sup>19</sup>, E. Pinat<sup>12</sup>, J. Posselt<sup>40</sup>, P. B. Price<sup>7</sup>, G. T. Przybylski<sup>8</sup>, L. Rädcl<sup>1</sup>, M. Rameez<sup>21</sup>, K. Rawlins<sup>3</sup>, P. Redl<sup>16</sup>, R. Reimann<sup>1</sup>, E. Resconi<sup>30</sup>, W. Rhode<sup>19</sup>, M. Ribordy<sup>24</sup>, M. Richman<sup>16</sup>, B. Riedel<sup>27</sup>, J. P. Rodrigues<sup>27</sup>, C. Rott<sup>17,d</sup>, T. Ruhe<sup>19</sup>, B. Ruzybayev<sup>31</sup>, D. Ryckbosch<sup>22</sup>, S. M. Saba<sup>10</sup>, T. Salameh<sup>38</sup>, H.-G. Sander<sup>28</sup>, M. Santander<sup>27</sup>, S. Sarkar<sup>32</sup>, K. Schatto<sup>28</sup>, M. Scheel<sup>1</sup>, F. Scheriau<sup>19</sup>, T. Schmidt<sup>16</sup>, M. Schmitz<sup>19</sup>, S. Schoenen<sup>1</sup>, S. Schöneberg<sup>10</sup>, A. Schönwald<sup>41</sup>, A. Schukraft<sup>1</sup>, L. Schulte<sup>11</sup>, O. Schulz<sup>30</sup>, D. Seckel<sup>31</sup>, Y. Sestayo<sup>30</sup>, S. Seunarine<sup>33</sup>, R. Shanidze<sup>41</sup>, C. Sheremata<sup>20</sup>, M. W. E. Smith<sup>38</sup>, D. Soldin<sup>40</sup>, G. M. Spiczak<sup>33</sup>, C. Spiering<sup>41</sup>, M. Stamatikos<sup>17,e</sup>, T. Stanev<sup>31</sup>, A. Stasik<sup>11</sup>, T. Stezelberger<sup>8</sup>, R. G. Stokstad<sup>8</sup>, A. Stöbl<sup>41</sup>, E. A. Strahler<sup>13</sup>, R. Ström<sup>39</sup>, G. W. Sullivan<sup>16</sup>, H. Taavola<sup>39</sup>, I. Taboada<sup>5</sup>, A. Tamburro<sup>31</sup>, A. Tepe<sup>40</sup>, S. Ter-Antonyan<sup>6</sup>, G. Tešić<sup>38</sup>, S. Tilav<sup>31</sup>, P. A. Toale<sup>36</sup>, S. Toscano<sup>27</sup>, M. Usner<sup>11</sup>, D. van der Drift<sup>8,7</sup>, N. van Eijndhoven<sup>13</sup>, A. Van Overloop<sup>22</sup>, J. van Santen<sup>27</sup>, M. Vehring<sup>1</sup>, M. Voge<sup>11</sup>, M. Vraeghe<sup>22</sup>, C. Walck<sup>34</sup>, T. Waldenmaier<sup>9</sup>, M. Wallraff<sup>1</sup>, R. Wasserman<sup>38</sup>, Ch. Weaver<sup>27</sup>, M. Wellons<sup>27</sup>, C. Wendt<sup>27</sup>, S. Westerhoff<sup>27</sup>, N. Whitehorn<sup>27</sup>, K. Wiebe<sup>28</sup>, C. H. Wiebusch<sup>1</sup>, D. R. Williams<sup>36</sup>, H. Wissing<sup>16</sup>, M. Wolf<sup>34</sup>, T. R. Wood<sup>20</sup>, K. Woschnagg<sup>7</sup>, D. L. Xu<sup>36</sup>, X. W. Xu<sup>6</sup>, J. P. Yanez<sup>41</sup>, G. Yodh<sup>23</sup>, S. Yoshida<sup>14</sup>, P. Zarzhitsky<sup>36</sup>, J. Ziemann<sup>19</sup>, S. Zierke<sup>1</sup>, M. Zoll<sup>34</sup>

- <sup>1</sup>III. Physikalisches Institut, RWTH Aachen University, D-52056 Aachen, Germany
- <sup>2</sup>School of Chemistry & Physics, University of Adelaide, Adelaide SA, 5005 Australia
- <sup>3</sup>Dept. of Physics and Astronomy, University of Alaska Anchorage, 3211 Providence Dr., Anchorage, AK 99508, USA
- <sup>4</sup>CTSPS, Clark-Atlanta University, Atlanta, GA 30314, USA
- <sup>5</sup>School of Physics and Center for Relativistic Astrophysics, Georgia Institute of Technology, Atlanta, GA 30332, USA
- <sup>6</sup>Dept. of Physics, Southern University, Baton Rouge, LA 70813, USA
- <sup>7</sup>Dept. of Physics, University of California, Berkeley, CA 94720, USA
- <sup>8</sup>Lawrence Berkeley National Laboratory, Berkeley, CA 94720, USA
- <sup>9</sup>Institut für Physik, Humboldt-Universität zu Berlin, D-12489 Berlin, Germany
- <sup>10</sup>Fakultät für Physik & Astronomie, Ruhr-Universität Bochum, D-44780 Bochum, Germany
- <sup>11</sup>Physikalisches Institut, Universität Bonn, Nussallee 12, D-53115 Bonn, Germany
- <sup>12</sup>Université Libre de Bruxelles, Science Faculty CP230, B-1050 Brussels, Belgium
- <sup>13</sup>Vrije Universiteit Brussel, Dienst ELEM, B-1050 Brussels, Belgium
- <sup>14</sup>Dept. of Physics, Chiba University, Chiba 263-8522, Japan
- <sup>15</sup>Dept. of Physics and Astronomy, University of Canterbury, Private Bag 4800, Christchurch, New Zealand
- <sup>16</sup>Dept. of Physics, University of Maryland, College Park, MD 20742, USA
- <sup>17</sup>Dept. of Physics and Center for Cosmology and Astro-Particle Physics, Ohio State University, Columbus, OH 43210, USA
- <sup>18</sup>Dept. of Astronomy, Ohio State University, Columbus, OH 43210, USA
- <sup>19</sup>Dept. of Physics, TU Dortmund University, D-44221 Dortmund, Germany
- <sup>20</sup>Dept. of Physics, University of Alberta, Edmonton, Alberta, Canada T6G 2E1
- <sup>21</sup>Département de physique nucléaire et corpusculaire, Université de Genève, CH-1211 Genève, Switzerland
- <sup>22</sup>Dept. of Physics and Astronomy, University of Gent, B-9000 Gent, Belgium
- <sup>23</sup>Dept. of Physics and Astronomy, University of California, Irvine, CA 92697, USA
- <sup>24</sup>Laboratory for High Energy Physics, École Polytechnique Fédérale, CH-1015 Lausanne, Switzerland
- <sup>25</sup>Dept. of Physics and Astronomy, University of Kansas, Lawrence, KS 66045, USA
- <sup>26</sup>Dept. of Astronomy, University of Wisconsin, Madison, WI 53706, USA
- <sup>27</sup>Dept. of Physics and Wisconsin IceCube Particle Astrophysics Center, University of Wisconsin, Madison, WI 53706, USA
- <sup>28</sup>Institute of Physics, University of Mainz, Staudinger Weg 7, D-55099 Mainz, Germany
- <sup>29</sup>Université de Mons, 7000 Mons, Belgium
- <sup>30</sup>T.U. Munich, D-85748 Garching, Germany
- <sup>31</sup>Bartol Research Institute and Department of Physics and Astronomy, University of Delaware, Newark, DE 19716, USA
- <sup>32</sup>Dept. of Physics, University of Oxford, 1 Keble Road, Oxford OX1 3NP, UK
- <sup>33</sup>Dept. of Physics, University of Wisconsin, River Falls, WI 54022, USA
- <sup>34</sup>Oskar Klein Centre and Dept. of Physics, Stockholm University, SE-10691 Stockholm, Sweden
- <sup>35</sup>Department of Physics and Astronomy, Stony Brook University, Stony Brook, NY 11794-3800, USA
- <sup>36</sup>Dept. of Physics and Astronomy, University of Alabama, Tuscaloosa, AL 35487, USA
- <sup>37</sup>Dept. of Astronomy and Astrophysics, Pennsylvania State University, University Park, PA 16802, USA
- <sup>38</sup>Dept. of Physics, Pennsylvania State University, University Park, PA 16802, USA
- <sup>39</sup>Dept. of Physics and Astronomy, Uppsala University, Box 516, S-75120 Uppsala, Sweden
- <sup>40</sup>Dept. of Physics, University of Wuppertal, D-42119 Wuppertal, Germany
- <sup>41</sup>DESY, D-15735 Zeuthen, Germany
- <sup>a</sup>Physics Department, South Dakota School of Mines and Technology, Rapid City, SD 57701, USA
- <sup>b</sup>Los Alamos National Laboratory, Los Alamos, NM 87545, USA
- <sup>c</sup>also Sezione INFN, Dipartimento di Fisica, I-70126, Bari, Italy
- <sup>d</sup>Department of Physics, Sungkyunkwan University, Suwon 440-746, Korea
- <sup>e</sup>NASA Goddard Space Flight Center, Greenbelt, MD 20771, USA

## **Acknowledgements**

We acknowledge the support from the following agencies: U.S. National Science Foundation-Office of Polar Programs, U.S. National Science Foundation-Physics Division, University of Wisconsin Alumni Research Foundation, the Grid Laboratory Of Wisconsin (GLOW) grid infrastructure at the University of Wisconsin - Madison, the Open Science Grid (OSG) grid infrastructure; U.S. Department of Energy, and National Energy Research Scientific Computing Center, the Louisiana Optical Network Initiative (LONI) grid computing resources; Natural Sciences and Engineering Research Council of Canada, WestGrid and Compute/Calcul Canada; Swedish Research Council, Swedish Polar Research Secretariat, Swedish National Infrastructure for Computing (SNIC), and Knut and Alice Wallenberg Foundation, Sweden; German Ministry for Education and Research (BMBF), Deutsche Forschungsgemeinschaft (DFG), Helmholtz Alliance for Astroparticle Physics (HAP), Research Department of Plasmas with Complex Interactions (Bochum), Germany; Fund for Scientific Research (FNRS-FWO), FWO Odysseus programme, Flanders Institute to encourage scientific and technological research in industry (IWT), Belgian Federal Science Policy Office (Belspo); University of Oxford, United Kingdom; Marsden Fund, New Zealand; Australian Research Council; Japan Society for Promotion of Science (JSPS); the Swiss National Science Foundation (SNSF), Switzerland.

## Model Independent Search For GRB Neutrinos Interacting Inside IceCube

THE ICECUBE COLLABORATION<sup>1</sup>,

<sup>1</sup>See special section in these proceedings

*jcasy8@gatech.edu*

**Abstract:** IceCube is a km-scale neutrino detector operating at the geographical South Pole. It is sensitive to high energy neutrinos. Many GRB models predict the generation of high energy neutrinos through various hadronic interactions at different stages of the burst such as the prompt phase, the early afterglow and/or a precursor phase. A potential neutrino lightcurve, however, remains unknown. We report a search of temporal and spatial correlation between neutrinos and a stacked list of GRBs on a time scale from  $\pm 10$  s to  $\pm 15$  days. Previous searches by IceCube that study correlations up to  $\pm 1$  day have focused on through-going tracks from muon neutrinos. As neutrino candidates we use the 28 events found between  $\approx 30$  TeV and  $\approx 1.2$  PeV using the high-energy starting event technique. This method is sensitive to neutrinos of all flavors over  $4\pi$  sr. The temporal and spatial correlation method reported here uses a likelihood ratio test. We search for correlations of neutrino events with 562 GRBs reported mostly by Fermi GBM and Swift BAT from May 2010 to May 2012.

**Corresponding authors:** James Casey<sup>1</sup>, Ignacio Taboada<sup>1</sup>

<sup>1</sup>Center for Relativistic Astrophysics & School of Physics, Georgia Institute of Technology, Atlanta, USA

**Keywords:** Neutrino, Gamma Ray Bursts, IceCube

### 1 Introduction

Gamma Ray Bursts (GRBs) have been suggested as sources for the highest-energy cosmic rays [1]. If this hypothesis is correct, neutrinos should also be produced [2, 3, 4]. Since neutrinos are neutral particles, they are not deflected by magnetic fields and point back to the sources of the highest energy cosmic rays. Several models predict the neutrino fluence to be sufficiently large to be detectable by the IceCube Neutrino Observatory. Previous searches with IceCube have failed to find a temporal and spatial correlation between GRBs and neutrinos. As a result, IceCube has been able to exclude those models in which GRBs are the only sources of the highest energy cosmic rays and the cosmic rays escape as neutrons [5]. Previous searches in IceCube looked for through-going tracks from  $\nu_\mu$  interactions, spatially correlated with bursts, and within  $\pm 1$  day of the burst ('model-independent') or during the keV-MeV gamma ray emission and assuming a hard signal spectrum ('model-dependent').

The null result reported by IceCube has triggered a revision of theoretical predictions of neutrino emission by GRBs. Present models have improvements, such as a more detailed particle physics simulation, that reduce the signal expectation in IceCube by about one order of magnitude [6]. However these updated models should still be within the reach of IceCube with a few years of data.

IceCube is a very high-energy neutrino telescope operating at the geographic South Pole. It consists of 5,160 digital optical modules (DOMs). Each DOM contains a photomultiplier tube, supporting hardware and electronics inside a pressure glass sphere. These DOMs are arranged on 86 strings frozen into the antarctic ice at depths from 1450 m to 2450 m instrumenting one cubic kilometer. The DOMs indirectly detect neutrinos by sensing Cherenkov light produced by charged secondary particles produced in

neutrino-matter interactions. A more detailed description of IceCube and its operation can be found in ref. [7].

Here we present a search for a correlation between 28 events found by IceCube using the high-energy starting event technique (HESE) and GRBs detected between May 31, 2010 and May 15, 2012. A total of 562 GRBs were reported by satellites, notably Fermi GBM and Swift BAT, in this time period [8]. All GRBs with a known trigger time and position during the two years of the HESE analysis were selected. The search reported here uses a likelihood ratio technique similar to the method used to search for neutrino point sources with IceCube [9] that relies on positional and temporal correlation between the GRB and neutrino event times and positions in the sky. Our search is able to study this correlation in timescales from  $\pm 10$  s to  $\pm 15$  days around each GRB.

### 2 High Energy Starting Events (HESE)

The Extremely High Energy (EHE) neutrino search and a follow-up HESE search have resulted in the first evidence of astrophysical neutrinos in IceCube [10, 11]. Because the very low rate, we can for the first time study correlations between GRBs and neutrinos over long time scales.

There are 2 main signatures for neutrinos in IceCube. Tracks are the result of deeply penetrating muons traveling for several kilometers in ice or rock at the energies relevant to IceCube. Charged current interactions of  $\nu_\mu$  (and a small contribution due to  $\nu_\tau$ ) result in track-like events. Cascades, or showers, are the result of secondaries such as electrons or hadrons interacting in the ice. Neutrinos of all flavors that interact via the neutral current result in cascades. Cascades are also produced by charged current interactions of  $\nu_e$  and  $\nu_\tau$ . For the latter flavor, a single cascade is observed if the  $\tau$  decay lengths in the detector is short. Cascades have length



of a few meters and from the point of view of IceCube they can be considered as point sources of light. Track-like events have very good angular resolution, but energy can only be measured via energy deposition in the instrumented volume. Cascades have poorer angular resolution but very good visible energy resolution.

The HESE technique [11] selects neutrino-like events by vetoing events in which the earliest light is observed in the outer part of the detector. The DOMs are also required to observe a total charge of at least 6000 photo-electrons. These vetoes significantly reduce the backgrounds of down-going cosmic ray muons and through-going muons from atmospheric neutrinos. The HESE search is sensitive to neutrinos of all flavors with neutrino interaction vertices in the fiducial volume of the detector. The HESE method, and thus the search reported here, is sensitive over  $4\pi$  sr. Track-like events selected by the HESE search have an angular resolution of  $\approx 1^\circ$ . Cascade-like events have median angular resolutions of  $10 - 15^\circ$  and visible energy resolutions of  $\approx 15\%$ . The HESE technique resulted in the observation of 28 events with reconstructed energies between  $\sim 30$  TeV and  $\sim 1.2$  PeV [11]. The observations were conducted using approximately one year of full detector exposure and one year of exposure with 79 strings in operation for a total of 662 days of livetime. The background expectation is  $10.6_{-3.9}^{+4.5}$  due in part to down-going muons that sneak through the veto and in part due to atmospheric neutrinos including prompt atmospheric neutrinos. This corresponds to an excess over background of  $4.1 \sigma$ . Of the 28 events, 21 are cascade-like and 7 are track like. This agrees with expectations of astrophysical neutrinos and vacuum oscillations under several astrophysical scenarios [12]. No evidence of a point source of neutrinos using all 28 events or using only the 21 cascade-like events is observed [11].

### 3 Method

We performed a search for spatial and temporal correlations between a stacked list of 562 GRBs and the 28 HESE events. The temporal search is performed with multiple overlapping windows that increase in size by 20 s up to one day and then increase in size by 2 hours up to 15 days. The shortest time window is  $\pm 10$  s and the longest time window is  $\pm 15$  days centered at the time of each GRB. The spatial correlation is performed using detailed event by event reconstruction information. This *model independent* analysis has not been optimized for any individual predicted GRB spectra and searches for broad time and space correlations with GRBs. Our search has been constructed using blind data techniques, where event times were kept hidden during analysis preparation, and the events themselves were used to characterize the background by randomizing the times of each event.

#### 3.1 Likelihood

For each time window  $\Delta T$  from  $\pm 10$  s to  $\pm 15$  days, we define a likelihood function for the correlation of an event with a set of GRB thus:

$$\mathcal{L}_e(n_s, \Delta T) = \frac{n_s}{N_E} * \bar{S}_e(\theta, \phi, t, \Delta T) + \left(1 - \frac{n_s}{N_E}\right) * B_e(\theta, \phi, t, \Delta T), \quad (1)$$

where  $N_E = 28$  is the number of HESE events,  $n_s$  is the unknown number of events correlated with GRBs,  $t$  is the time difference between GRB  $g$  and HESE event  $e$ , and  $\theta$  and  $\phi$  are the relative location of the GRB and the HESE event and  $B_g$  is the background (accidental correlation) probability density function (PDF).  $\bar{S}_e$  is the weighted signal probability density function given by:

$$\bar{S}_e(\theta, \phi, t, \Delta T) = \frac{1}{N_G} \sum_g S_{g,e}(\theta, \phi, t, \Delta T) \quad (2)$$

where the sum is done over the signal PDF  $S_{g,e}$  for all GRBs coincident with a given event  $e$  for a given time window  $\Delta T$  and  $N_G$  is the number of GRBs.

The likelihood function that describes the correlation between all events and all GRBs is:

$$\mathcal{L}(n_s, \Delta T) = \prod_e \mathcal{L}_e(n_s, \Delta T) \quad (3)$$

The likelihood ratio is  $\Lambda(n_s) = \mathcal{L}(n_s, \Delta T) / \mathcal{L}(n_s = 0, \Delta T)$ . And the most likely value of  $n_s$ , called  $\hat{n}_s$ , is found by maximizing  $\lambda = 2 \ln(\Lambda)$  as a function of  $n_s$  for each time window  $\Delta T$ . The value of  $\lambda$  evaluated at  $\hat{n}_s$  for each time window  $\Delta T$  is used as a test statistic  $\hat{\lambda}(\Delta T)$ .

The test statistic which is calculated for each time window is used to determine the pre-trials  $p$ -value for that time window.

#### 3.1.1 Signal PDF

The signal PDF is composed of two parts: spatial and temporal.

$$S_{g,e}(\theta, \phi, t, \Delta T) = P_{s,g,e}(t, \Delta T) P_{s,g,e}(\theta, \phi) \quad (4)$$

The temporal component is a normalized step function based on the time window being examined. This window extends from  $-\Delta T$  to  $+\Delta T$  of time difference between an event  $e$  and a GRB  $g$ . Any event inside this time window has a normalized PDF value, and the signal PDF outside this window is zero.

$$P_{s,g,e}(t, \Delta T) = \begin{cases} \frac{1}{2\Delta T} & |t_e - t_g| < \Delta T \\ 0 & |t_e - t_g| > \Delta T \end{cases} \quad (5)$$

The spatial PDF of each event is based on the reconstructed likelihood map. This is a more elaborate choice than previously used for point source searches in IceCube [9]. It is necessary to use the reconstruction likelihood space for each event, specifically for cascades. Event reconstruction is performed using the time and charge of each pulse reported by the DOMs. Each reconstruction likelihood map is smoothed using the uncertainty of the GRB position as reported by the satellites and an IceCube systematic uncertainty based on the type of event (track or cascade). The smoothing is done using both uncertainties added in quadrature. GRBs reported by Fermi GBM have an uncertainty in localization of  $3-10^\circ$  [13], while other satellites typically localize GRBs with much better accuracy than IceCube's angular resolution. For HESE track-like events the IceCube systematic uncertainty is  $1^\circ$  and it is  $10^\circ$  for cascade-like HESE events. The smoothing also minimizes the effects of the discrete binning inherent in the reconstruction likelihood maps.

To optimize CPU usage, the smoothing is done using the Fourier transformation on the surface of a sphere of the

smoothing function and the reconstruction likelihood map [14]. After the reconstruction likelihood has been smoothed, it is normalized and a minimum floor is set 10 orders of magnitude below the peak to simplify the calculation. The information used in  $P_{s,g,e}(\theta, \phi)$  is provided by the normalized and smoothed event reconstruction likelihood map. Figure 1 shows one such normalized and smoothed reconstruction likelihood.

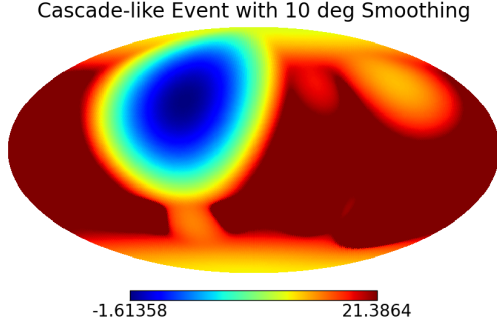


**Fig. 1:** Normalized Smoothed Likelihood Reconstruction Map for one of the HESE events. The map is in log space with a linear color scale. The large solid red color corresponds to the minimum likelihood value artificially put into the map.

### 3.1.2 Background PDF

The background PDF is also composed of temporal and spatial components.

$$B_e(\theta, \phi, t, \Delta T) = P_{b,e}(t, \Delta T)P_{b,e}(\theta, \phi), \quad (6)$$

The temporal component is given by

$$P_{b,e}(t, \Delta T) = \frac{1}{\tau}, \quad (7)$$

with  $\tau = 1/\text{lifetime}$ . The  $1/\tau$  accounts for the normalization.

The spatial component is given by

$$P_{b,e}(\theta, \phi) = \frac{1}{4\pi}. \quad (8)$$

We approximate the background PDF as  $1/4\pi$ . The true distribution is poorly measured since we are limited to 28 events. This approximation is reasonable since the variation scale small enough for the event spatial distribution and GRBs are known to be uniformly distributed in the sky.

### 3.2 Test Statistic

The test statistic gives us a measure of how signal-like a set of events is in a given time window. Since it is possible that an event and GRB could show a measure of significance by random chance, we use a Monte Carlo simulation to generate a set of scramblings to characterize the test statistic distribution for accidental coincidences.

Each scrambling is done by randomizing the event times where the event times are randomly generated from detector lifetime. For this analysis we have generated  $10^5$  scramblings. The full set of 562 GRBs and 28 time randomized events are used to generate the likelihood ratio. For each time window in each scrambling, the likelihood

ratio is maximized with respect to  $n_s$  to find  $\hat{n}_s$ . A larger test statistic implies a more signal-like event distribution in that time window.

For each time window, we generate a distribution of test statistics using all of the scramblings. The distribution of test statistics gives us a characterization for the test statistic assuming an accidental correlation. By comparing the test statistic for the actual event times for a given time window, we get a pre-trials  $p$ -value for that time window that indicates how signal-like the test statistic is compared to the random cases.

Figure 2 shows the test statistic distribution for  $\sim 10^5$  scramblings for a time window of 100 s before and after each GRB, and figure 3 is the distribution for 10,000 s.

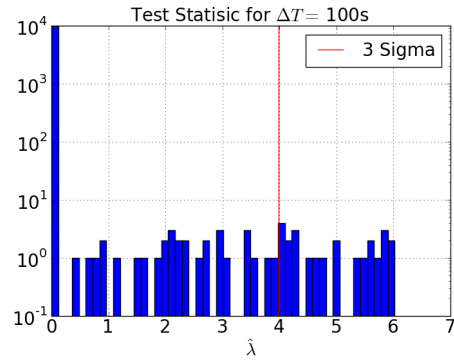


**Fig. 2:** Null hypothesis distribution of  $\hat{\lambda}$  (100 s), the test statistic for 100 s. This distribution was produced with  $10^5$  scramblings. The location of a 3-sigma pre-trial accidental correlation is marked by a vertical line.

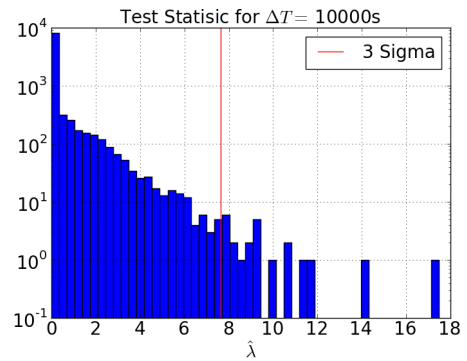


**Fig. 3:** Null hypothesis distribution of  $\hat{\lambda}$  (10,000 s), the test statistic for 10,000 s. This distribution was produced with  $10^5$  scramblings. The location of a 3-sigma pre-trial accidental correlation is marked by a vertical line.

## 4 Trials Factor Calculation

Since we are examining multiple overlapping time windows, we have to generate a post trials  $p$ -value. The pre-trials  $p$ -value is the significance for a set of events for a single time window, but since the time windows are not entirely independent of one another, we create a distribution of  $p$ -values based on the most significant (smallest)  $p$ -value for each scrambling.

After the test statistic distribution is generated for each time window, a  $p$ -value is determined for each time window in each scrambling. After all the  $p$ -values have been determined for a scrambling, the smallest  $p$ -value (or most extreme) for that scrambling is selected to generate a global distribution of  $p$ -values. After we have the distribution of the most significant  $p$ -values for all random scramblings, we find the most significant  $p$ -value over all time windows for the events with the unblinded times. The post trials  $p$ -value is the  $p$ -value of the most significant  $p$ -value over all time windows for the unblinded events compared to the distribution of the most significant  $p$ -values from the random scramblings. After the event times are unblinded, the post trials  $p$ -value is used to determine the significance of the events compared to the random scramblings.

## 5 Event Sensitivity

The Feldman Cousins 90% C.L. average upper limit [15] is calculated for each time window using the background  $\mu = \langle \hat{n}_s(\Delta T) \rangle$  for all scramblings. This average upper limit is our event sensitivity. It gives the upper limit on the number of events given the background  $\mu$  for a null measurement. Figure 4 shows the average upper limit in each time window from 10 s to 15 days.

The average upper limit is found by taking the sum of the Feldman Cousins upper limit for  $n$  observed events with a background of  $\mu$  weighted by the Poisson probability of seeing  $n$  events with background  $\mu$  for all  $n$ .

$$\langle u.l. \rangle = \sum_{n=0}^{\infty} P(n, \mu) * FC(n, \mu) \quad (9)$$

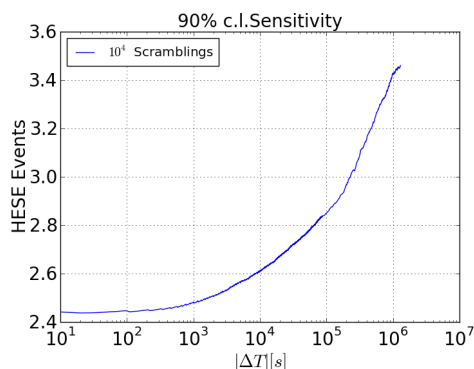


Fig. 4: Event sensitivity as a function of time window.

## 6 Summary

Using high energy events that interact within a fiducial volume of IceCube, we continue to probe cosmic ray production in GRBs. We focus on a model independent search over  $\pm 15$  days for high energy neutrinos coincident in time and space with GRBs. Due to low background rates and increased event type sensitivity, we have the opportunity to explore a previously unexamined test regime.

## References

- [1] Vietri M., ApJ. 453 (1995) 883-889 doi:10.1086/176448.
- [2] Waxman E. & Bahcall J., Phys. Rev. Lett. 78 (1997) 2292-2295 doi:10.1103/PhysRevLett.78.2292.
- [3] Waxman E. & Bahcall J., Phys. Rev. D 59 (1999) 023002 doi:10.1103/PhysRevD.59.023002.
- [4] Mészáros P. & Waxman E., Phys. Rev. Lett. 87 (2001) 171102 doi:10.1103/PhysRevLett.87.171102.
- [5] Abbasi, R. et al., Nature 484 (2012) 351 doi:10.1038/nature11068.
- [6] Hümmel, S., Baerwald, P. & Winter, W., Phys. Rev. Lett. 108 (2012) 231101 doi:10.1103/PhysRevLett.108.231101.
- [7] A. Achterberg et al., Astropart. Phys. 26 (2006) 155 doi:10.1016/j.astropartphys.2006.06.007.
- [8] Aguilar, J.-A., arXiv:1110.5946 (2011) and references therein.
- [9] Braun J. et al., Astropart. Phys. 29 (2008) 299-305 doi:10.1016/j.astropartphys.2008.02.007.
- [10] M. G. Aartsen et al., arXiv:1304.5356 (2013).
- [11] IceCube Coll., paper 0650 these proceedings.
- [12] Kashti T. & Waxman E. Phys. Rev. Lett. 95 (2005) 181101 doi:10.1103/PhysRevLett.95.181101.
- [13] Paciesas, W. S. et al., Astropart. Phys. 199 (2006) 18.
- [14] Baddour, N. J., Opt. Soc. AM. A 27 (2010) 2144 doi:10.1364/JOSAA.27.002144.
- [15] Feldman, G. & Cousins, R. Phys. Rev. D 57 (1998) 3873 doi:10.1103/PhysRevD.57.3873.



## Ultra-high energy neutrino online alert system for GRB and transient astronomical sources

THE ICECUBE COLLABORATION<sup>1</sup>,

<sup>1</sup>See special section in these proceedings

aya@hepburn.s.chiba-u.ac.jp

**Abstract:** The IceCube neutrino observatory is capable of detecting ultra-high energy cosmic neutrinos of PeV – EeV energies. The initial search of the ultra-high energy neutrinos using the fully completed IceCube detector has detected two neutrino events with energies above 1 PeV. The next challenge is an identification of their origin. In this paper, we propose to extend IceCube’s online follow-up beyond PeV energies, thus to the Southern sky, by performing the search process in a real time manner. A generated online alert of an ultra-high energy neutrino-induced muon or tau event would trigger follow-up observations in the X-ray and the gamma-ray bands to search for transient phenomena coincident in time and space. We describe the technique implemented in the ultra-high energy alert system and discuss their expected performance. The future prospects are also discussed in context of the field of view of an air Cherenkov telescope or Swift/XRT.

**Corresponding authors:** Aya Ishihara<sup>1</sup>, and Shigeru Yoshida<sup>1</sup>,

<sup>1</sup> Department of Physics, Graduate School of Science, Chiba University, Chiba 263-8522, Japan

**Keywords:** cosmic-ray, neutrinos, ultra-high energy.

### 1 Introduction

High energy cosmic neutrinos are important messengers to probe the origin of high energy cosmic rays. Neutrinos up to EeV energies are expected to be produced in the cosmic-ray acceleration processes at the source site. A neutrino penetrates over cosmological distance without being deflected by cosmic magnetic field nor absorbed by the photon field. Therefore, a straightforward interpretation of their arrival direction as the origin of cosmic-rays is possible.

The IceCube neutrino observatory [1] at the geographic South Pole is now in full operation. IceCube is a cubic kilometer scale deep underground Cherenkov neutrino detector. The IceCube detector construction was completed in December, 2010. The IceCube array comprises 5160 optical sensors on 86 cables, over a 1 km<sup>3</sup> fiducial volume of ice at a depth between 1450 m and 2450 m. Searches for extraterrestrial neutrinos with energies above the TeV range [2, 3] and above the PeV range [4, 5] have been performed with partially completed detector. The first search for very high energy diffuse neutrinos using the fully completed IceCube detector has detected two events of neutrinos above PeV energies [6]. The followup search of the PeV events revealed a further excess of events over the expected background distributions [7]. However, no significant point-source of neutrinos was observed. One of the interesting hypotheses to explain these recent observations are that observed ultra-high energy cosmic neutrinos are originated from transient sources, such as gamma-ray bursts (GRBs) or active galactic nucleus (AGN) flares.

Optical and gamma-ray follow-up observations prompted by neutrino signals have been under active study in IceCube [8, 9]. These follow up alert systems have also been in a state of stable operation. Because of a large amount of downward-going muon background in IceCube, currently

the real-time event searches are limited in the Northern sky and an alert is generated when multiple neutrino events are detected in a given directional and time window for the further background rejection. In the ultra-high energy region, these directional and multiplet conditions can be relaxed because the background event rates steeply decrease with energies. Therefore a real-time alert triggered by a detection of single well reconstructed ultra-high energy neutrino would provide a powerful tool to identify high energy astronomical phenomena which emit cosmic rays for a short period of time in the Southern sky. In this paper, we describe the technique to be implemented in the online ultra-high energy alert system with IceCube. Future prospects are also discussed.

### 2 Ultra-high energy neutrinos in IceCube

Neutrino event signatures in IceCube are determined using the Cherenkov light output from the penetrating high energy charged particles in ice. These charged particles are induced by charged-current, neutral-current, or Glashow resonance interactions of neutrinos and the Earth. Neutrino events in IceCube are distinguished as a track-like light pattern originating from neutrino-induced muons or high energy taus (tracks) and a spherical light pattern produced by hadronic or electromagnetic particle showers (cascades). While the previous searches above PeV energies did not distinguish these event topologies and were sensitive to both type of events, the directional resolution of track type events is significantly higher than that of cascade-like events. Expected angular resolutions for well reconstructed track-like events are  $\sim 1^\circ$  and  $\sim 10^\circ$  for cascade-like events. Therefore when considering the precision of the directional reconstruction and the field of view of follow-up instruments, only track-like events are considered as

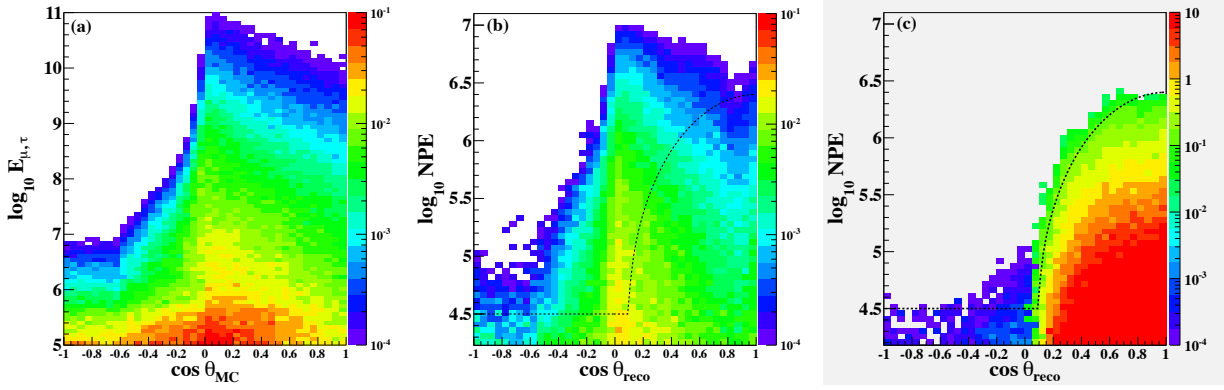


**Fig. 1:** Event number distributions from the Monte Carlo simulation of 1 year livetime of the full IceCube detector. The color scale (z-axis) represents the number of events per year per bin. (a) the signal distribution as a function of Monte Carlo truth muon and tau energies and cosine of zenith angle ( $\cos \theta_{MC}$ ). (b) the signal distribution as a function of NPE and cosine of reconstructed zenith angle ( $\cos \theta_{reco}$ ). (c) the atmospheric background distribution as a function of NPE and cosine of reconstructed zenith angle ( $\cos \theta_{reco}$ ). The lines in the panels (b) and (c) indicate the final selection criteria.

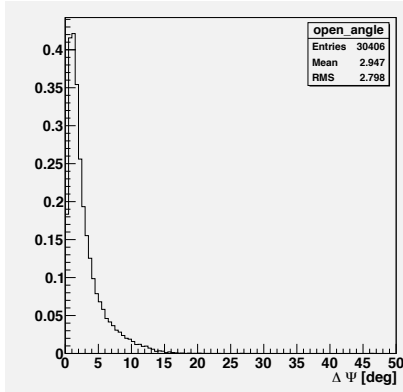


**Fig. 2:** The angle difference between the Monte Carlo truth direction and reconstructed direction for the event selection. Signal model is assumed to follow a  $E^{-2}$  power-law flux between PeV and 100 PeV. The selected events are to be further reconstructed with more computationally intensive algorithms for the alert information.

candidates. These track-like signals can be selected with a goodness-of-fit parameter from an event reconstruction using a track hypothesis.

Figure 1 (a) shows the neutrino-induced muon and tau track event distributions as function of truth energy and zenith angle, with the condition of at least 1000 photo-electrons observed by the IceCube detector. Neutrino-induced events which reaches as muon and tau track at 880 m from the IceCube center is considered in the plot. Energies of muons and taus are represented at the position of 880 m radius. Signal neutrino flux on the Earth surface is all flavor sum of neutrinos represented by a  $E^{-2}$  power-law flux with assumed 1:1:1 neutrino flavor ratio and 1:1 neutrino to anti-neutrino ratio. The all flavor total neutrino flux is assumed to be  $E^2 \phi_{\nu_e + \nu_\mu + \nu_\tau} = 3 \times 10^{-8} \text{ GeV m}^{-2} \text{ sec}^{-1} \text{ sr}^{-1}$ .

It can be observed that due to the energy dependence of the neutrino interaction cross section, the mean free path of ultra- to extremely-high energy neutrinos is much shorter than the typical path length in the Earth, thus a large part of

the high energy neutrino signal is expected from directions close to the horizon with downward-going track geometries.

### 3 Event selection

The dominant background in the downward-going region is atmospheric muons. As the zenith angle distribution of atmospheric muons peaks in the downward-going direction and sharply decreases towards the horizon with a cut-off at a  $\theta \sim 80^\circ$  due to absorption in the Earth, the rejection of atmospheric muons is achieved by using reconstructed zenith angle information. In addition, the energy spectra of signal neutrinos of astrophysical origin is expected to be much harder than steeply falling atmospheric muon spectra. Combination of these features allow us to form a reconstructed zenith angle dependent energy threshold as the selection criteria. In this study the total number of observed photo-electrons in each event (NPE) is used as a proxy of the deposited energy in the IceCube detector. Figure 1 (b) shows the neutrino induced muon and tau track signal event distributions as a function of cosine of reconstructed zenith angle and NPE. It can be observed that the feature of the event distribution in the panel (a) are reproduced using the simple experimental observables. The dashed lines in Fig. 1 (b) and (c) are the final level selection criteria determined from the background simulations. Events above the line are considered to be signal event candidates and directional information is sent for optical follow up studies. Corresponding cosmic ray induced atmospheric background distribution is shown in Fig. 1 (c).

Final optimization is still to be decided. Current selection criteria shown in Fig. 1 (b) and (c) expects total background event rate, which corresponds to a fake alert rate of 0.1 events/year, while 2 events per year of signal event rate is predicted from a power-law flux of the level  $E^2 \phi_{\nu_e + \nu_\mu + \nu_\tau} = 3 \times 10^{-8} \text{ GeV m}^{-2} \text{ sec}^{-1} \text{ sr}^{-1}$  with the same selection criteria. The angle differences between the Monte Carlo truth direction and reconstructed direction  $\Delta\Psi$  used for the event selection which is designed to be very fast algorithm [10] are shown in Fig. 2. The median resolution of the fast reconstruction is estimated to be  $2.0^\circ$ . With an improved optimization of the geometrical reconstruction

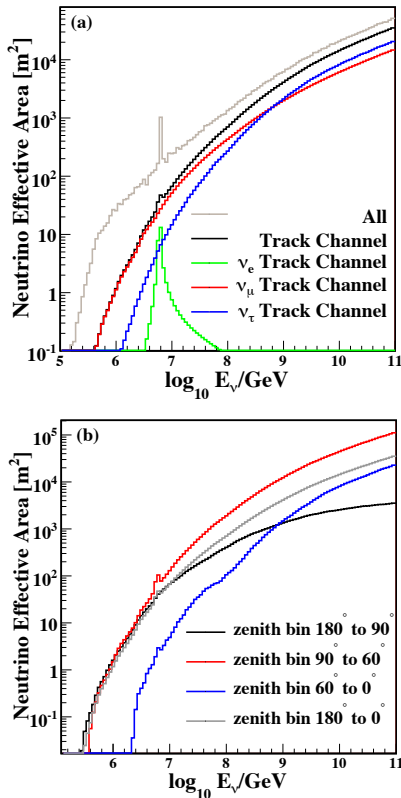


**Fig. 3:** The effective areas for the final selection criteria. (a) the  $4\pi$  average neutrino effective areas and (b) different zenith angle band averaged neutrino effective areas.

in particular for the horizontal direction, the further reduction of background events and enhanced number of signal events can be expected.

#### 4 Performance

Figure 3 presents the neutrino effective area as a function of energies with the selection criteria defined in the previous section. Neutrino effective area is the equivalent area at the Earth's surface in which neutrinos are detected with 100% efficiency and proportional to expected signal event rates. The neutrino effective areas for the track like events is represented by the black line in the panel (a) in Fig. 3. The comparison with the gray line which represents the effective areas for all the events including both cascade and track topologies indicates an increase of track event contribution with energies. The propagation length of muon or tau tracks increases with energies as well as an increase of neutrino-nucleon cross-section is expected. Thus the neutrino-induced muon and tau tracks allows us effectively detects signal induced events at high energies. Tau events appear to be cascade like at PeV but at the higher energies, the track-like feature emerges.

Figure 3 (b) shows the neutrino effective area as a function of energies for different zenith angle bands. The performance for the zenith angle between  $90^\circ$  and  $60^\circ$  is considerably higher than that in the other zenith angles at high energies. This indicates that we need follow up telescopes capable of observing these directions.

#### 5 Summary and prospects

We have developed an initial algorithm for the ultra-high energy neutrino event alert system with IceCube. Our sensitivity for ultra-high energy neutrinos has its peak for zenith angle band approximately from  $60$  to  $90$  degree, implying a good observation coverage of the Southern sky. The current study expands our effective field of view of the on-line alert system that has been limited to the Northern hemisphere due to the vastly dominated atmospheric muon background at TeV energies. The expansion, therefore, allow us to access to a group of the galactic objects of interest. A coordination with the existing high energy gamma-ray air Cherenkov telescope in the Southern hemisphere, i.e. the High Energy Stereoscopic System (H.E.S.S.) [11] will be in our scope when the online selection procedures discussed here is finalized. Because of a fairly low background event rates or a fake alert rate of about 0.1 events/year expected from the current study, we would consider relatively large time window for the multi-wavelength correlation study. A method of significance calculation for an event detection is to be decided.

The selection procedures described here have already been implemented in the offline analysis of ultra- to extremely high energy cosmic neutrino searches using the IceCube 2012 data [6]. In contrast to the diffuse neutrino searches, the online signal selection to prompt a follow-up observation needs to retain signal events with a good angular resolution only. Therefore a more sophisticated algorithm to reconstruct track geometry with better precision are currently under study. A loose cut using the fast algorithm described in this paper reduces the expected event rates to a few events per year. The further reconstruction process for these interesting events does not consume the computer resources at the South Pole. Finally, the best available information about the well reconstructed track will be sent to the alert system for the follow-up studies. IceCube has already implemented the established online alert systems [8, 9]. Integration of the very high energy neutrino information into the system would extend IceCube's capability to perform the online analysis to the Southern sky.

This work was supported by Grants-in-Aid for Scientific Research (Grant Number 22340048 and 25247031) from the JSPS in Japan.

#### References

- [1] IceCube collaboration, A. Achterberg *et al.*, *Astropart. Phys.* 26 (2006) 155.
- [2] IceCube collaboration, R. Abbasi *et al.*, *Phys. Rev. D* 84 (2011) 082001.
- [3] A. Schukraft for the IceCube collaboration, e-print arXiv:1302.0127 (2013).
- [4] IceCube Collaboration, R. Abbasi *et al.*, *Phys. Rev. D* 82 (2010) 072003.
- [5] IceCube collaboration, R. Abbasi *et al.*, *Phys. Rev. D* 83 (2011) 092003.
- [6] IceCube collaboration, M. G. Aartsen *et al.*, e-print arXiv:1304.5356 [astro-ph:HE] (2013).
- [7] IceCube Coll., paper 0650 these proceedings.
- [8] IceCube Coll., paper 0852 these proceedings.
- [9] IceCube Coll., paper 0537 these proceedings.
- [10] IceCube Coll., paper 0807 these proceedings.
- [11] H.E.S.S. Coll., these proceedings.

## Searches for multiple neutrino sources in the Cygnus region and beyond with three years of IceCube data

THE ICECUBE COLLABORATION<sup>1</sup>,

<sup>1</sup>See special section in these proceedings

Sirin.Odrowski@icecube.wisc.edu

**Abstract:** The IceCube neutrino telescope with its large detection volume and full-sky field of view is a unique instrument to study high-energy neutrino emission within the Galaxy and beyond. The detection of such neutrino emission would provide invaluable information about the origin of the high-energy cosmic radiation. In this contribution, we present two searches for multiple faint sources of high-energy neutrinos using three years of data collected by the partial IceCube detector before its completion. The analyses apply the multi-point-source (MPS) method to search for clustering, with a modification based on event energy-weighting in order to improve sensitivity. In the first search, we analyze the Cygnus region, a part of the Galaxy that may contain several cosmic-ray accelerators within a confined area of the sky and is located at a favorable position for IceCube. In the second search, we expand the region of interest beyond the galactic plane and study the small-scale correlations of events in the entire northern and southern skies, respectively.

**Corresponding authors:** Sirin Odrowski<sup>1</sup>, Anna Bernhard<sup>2</sup>,

<sup>1</sup> Dept. of Physics, University of Alberta, Edmonton, Alberta, Canada T6G 2E1

<sup>2</sup> Technische Universität München, D-85748 Garching, Germany

**Keywords:** IceCube, neutrino astronomy

### 1 Introduction

High-energy neutrinos may be produced in the interaction of accelerated protons or nuclei with matter or radiation fields in or near their sources. In the absence of leptonic production channels, they are unambiguous tracers of hadronic interactions and may as such provide insight into the origin of the high-energy cosmic radiation. The IceCube detector [1], which instruments a cubic kilometer of the antarctic ice with a three-dimensional grid of light sensors, is a unique facility for the search for extraterrestrial neutrinos.

The IceCube neutrino telescope has been built in several stages, adding new light sensors on units called *strings* each year from 2005 to 2011. Since then, the IceCube detector operates in its complete 86-strings configuration. The data collected between May 2008 and May 2011 were used in this contribution. These data were taken with three different partial configurations of the IceCube detector: the 40-strings, 59-strings and 79-strings configurations. 108,288 muon neutrino candidates in the northern sky with energies above  $\sim 100$  GeV were extracted from these data. In the southern sky, 146,047 events were selected to search for neutrinos among the background of down-going muons which is dominant in this part of the sky.

An unbinned likelihood search for point-like neutrino emission at any position on a fine grid across the sky has already been applied to the data [2]. The two approaches presented here are complimentary to this search. Both are based on the small scale clustering of events, a strategy that was applied to cosmic-ray data [3] because cosmic rays are deflected by magnetic fields of uncertain strength. The expected distance between the direction of the cosmic primary and the location of its source is therefore not

well constrained. Neutrinos are not deflected by magnetic fields, but an energy-dependent angular resolution and the possibility for extended sources implies that it is of advantage to be sensitive to a wide range of possible spatial signal distributions.

### 2 Analysis of the Cygnus region

The Cygnus region is a particularly promising region for the acceleration of galactic cosmic rays and the subsequent production of high-energy neutrinos in the northern hemisphere. It is roughly located at galactic longitudes between  $70^\circ$  and  $90^\circ$  and extends  $4^\circ$  and  $8^\circ$  below and above the plane, respectively. It comprises objects from the local arm, the Perseus arm and the outer arm of the Milky Way superimposed in a small region of the sky. Since it contains some of the nearest and most massive starforming regions as well as massive giant molecular cloud complexes, it is a very interesting target for neutrino searches. Moreover, strong TeV  $\gamma$ -ray emission from this area of the sky has been observed [6, 7].

#### 2.1 Energy-weighted multi-point-source analysis

The multi-point-source analysis (MPS) [4] is a non-parametric statistical test based on the distribution of pairwise calculated spatial distances between events. The analysis measures the amount of clustering as a function of a clustering scale  $\theta$  and compares the observation to the background expectation. It was developed to search for multiple (neutrino) sources inside a search region that is larger



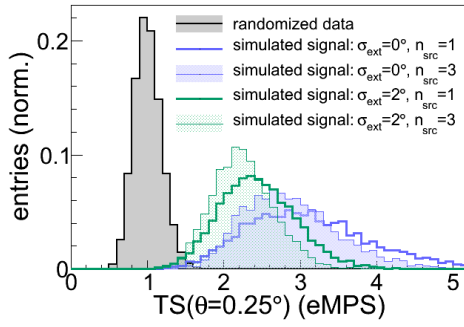


**Fig. 1:** Test statistic of the eMPS analysis at a clustering scale  $\theta$  of  $0.25^\circ$  for randomized data and four different simulated signal models at their discovery flux level. Signal scenarios with one and three sources and point-like ( $\sigma_{ext} = 0$ ) as well as extended emission patterns modelled by a Gaussian with a standard deviation of  $\sigma = 2^\circ$  are shown.

than the angular resolution of the detector. The method was applied to IceCube data in [5] to search for astrophysical neutrinos inside the Cygnus region. Since astrophysical neutrinos are often expected to have harder spectra than the atmospheric neutrino background, the method has now been extended to include energy-weights. With  $\Psi$  being the spatial distance between two events, the test statistic of the energy-weighted multi-point-source analysis (eMPS) is defined as a function of the clustering scale  $\theta$  by

$$TS(\theta) = \frac{\text{obs. weighted no. pairs with } \Psi \leq \theta}{\text{avg. weighted no. bg. pairs with } \Psi \leq \theta}, \quad (1)$$

and more precisely by

$$TS(\theta) = \frac{\sum_{i \in P} \sum_{j \in S, i \neq j} W(E_i) \cdot W(E_j) \cdot \Theta(\theta - \Psi_{ij})}{\langle \sum_{m \in P} \sum_{n \in S, m \neq n} W(E_m) \cdot W(E_n) \cdot \Theta(\theta - \Psi_{mn}) \rangle_{bg}}. \quad (2)$$

Here, the set of events  $i$  inside the search region is denoted by  $P$  and  $S$  is the set of all events  $j$ . Thus, only event pairs with at least one event inside the search region are counted.  $\Theta$  is the Heaviside function. The background expectation  $\langle \dots \rangle_{bg}$  enters in the denominator and is obtained by averaging over a large number of pseudo-experiments performed on background-only data.  $W(E_i)$  is the energy weight for event  $i$ .

The energy weights  $W(E_i)$  are obtained from the pdf  $\mathcal{P}(E)$  of the reconstructed energies in the background by using the probability to observe an event with equal or higher energy in the background.  $W(E_i)$  is given by

$$\begin{aligned} W(E_i) &= 1 - \int_{E_i}^{\infty} \mathcal{P}(E) dE \\ &= \int_0^{E_i} \mathcal{P}(E) dE. \end{aligned}$$

In this way, the energy weights do not depend on a specific signal model and the extension of the method preserves the generality of the original test. Larger weights are assigned to events with higher energies than to events with lower energies. Figure 1 shows the distribution of the test statistic at  $\theta = 0.25^\circ$  for randomized data and four different simulated signal models at their respective discovery flux level.

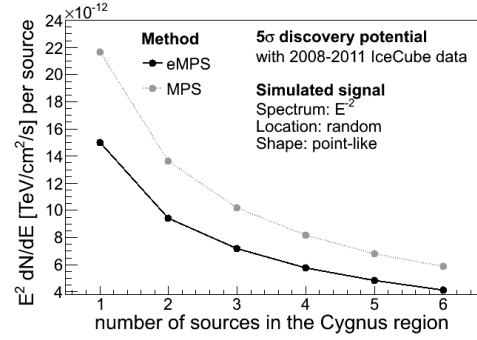


**Fig. 2:** The discovery flux for point-like  $E^{-2}$  spectra sources inside the Cygnus region obtained with MPS and eMPS as a function of the number of simulated sources.

The agreement of the observed data with the background expectation is quantified by the smallest observed  $p$ -value in any of the  $\theta$ -bins corrected for the trials incurred by testing multiple values of  $\theta$ . Since  $TS(\theta)$  is a cumulative function, the bins are highly correlated and the effective number of trials is less than the number of bins.

## 2.2 Application to the Cygnus region

The eMPS analysis has been applied to the IceCube data collected with the 40-strings, 59-strings and 79-strings configurations. A  $11 \times 7$  degree region in galactic coordinates has been defined to comprise the most active part of the Cygnus region. The selected region extends from  $72^\circ$  to  $83^\circ$  in galactic longitude and from  $-3^\circ$  to  $4^\circ$  in galactic latitude and is identical to the region studied in [5]. Clustering scales  $\theta$  up to  $5^\circ$  evaluated in  $0.25^\circ$  steps have been considered.

The event weights  $W(E_i)$  were calculated from the observed data. The energy-dependence of the background with declination was accounted for by dividing the data into five declination bands. The expected number of weighted event pairs as a function of  $\theta$  was obtained from  $3 \times 10^7$  pseudo-experiments performed on randomized experimental data from the same declination band. The randomization was performed by assigning a random right ascension to each event while keeping its declination and energy unchanged.

The performance of the statistical test was quantified by the discovery flux, defined as the flux that is necessary to obtain a  $5\sigma$  deviation from the background in 50% of all pseudo-experiments which were performed with a simulated signal of this strength. Figure 2 shows the discovery flux for sources with an  $E^{-2}$  energy spectrum as a function of the simulated number of sources inside the region. All sources were simulated with the same strength and the  $5\sigma$  threshold was corrected for the trials incurred by testing different clustering scales  $\theta$ . The eMPS method leads to an improvement of 45% or more with respect to the original MPS method for this spectrum. For neutrino spectra of the form  $E^{-2} \cdot e^{-E/E_c}$  with a cutoff energy  $E_c$ , the eMPS method yields a better discovery potential for cutoff energies down to 10 TeV. The discovery flux per source decreases with the number of sources inside the region as expected. For a single  $E^{-2}$  source, the discovery flux is about twice the one of the standard point source analysis at this declination [2]. The latter is however not corrected for the trials incurred by the application of the test to the whole northern hemisphere. The trial-corrected discovery flux of



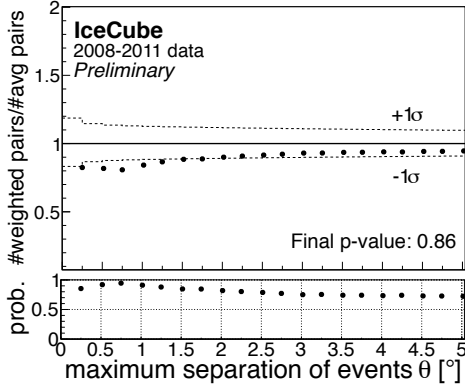


**Fig. 3:** Results from the search for neutrino emission inside the Cygnus region with the eMPS method using three years of data from IceCube taken in partial configurations of the detector. The upper panel shows the observed values of the test statistic as a function of the clustering scale  $\theta$ . The lower panel shows the probability to observe a similar or stronger fluctuation in the background.

the eMPS analysis crosses the local discovery flux of the standard point source analysis at about three sources in the region. Since no local significance above  $5\sigma$  was found in the standard point source analysis at any point in the sky, it is excluded that the analysis of the Cygnus region observes a single  $E^{-2}$ -source at a flux of  $1.5 \cdot 10^{-11} \text{TeV cm}^{-2} \text{s}^{-1}$ . With its sensitivity to a signal from multiple point sources, the eMPS analysis of the Cygnus region can in principle detect signals that the standard point source analysis cannot. In addition to multiple point sources, the analysis is also sensitive to extended sources or diffuse emission inside the region.

### 2.3 Results for the Cygnus region

The eMPS analysis was applied to the IceCube data collected from 2008 to 2011 with the partial 40-, 59- and 79-strings configurations. Figure 3 shows the measured test statistic as a function of the clustering scale  $\theta$ . Less events than expected have been observed in the region, and the measured values of the test statistic are below one at all clustering scales  $\theta$ . The trial-corrected p-value for this observation is 86%. The results are consistent with the non-observation of a point source inside the Cygnus region and the results of a stacking of neutrino events observed near Milagro sources [2].

## 3 Search for a small-scale anisotropy

The approach to search for a small-scale clustering of neutrino events can be naturally extended beyond the Cygnus region. Instead of a selected region, a whole hemisphere can be studied by the use of an autocorrelation function. The aim is to be sensitive to a population of sources at unknown positions and with unknown energy spectra and spatial extensions.

### 3.1 Method

Like the analysis discussed, the test is based on pairwise calculated spatial distances between events. The test statistic is defined as a function of a clustering scale  $\theta$  and a

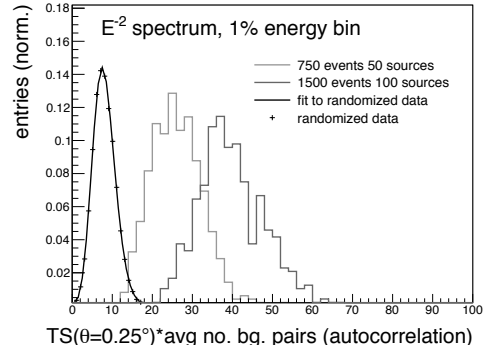


**Fig. 4:** The test statistic of the autocorrelation analysis at  $\theta = 0.25^\circ$  and in the bin that contains the 0.1% highest energy events, multiplied by the average number of pairs in the randomized data. The randomized data is fitted with a Gamma distribution and two signal scenarios with a uniform distribution of  $E^{-2}$  sources in the northern sky are shown. In the first, 1500 events were distributed over 50 sources according to the acceptance of the detector, and in the second, 2000 events were shared among 100 sources.

minimum energy  $E_{min}$  by

$$TS(\theta, E_{min}) = \frac{\text{obs. no. pairs with } \Psi \leq \theta, E_{1,2} \geq E_{min}}{\text{avg. no. bg. pairs with } \Psi \leq \theta, E_{1,2} \geq E_{min}}, \quad (3)$$

or, more precisely, by

$$TS(\theta, E_{min}) = \frac{\sum_{i,j \in H, i \neq j} \Theta(\theta - \Psi_{ij}) \cdot \Theta(E_{i,j} - E_{min})}{\langle \sum_{m,n \in H, m \neq n} \Theta(\theta - \Psi_{mn}) \cdot \Theta(E_{m,n} - E_{min}) \rangle_{bg}}. \quad (4)$$

Here,  $\Theta$  is again the Heaviside function, and the background expectation in the denominator is the average over pseudo-experiments on data without signal contribution.  $H$  denotes the set of all events under consideration. In the application here, events in the northern and the southern hemisphere of the sky are considered separately and one test will be performed for each hemisphere. Here, we describe the performance for the northern hemisphere and results for the southern sky will be reported later.

The result of the test is a two-dimensional matrix of the test statistic in bins of  $\theta$  and  $E_{min}$  and the significance of the observation is given by the smallest  $p$ -value in any of the bins corrected for the trials incurred by testing multiple bins.

### 3.2 Application to the northern hemisphere

The performance of the proposed test is evaluated for the northern hemisphere, using the data collected by the 40-, 59- and 79-strings configurations of IceCube. Clustering scales  $\theta$  up to  $5^\circ$  are tested in  $0.25^\circ$  steps. Four energy bins are defined based on the observed energy distribution in the data. The first bin contains all the data, and the thresholds for the other bins are defined such that they contain the 10%, 1% and 0.1% highest energy events observed in the data. By using different energy thresholds, the discovery potential for highly energetic signals is improved while the sensitivity to sources with soft energy spectra is retained. The denominator in the test statistic is obtained from pseudo-experiments with data which was randomized in the right ascension.

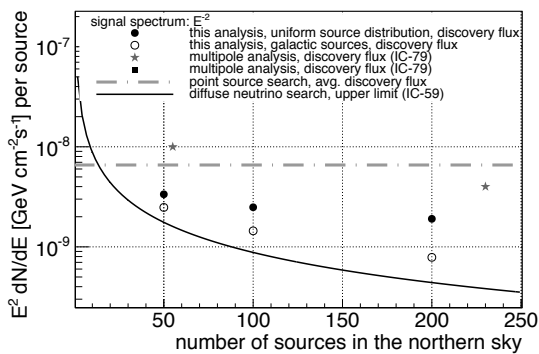


**Fig. 5:** The  $5\sigma$  discovery flux for  $E^{-2}$  neutrino sources with the autocorrelation analysis is compared to the discovery flux of the point source search in the same data [2] and a multipole analysis of the 79-string data. The upper limit of the diffuse neutrino flux search in the 59-string data [9] is also shown.

The data used here contain more than 100,000 events and the evaluation of the discovery potential is thus computationally challenging. More than 20,000 pseudo-experiments with randomized data were performed and the distributions of the test statistic for each value  $\theta$  and  $E_{min}$  were fitted. A Gamma-distribution was used in the two highest energy bins. For large numbers of pairs, the Gamma-distribution converges to a Gaussian. The energy bins which contain all events and the 10% highest energy events were thus fitted with a Gaussian distribution. Figure 4 shows the distribution of the test statistic for randomized data and the fit with a Gamma distribution for a clustering scale  $\theta$  of  $0.25^\circ$  and in the energy bin which contains 0.1% of the data. Also shown are two simulated signal scenarios with a uniform distribution of sources in the northern sky. The fit describes the data well and the signal is clearly distinguishable from the background expectation. Randomized data will also be used for the evaluation of the  $p$ -values.

Figure 5 presents the  $5\sigma$  discovery potential for sources with  $E^{-2}$  neutrino spectra as a function of the number of sources. The first signal model considered here were sources with equal strength and a uniform distribution across the northern sky. The detector acceptance was taken into account and the total number of events in the sample was kept constant in the signal simulation. The second scenario is a spatial distribution according to the Green catalogue [8] of SNR in the Milky Way and exhibits a larger clustering between the sources compared to the first scenario. The figure shows that the discovery flux per source decreases with the number of sources in both scenarios. If there are more than 50 sources of the same strength in the northern sky, this analysis is able to detect a signal that the standard likelihood point source analysis [2] would not see. While a discovery of a population of sources with an  $E^{-2}$  neutrino spectrum is already excluded by a search for a diffuse neutrino flux in the 59-string data [9], this analysis will be able to provide valuable information should a diffuse flux emerge in the future. Since it uses a data-driven background estimation, it is more robust against systematic uncertainties. Furthermore, it might eventually unveil the first hint for a clustering in such a signal.

Figure 6 shows the discovery potential for neutrino sources with an  $E^{-2}$  spectrum and a cutoff energy of 10 TeV.

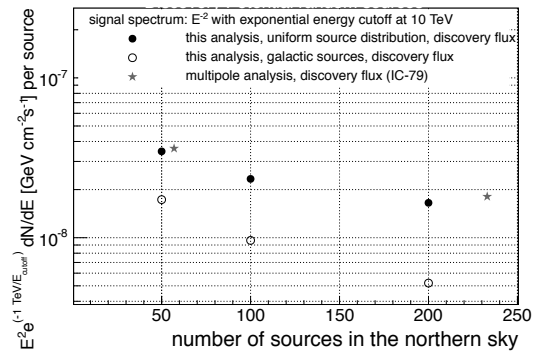


**Fig. 6:** The  $5\sigma$  discovery flux for  $E^{-2}$  neutrino sources with an exponential energy cutoff at 10 TeV with the autocorrelation analysis.

Soft spectra like these are less accessible by diffuse neutrino searches. For this spectrum, the analysis is also sensitive to the clustering between sources, as can be seen from the difference between the discovery flux for uniformly distributed sources and for sources within the galactic plane.

## 4 Conclusions

Two analyses based on the small scale clustering of neutrino events in the IceCube data have been presented. The first is a dedicated search for neutrino emission inside the Cygnus region and uses an extension of the MPS method. The analysis is sensitive to multiple neutrino sources inside the region as well as to a diffuse emission and makes no assumption about the position, extension and energy spectra of the hypothetical neutrino sources. The method has been applied to the data collected with the 40-, 59- and 79-strings configurations of IceCube and no significant deviation from the background has been observed. The  $p$ -value of the observation is 88%. The second analysis extends the generality of the above test and searches for a small scale clustering of neutrino events in the northern hemisphere. The performance of the method has been evaluated and it has been shown that the analysis is sensitive to both hard and soft spectra. Moreover, it may eventually provide the first hint of a clustering should a diffuse flux be discovered in the future.

## References

- [1] A. Achterberg et al., *Astropart. Phys.* 26, 155 (2006).
- [2] M. G. Aartsen et al., contribution 550, these proceedings (2013).
- [3] C. Finley and S. Westerhoff, *Astropart. Phys.* 21, 359 (2004).
- [4] Y. Sestayo and E. Resconi, *Astropart. Phys.* 44, 15 (2013).
- [5] R. Abbasi et al., *Astrophys. J.* 763, 33 (2013).
- [6] A. A. Abdo et al., *Astrophys. J. L.*, 658, 33 (2007).
- [7] E. Aliu for the Veritas collaboration, 32nd ICRC, Beijing (2011).
- [8] D. A. Green, *Bulletin of the Astronomical Society of India* 37 (1), 45 (2009).
- [9] A. Schukraft for the IceCube Collaboration, *Nucl. Physics B Proc. Suppl.*, in press (2013).

## High-Energy Gamma-Ray Follow-Up Program Using Neutrino Triggers from IceCube

THE ICECUBE COLLABORATION<sup>1</sup>

<sup>1</sup>See special section in these proceedings

dariusz.gora@desy.de

**Abstract:** We present the status of a neutrino-triggered program in IceCube that generates real-time alerts for gamma-ray follow up observations by Air Shower Cherenkov telescopes (e.g. MAGIC and VERITAS). While IceCube is capable of monitoring the whole sky continuously, high energy gamma-ray telescopes have restricted fields of view and in general may not be likely to be observing a potential neutrino-flaring source at the time such neutrinos are recorded. The use of neutrino-triggered alerts thus aims at increasing the availability of simultaneous multi-messenger data, which can increase the discovery potential as well as constrain the phenomenological interpretation of the high energy emission of selected source classes (e.g. blazars). The requirements of a fast and stable online analysis of potential neutrino signals and its operation will be discussed, and first results of its performance shown.

**Corresponding authors:** Robert Franke<sup>1</sup>, Elisa Bernardini<sup>1</sup>, Dariusz Góra<sup>1,2</sup>

<sup>1</sup> DESY Zeuthen, 15738 Zeuthen, Germany

<sup>2</sup> Institute of Nuclear Physics PAN, Radzikowskiego 152, Cracow, Poland

**Keywords:** IceCube, neutrino, NToO, blazars.

### 1 Introduction

Active Galactic Nuclei (AGN) and Gamma Ray Bursts (GRB) are often claimed to be the sources of ultra high energy cosmic rays (UHECR). Models describing the acceleration of atomic nuclei in these objects also predict a significant flux of high energy neutrinos from the decay of charged pions. The magnitude of the predicted neutrino flux, and hence the chance to discover these neutrinos, depends strongly on the models considered. For blazars, a subclass of AGNs, Flat Spectrum Radio Quasars (FSRQs) are predicted to be more promising candidates than BL-Lac objects in [1], whereas in [2] the opposite is predicted. The proton blazar model [3], which considers proton-proton interactions, predicts that the Low synchrotron peaked BL-Lac objects (LBL) are more likely to produce a significant neutrino emission than the High synchrotron peaked BL-Lacs (HBL). However, a photo-hadronic model in [1] leads to the conclusion that GeV bright FSRQs are promising neutrino sources, regardless of their spectral index.

The detection of cosmic neutrinos by high-energy neutrino telescopes is very challenging due to the small neutrino interaction cross-section and because of a large background of atmospheric neutrinos. Thus, simultaneous measurements using neutrino and electromagnetic observations (the so-called “multi-messenger” approach) can increase the chance to discover the first neutrino signals by reducing the trial factor penalty arising from the observation of multiple sky regions over different time periods.

Recent results obtained by the IceCube Collaboration [4] indicate that high-energy neutrino telescopes have reached a sensitivity to neutrino fluxes comparable to the observed high energy gamma-ray fluxes of Blazars in the brightest states (e.g. the flares of Markarian 501 in 1997 [5], Markarian 421 in 2000/2001 [6] and 2009 [7]

and PKS 2155304 in 2006 [8]). Under the assumption that the possibly associated neutrino emission is characterized by a flux enhancement comparable to what is observed in gamma-rays in such states, neutrino flares could be extracted from the sample of neutrino events with a reasonable significance.

For sources which manifest large time variations in the emitted electromagnetic radiation, the signal-to-noise ratio can be increased by searching for periods of enhanced neutrino emission (a time-dependent search). Of special interest is the relation of these periods of enhanced neutrino emission with periods of strong high-energy  $\gamma$ -ray emission. However, as Imaging Air Cherenkov Telescopes (IACTs) such as MAGIC [9] or VERITAS [10] have a small field-of-view and are not continuously operated such correlation studies are not always possible after the flare. Therefore it is desirable to ensure the availability of simultaneous neutrino and high-energy  $\gamma$ -ray data for periods of interests. This is achieved by an online neutrino flare search that alerts a partner IACT experiment when an elevated rate of neutrino events from the direction of a source candidate is detected.

Such a Neutrino Triggered Target of Opportunity program (NToO) using a list of pre-defined sources was developed already in 2006 using the AMANDA neutrino telescope to initiate quasi-simultaneous gamma-ray follow-up observations by MAGIC [11]. We present here a refined and enhanced implementation using the IceCube neutrino detector.

IceCube is a cubic-kilometer neutrino detector installed in the ice at the geographic South Pole [12] between depths of 1450 m and 2450 m. Detector construction started in 2005 and finished in 2010. Neutrino reconstruction relies on the optical detection of Cherenkov radiation emitted by secondary particles produced in neutrino interactions in the surrounding ice or the nearby bedrock.

## 2 Selection of target sources

The most interesting objects as a target for gamma-ray follow-up observations triggered by IceCube events are promising sources of TeV neutrinos, which are either known to exhibit a bright GeV flux in gamma-rays and show extrapolated fluxes detectable by IACTs, or are already detected by IACTs and are variable. We consider two different target source lists. One list was selected based on the the second Fermi point-source catalog [13]. The following criteria were applied:

- Redshift  $< 0.6$
- Fermi variability index  $> 41.64$  (corresponding to the 99% confidence level of the source being variable)
- Spectral index as observed with Fermi  $< 2.3$  (BL Lacs only)
- Fermi flux  $[1 - 100 \text{ GeV}] > 1 \cdot 10^{-9} \text{ ph cm}^{-2} \text{ s}^{-1}$  (BL Lacs only)
- Fermi flux  $[0.1 - 1 \text{ GeV}] > 7 \cdot 10^{-8} \text{ ph cm}^{-2} \text{ s}^{-1}$  (FSRQs only)

These selection criteria result in 21 sources on the list in total (three FSRQs and 18 BL Lacs). This selected list of target sources was combined with lists provided by the partner experiments (currently MAGIC and VERITAS) covering the Northern hemisphere ( $\delta > 0^\circ$ ). In total 109 sources are included in the follow-up program.

## 3 Neutrino event selection

The basis for the neutrino event selection is an on-line filter that searches for high-quality muon tracks. The full-sky rate of this filter is about 40Hz for IceCube in its 2012/2013 configuration with 86 deployed strings. This rate is strongly dominated by atmospheric muons. In order to efficiently select neutrinos events from this sample several elaborate reconstruction algorithm have to be applied. However, as the computing resources at the South Pole are limited, this is only possible at a lower event rate. The so-called Online Level2 filter selects events that were reconstructed as upgoing ( $\theta > 80^\circ$ ,  $\theta = 0^\circ$  equals vertically down-going tracks) with a likelihood reconstruction that takes into account the time of arrival of the first photon at each Digital Optical Module (DOM) and the total charge recorded in that module. By requiring a good reconstruction quality the background of misreconstructed atmospheric muons is reduced. The parameters used to assess the track quality are the likelihood of the track reconstruction, the number of unscattered photons with a small time residual w.r.t. the Cherenkov cone and the distribution of these photons along the track. The reduced event rate of approximately 5 Hz can then be reconstructed with more time intensive reconstructions, like angular resolution estimators and likelihood fits applied to different subsets of the recorded photons. Based on these reconstructions the final event sample is selected by employing different quality cuts. These cuts are optimized to achieve a good sensitivity for flares of different time durations. The event selection results in an event rate of about 2 mHz and a median angular resolution of  $0.5^\circ$  for an  $E^{-2}$  signal neutrino spectrum. The median resolution for events with  $E > 10^6 \text{ GeV}$  is  $< 0.4^\circ$ , see Figure 1.

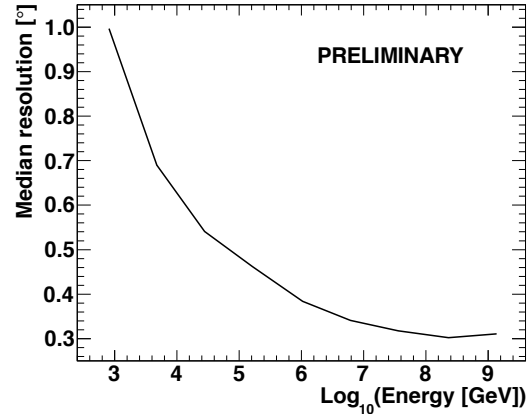


**Figure 1:** Median angular resolutions in degrees for the final selected neutrino sample as a function of neutrino energy.

## 4 The time-clustering algorithm

The timescale of a neutrino flare is not fixed a-priori and thus a simple rolling time window approach is not adequate to detect flares. The time clustering approach that was developed for an unbiased neutrino flare search [14] looks for any time frame with a significant deviation of the number of detected neutrinos from the expected background. The simplest implementation uses a binned approach where neutrino candidates within a fixed bin around a source are regarded as possible signal events.

Let  $T = \{t_i\}$  denote the times of all detected neutrino events in the on-source bin of a given source in the source list and let  $t_0$  be the last detected neutrino in that on-source bin (i.e.  $t_0 = \max t_i$ ). For all time periods  $[t_i, t_0]$  the expected background  $N_{\text{bck}}^{i,0}$  is calculated and compared to the actual number of observed neutrinos  $N_{\text{obs}}^{i,0}$  in that time period. In order to calculate  $N_{\text{bck}}^{i,0}$  the detector efficiency as a function of the zenith, azimuth angle and the detector uptime has to be taken into account. The chance probability to observe  $N_{\text{obs}}^{i,0}$  due to a background fluctuation is then calculated according to

$$\sum_{k=N_{\text{obs}}^{i,0}-1}^{\infty} \frac{(N_{\text{bck}}^{i,0})^k}{k!} e^{-N_{\text{bck}}^{i,0}}. \quad (1)$$

Typical flares in high energy gamma-rays have a maximal duration of several days. Therefore we constrain our search for time clusters of neutrinos to a maximum duration of 21 days (i.e.  $t_0 - t_i < 21 \text{ days}$ ). This has the additional benefit of reducing the trial factor penalty.

## 5 Data stability monitoring

A dedicated monitoring system was implemented to minimize the rate of false alerts due to problems with the detector itself. The IceCube detector works very stably, but sometimes unexpected problems with the data acquisition (DAQ) system or the filtering software can appear. IceCube has a very extensive monitoring of the DAQ system and South Pole online processing. The results of these monitoring systems are, however, only available with a certain



delay after the data was taken. Thus they are not yet available in time for a real-time alert system. In order to ensure that alerts are issued only during stable running conditions a simple but powerful online stability monitoring scheme was developed. All detector trigger- and filter rates are continuously measured in time bins of 10 minutes. These data are stored in an SQL database at the South Pole and are generally accessible a few minutes after the respective time bin ended. The rates and ratios of rates relevant for the selection of good quality neutrino-induced muon tracks are compared to an exponential running average of these rates to detect significant deviations. The results from that system were compared to the results from the offline monitoring data from IceCube in its 59-string configuration. Periods of reduced data quality were identified with very high efficiency by the simple online monitoring scheme. The fraction of data marked as *bad* periods is about of 8%.

## 6 Technical design of the alert system

The Gamma Follow-Up system runs online at the South Pole with minimal human intervention. In order to maximize the uptime of the system it has to be very stable. The main design driver was that the failure of any of the sub-components should not lead to the loss of the online program's data. Therefore all components have been separated as much as possible and intermediate results are stored frequently.

In the first step, the selection of neutrino candidate events (see Sec. 3) happens inside the IceCube data processing system at South Pole. Each event is serialized to the text-based and human-readable JSON (JavaScript Object Notation) format and written to a dedicated directory on disk. The event directory is checked for new events every 30 seconds by the daemon that runs the time clustering algorithm. This daemon keeps a list of events it has detected in the last 21 days from each of the monitored sources and adds new events to the appropriate list if the detector was stable when the event was detected. For each new event that falls into the search bin of one of the monitored sources the time-clustering algorithm for that particular source is run.

If the significance for an evaluated event cluster exceeds a certain threshold (see below), an alert message containing the source name, event positions, event times and the significance of the cluster is generated. The alert message is then sent to the University of Wisconsin via the IceCube Teleport System (ITS) which uses the Iridium satellites. This low bandwidth connection has a very high availability and allows to send short messages from the South Pole without any significant delay. Once the message arrives in the North it is checked to see whether it represents a *real alert* or a *test alert* from a monitoring source (see Sec. 7 for an explanation of the difference). If it is a *real alert*, the alert is forwarded to the respective partner experiment, MAGIC or VERITAS or to both of them if the alert significance is above the threshold for MAGIC and VERITAS. Currently the alerts are forwarded via email and follow-up observations are initiated by hand. Future setups might initiate automatic follow-up observations.

For an efficient monitoring of the follow-up system, all alerts (real and test) are filled into a database and a monitoring web page is updated. Each alert can be reviewed and basic information like the coordinates of the contributing events can be inspected (as an example see Figure 2).

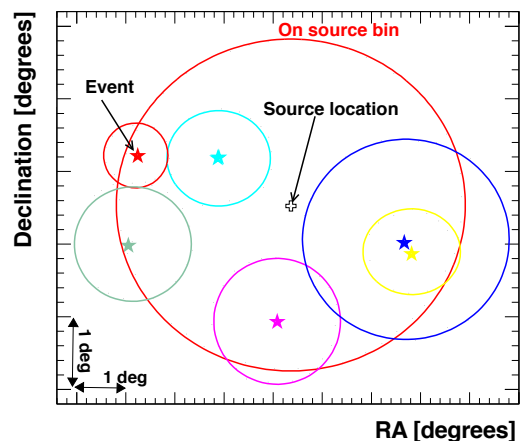


**Figure 2:** Angular distribution of events (star symbols) for the alert that was sent to VERITAS on November, 9th 2012. The weighted average of the contributing events is calculated using an event-by-event angular resolution estimator. The circle indicates the size of the on-source bin. The name of the source and coordinates are not given, in order to avoid biasing other IceCube analyses.

This allows a fast human inspection of alerts, even before the full IceCube event data arrives in the North. Furthermore global properties of all alerts received to date, like their rate, significance and time length distribution are plotted and monitored.

The total time delay between the (latest) neutrino event detected by IceCube and the moment that alert is forwarded to the partner experiment is on the order of several minutes.

## 7 Monitoring of the alert system

A monitoring system was developed to control that the follow-up alert system is functioning at all times. In order to achieve this, so-called *test alerts* with a very low significance threshold are generated for 2000 so-called monitoring sources. These monitoring pixels are randomly distributed over the Northern sky and are added to the source list used by GFU system. The *test alerts* are generated with a very low significance threshold to generate enough statistics. To guarantee blindness for these sky locations the *test alerts* are generated not from the physical sky coordinates of data events but a scrambled representation. The blindness is achieved by using the previous neutrino event time in the transformation from detector to sky coordinates for the current event instead of its own time. Due to the low neutrino event rate ( $\sim 2$  mHz) this lead to a random shift in right ascension on the order of several degrees. These test alerts are sent to the North in the same way as the physics alerts. The regular arrivals of these test alerts is monitored. If no alert is received for more than 6 hours a warning email is issued so the cause can be investigated. Warning emails are reissued every 2 hours if no new alert has been received. Each test alert is displayed on the monitoring web page (see Sec. 6). Up to now (May 2013) more than 6500 test alerts have been received.



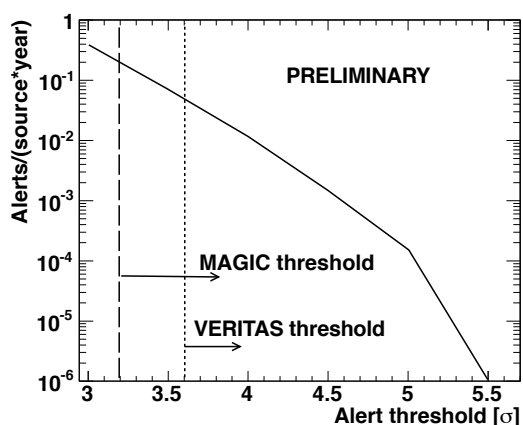


**Figure 3:** Expected number of accidental background alerts per year for a source at declination 14 deg as a function of the alert threshold expressed in units of standard deviations corresponding to a one-sided p-value.

## 8 Results and Outlook

The GFU system is based on a time-clustering approach to look for any time frame with a significant deviation of the number of detected neutrinos from the expected background. If the cluster of events with the highest significance exceeds a certain threshold the detector stability will be checked and an alert will be sent to a Cherenkov telescope (e.g. MAGIC and VERITAS) to initiate a follow-up observation. The number of accidental background alerts needs to be estimated in order to calculate a total significance of all the alerts generated by the program as well as to set sensible alert thresholds in order not to overwhelm the partner experiment with follow-up requests. The number of follow-up requests allowed in a given time period is fixed by the Time Allocation Committees of the partner experiments. Figure 3 shows the number of accidental background alerts as a function of the alert significance threshold. For threshold of  $3.2\sigma$  (MAGIC) this would result in a fake alert rate of about 0.1 alerts/(source · year). Thus, given the number of sources (about of 70) in this program for the MAGIC experiment the results in about 3 background alerts per year, taking into account an average source visibility of 40%. For the VERITAS telescope, a higher alert threshold ( $3.6\sigma$ ) leads to 1 expected background alert per year.

The system described here has been implemented and is fully operational since March, 14th 2012. Since this time one alert was forwarded to MAGIC in September 2012, and one to VERITAS in November 2012. The space distribution of the events contributing to the alert from November 2012 is shown in Figure 2. The  $-\log_{10}(p\text{-value})$  of event clusters is 4.6 (pre-trial). However, the binned method does not use energy or resolution information, and taking into account this information by using the unbinned maximum-likelihood method [15] the p-value of the event cluster would increase (i.e. become less significant) by a factor of 100. This is due to the fact that the events are clustered around the edge of the on-source bin, and not around the source position. This is better accounted for in the unbinned likelihood analysis where the individual event resolutions are taken into account.

Several enhancements to the program are possible and

planned. A maximum-likelihood based significance calculation taking into account an event-by-event angular reconstruction uncertainty estimation and an energy estimation of the event will further improve the sensitivity to neutrino flares. Improvements of the current neutrino selection by using Boosted Decision Trees (BDT) and an extension of the program to the Southern sky are planned. The current on-line alert system is limited to the Northern hemisphere due to the enormous atmospheric muon background at TeV energies. Due to this the expected sensitivity for the Southern sky will be about factor of 10 less than for the Northern sky. However, a recent IceCube search for neutrinos of EeV energy found two events at energies of 1 PeV [16] and 26 new events with energies between 30 and 300 TeV [17]. Therefore an extension of the on-line follow up program to the Southern hemisphere could help to identify sources of these ultra-high energy neutrinos and in consequence the high energy astronomical phenomena which emit cosmic rays for a short period of time. This idea is more extensively discussed in [18].

## References

- [1] A.M. Atoyan, C.Dermer, *New Astron. Rev.* 48 (2004) 381.
- [2] A. Neronov, M. Ribordy, *Phys. Rev. D* 80 (2009) 083008.
- [3] A. Mucke, et al., *Astropart. Phys.* 18 (6) (2003) 593.
- [4] J.L. Bazo Alba et al. for the IceCube Collaboration, *Proc. 31st ICRC*, ArXiv eprints (2009), arXiv:0908.4209.
- [5] F. Aharonian et al., *A&A*, **349** (1999) 1128.
- [6] F. Aharonian et al., *A&A*, **393** (2002) 8999.
- [7] I. Donnarumma, et al., *Astrophys. J.* 691 (2009) L13.
- [8] F. Aharonian et al., *Astrophys. J.*, 664 (2007) pp. L71.
- [9] MAGIC Collaboration: <http://magic.mppmu.mpg.de/>.
- [10] VERITAS Collaboration: <http://veritas.sao.arizona.edu/>.
- [11] M. Ackermann et al., *Proc. 29th ICRC*, ArXiv eprints (2005), arXiv:astro-ph/0509330.
- [12] A. Achterberg et al., *Astropart. Phys.* 26 (2006) 155.
- [13] Fermi LAT Second Source Catalog, <http://heasarc.gsfc.nasa.gov/W3Browse/fermi/fermilpsc.html>.
- [14] K. Satalecka et al., for the IceCube Collaboration, *Proc. 30th ICRC*, ArXiv eprints (2007), arXiv:0711.0353 [astro-ph.HE].
- [15] R. Abbasi et al., *Astrophys. J.* 732(1) (2011) 18.
- [16] M.G. Aartsen et al., ArXiv eprints (2013), arXiv:1304.5356 [astro-ph.HE].
- [17] IceCube Coll., paper 650 these proceedings.
- [18] IceCube Coll., paper 409 these proceedings.

## Search for multi-flares of high energy neutrinos from Active Galactic Nuclei with the IceCube detector

THE ICECUBE COLLABORATION<sup>1</sup>,

<sup>1</sup>See special section in these proceedings

angel.cruz@desy.de

**Abstract:** Active Galactic Nuclei (AGN) are among the best candidates for sources of high energy cosmic rays. One of their properties is the extreme variability of their electromagnetic emission at different wavelengths, with flare durations ranging from minutes in some cases to several weeks in others. Flares of neutrino emission may occur within similar time windows as these photon flares if protons are also accelerated in the same AGN relativistic jet. Here we present a statistical test to look for two or more flares separated in time (multi-flare) from selected AGN classes such as Flat Spectrum Radio Quasars (FSRQs) and BL-Lacs. This method does not rely on the detailed knowledge of the EM light-curves at a given wavelength, and it allows a time lag between the EM flares and the possible neutrino flares, which is predicted in some emission models. The duration of the potential neutrino flares is a result of this approach, not an input. An extension of this method performs an additional stacked flare search using a list of promising neutrino sources belonging to the same AGN class and selected from the 2nd Fermi-LAT AGN catalog. The performance and results of the method and its extension applied to one year of IceCube data in its 79-string configuration (IC79) are presented. No significant set of events was found in the IC79 period. Fluence upper limits are set for the most significant time windows found.

**Corresponding authors:** Angel Cruz<sup>1</sup>, Dariusz Góra<sup>1,2</sup>, Elisa Bernardini<sup>1</sup>

<sup>1</sup> DESY, D-15738 Zeuthen, Germany

<sup>2</sup> Institute of Nuclear Physics PAN, Radzikowskiego 152, 31-342 Cracow, Poland

**Keywords:** IceCube, Neutrino Astronomy, Neutrino Flares, Time-Dependent

### 1 Introduction

The origin of cosmic rays, especially at primary energies above  $\sim 10^{18}$  eV, remains the subject of intense research more than 100 years since their discovery. Active Galactic Nuclei (AGN) are believed to satisfy the necessary conditions to emit charged particles at such high energies [1]. Within the context of hadronic models, neutrinos should be produced in interactions of these particles inside the AGN jet [2, 3]. One of the aims of the IceCube neutrino observatory is to be sensitive to this high energy neutrino flux. IceCube is a cubic-kilometer neutrino detector installed in the ice at the geographic south pole between depths of 1450 m and 2450 m [4]. Detector construction started in 2005 and finished in 2010. The reconstruction of neutrino-induced events relies on the optical detection of Cherenkov radiation emitted by secondary particles produced in neutrino interactions in the surrounding ice or the nearby bedrock.

In order to distinguish astrophysical neutrino signal events from background events generated in the atmosphere (neutrinos and muons), energy and direction reconstructions have been used in several searches for localized excesses (time-integrated methods [5, 6]). An additional way to improve signal-background discrimination is the use of arrival time information to reduce the effective background. AGN are known to show time variability at different wavelengths and in various time scales [7]. The associated neutrino emission may exhibit similar variability and this is used in time-dependent methods to improve the detection probability with respect to time-integrated approaches. One such method aims to find a significant set of events clustered in time at any point in the sky (untriggered

search [8, 9]). Another approach takes into account information extracted from  $\gamma$ -ray light-curves in the GeV band for a set of selected AGN. This method defines periods of high  $\gamma$ -ray states where neutrinos are expected simultaneously (triggered search [8, 9]).

Here we describe two additional time-dependent methods that are sensitive to a set of neutrino events which form not only a single flare, as assumed in the untriggered search, but are distributed in several weak flares [10]. These multiple flares need not be synchronous with the  $\gamma$ -ray light curve as considered in the triggered search, permitting large time delays or different durations as proposed in some emission models [11, 12].

The event selection for these two analyses is the same used in time-integrated searches with the 79-string configuration of IceCube going from May-2010 until May 2011 [6]. It consists of 109 866 events (50 857 arriving from the northern sky and 59 009 arriving from the southern sky) with a median angular resolution better than  $1^\circ$  for neutrino energies larger than 1 TeV at which the current analyses are sensitive (see Ref. [6] for details).

### 2 Method

A point-source of astrophysical neutrinos is expected to manifest itself in the data as a clustering of events in space (around the position of the source candidate  $\vec{x}_s$ ) which have a different spectral index ( $\gamma_s$ ) from the atmospheric neutrino and muon spectra. Time-integrated searches [5] are based on a likelihood built with background and signal probability density functions (PDFs) evaluated

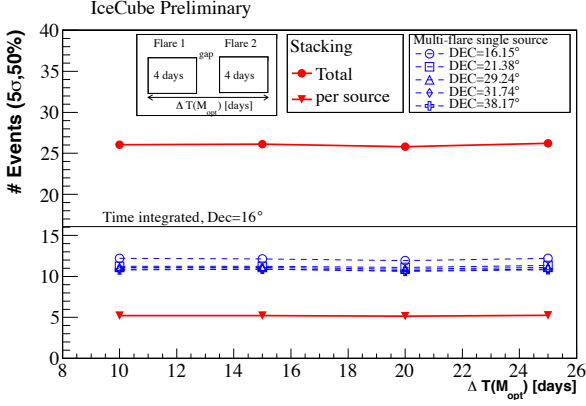


**Figure 1:** Discovery potential as a function of the simulated flare activity time,  $\Delta T(M_{\text{opt}})$ , for the double-flare example. The dashed lines correspond to the single source cases and the solid lines correspond to the stacking case.

for each event  $i$  of the data sample. These PDFs depend on the event reconstructed direction ( $\vec{x}_i$ ) and energy ( $E_i$ ). The signal PDF,  $S_i(\vec{x}_s, \gamma_s) = S^{\text{Space}}(\vec{x}_s, \vec{x}_i) S^{\text{Energy}}(E_i, \gamma_s, \vec{x}_i)$ , is calculated from simulations while the background PDF,  $B_i = B^{\text{Space}}(\vec{x}_i) B^{\text{Energy}}(\vec{x}_i, E_i)$ , is constructed directly from data. The likelihood to be maximized is defined as:

$$\mathcal{L}(n_s, \gamma_s, \vec{x}_s) = \prod_{i=1}^N \left( \frac{n_s}{N} S_i(\vec{x}_s, \gamma_s) + \left(1 - \frac{n_s}{N}\right) B_i \right), \quad (1)$$

where  $n_s$  (the number of signal events) and  $\gamma_s$  (the signal spectral index) are free parameters.  $N$  is the total number of events considered. For a point-source analysis this is the number of events in a declination band around the source candidate position  $\vec{x}_s$  during the considered data live time. The final significance is calculated from a test statistic (TS) defined as the ratio between the null and the best-fit hypothesis:  $-2 \log(\mathcal{L}(n_s=0)/\mathcal{L}(\hat{n}_s, \hat{\gamma}_s, \vec{x}_s))$ , where  $\hat{n}_s$  and  $\hat{\gamma}_s$  maximize the likelihood [5].

The variability in AGN electromagnetic emission may be exploited to further reduce the atmospheric background. For this purpose time-dependent methods such as the untriggered, triggered [6, 8], and multi-flare searches [10], include additional signal,  $S^{\text{Time}}$ , and background,  $B^{\text{Time}}$ , PDFs dependent on the event arrival time  $t_i$ . These methods differ in the functional form of the signal time PDF. In the untriggered search for example,  $S^{\text{Time}}$  is a Gaussian function with its width and centroid taken as free parameters in the likelihood maximization, whereas in the triggered search it is modeled from Fermi light-curves [6].

## 2.1 Multi-flare method for a single source

The first step in the present analysis is the construction of time intervals  $j$  with duration  $\Delta t_j$ . The intervals are defined by the arrival times of consecutive ‘‘signal-like’’ events, i.e.  $S_i/B_i > 1$ , where  $S_i$  and  $B_i$  only include space and energy information. The region around the declination of the source candidate  $\delta_s$  is defined as  $\delta_s \pm 5^\circ$ . The background PDF is assumed to be flat in time,  $B^{\text{Time}}(t_i) = 1/\Delta T_{\text{Data}}$ . Here  $\Delta T_{\text{Data}}$  is the length of the search time window, namely 80 days around the flare alert selected for each source, see section 4. Within this declination band and time search window there are on the order of 2000 events from which about 2% are ‘‘signal-like’’ (depending on  $\delta_s$ ).

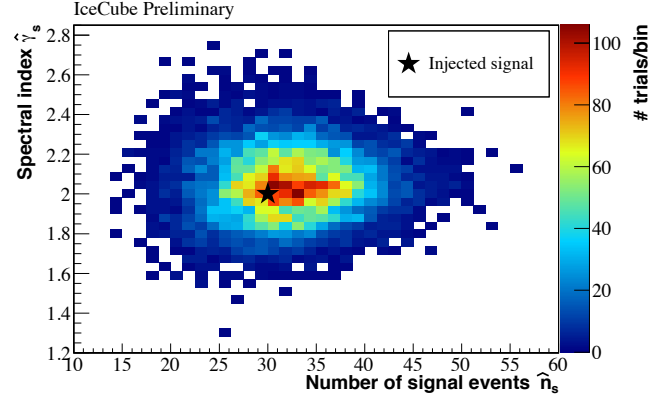


**Figure 2:** Best fit parameters  $\hat{n}_s$  and  $\hat{\gamma}_s$  for a set of  $10^5$  simulated trials in the stacking analysis.

The signal time PDF is defined as  $S^{\text{Time}}(t_i, \Delta t_j) = 1/\Delta t_j$  if the event  $i$  is inside the time window  $j$  and zero otherwise.

In the second step the test statistic  $TS_j$  is calculated for each time window,  $\Delta t_j$ , and then used to rank it in an ordered list. In the final step the algorithm selects from this list a subset of  $M_{\text{opt}}$  time windows. For this purpose a global likelihood is defined using a modified signal term:

$$S_i^{\text{tot}}(\vec{x}_s, \gamma_s, M) = \frac{\sum_{j=1}^M w^j \times S_i(\vec{x}_s, \gamma_s) \times S^{\text{Time}}(t_i, \Delta t_j)}{\sum_{j=1}^M w^j}, \quad (2)$$

where  $w^j = TS_j$  and  $M$  is the index running over the elements of the ordered list. A global test statistic is then calculated as:

$$\widetilde{\text{TS}}(M) \equiv -2 \log \left[ \frac{\mathcal{L}(n_s=0)}{\mathcal{L}(\hat{n}_s, \hat{\gamma}_s, \vec{x}_s, M)} \right]. \quad (3)$$

Starting from the time window that provided the largest value of  $TS_j$ , i.e.  $M=1$ , and following with the next in significance, the final number of  $M_{\text{opt}}$  time windows that constitute the potential multi-flare signal is chosen according to the maximum of  $\widetilde{\text{TS}}(M)$  [10]. The resulting flare activity time,  $\Delta T(M_{\text{opt}})$ , is defined as the time interval between the arrival time of the first event in the first time window and the arrival time of the last event in the last time window (see sub-figure in the upper-left of Figure 1). The final significance is estimated from Monte Carlo simulations by applying the same analysis to a large set of scrambled datasets (trials) [10, 13].

## 2.2 Multi-flare stacking method

An extension of the multi-flare method was developed to consider several flaring sources that belong to a particular AGN category (FSRQs or BL-Lacs) in a single statistical test. The signal term in the likelihood is replaced by the weighted sum of the contribution of each source  $k$  [5]:

$$S_i^{\text{Stacking}} = \frac{\sum_{k=1}^{N_s} W_k(\gamma_s, \vec{x}_k) \times S_{i,k}^{\text{tot}}(\vec{x}_k, \gamma_s, M_{\text{opt},k})}{\sum_{k=1}^{N_s} W_k(\gamma_s, \vec{x}_k)}, \quad (4)$$

where  $N_s$  is the number of sources in an AGN category and  $W_k(\gamma_s, \vec{x}_k)$  is the relative detector acceptance calculated from simulations as the number of events expected from a source at a certain location in the sky  $\vec{x}_k$  following a differential energy spectrum proportional to  $E^{-\gamma_s}$ . The signal

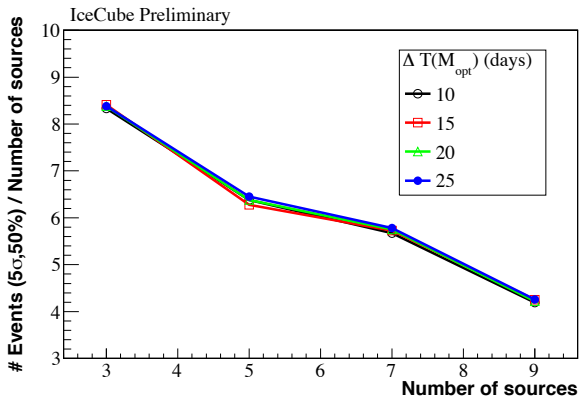


**Figure 3:** Discovery potential per source (total divided by the number of contributing sources) as a function of the number of stacked sources for different injected flare activity times in the double-flare example.

PDF of each individual contribution,  $S_{i,k}^{\text{tot}}(\vec{x}_k, \gamma_s, M_{\text{opt},k})$ , is given by eq. (2) with  $M_{\text{opt},k}$  calculated by applying as a first step the multi-flare method to each selected source  $k$ . As in the previous section the spectral index,  $\gamma_s$ , and the total number of signal events,  $n_s$ , are free parameters in the likelihood minimization. The spectral index is assumed to be the same for all the  $k$  sources in a particular category. The parameter  $n_s$  in this case accounts for the sum of signal events produced in all the sources in the category.

### 3 Performance

As an illustrative example two simulated neutrino flares separated in time (double-flare) are considered as a signal hypothesis. This configuration may not be observed in the untriggered search because the assumed single Gaussian time structure is less efficient for large time gaps between the individual flares. Figure 1 shows the discovery potential, defined as the average number of signal events required to achieve a p-value less than  $2.87 \times 10^{-7}$  (one-sided  $5\sigma$ ) in 50% of the trials, as a function of the flare activity time for 5 of the selected FSRQs (see section 4) in dashed lines. The discovery potential is approximately constant and below the time integrated search for the range of flare activity times tested in this example. This feature of the method represents an improvement in the sensitivity for large time gaps when compared with the untriggered approach (see more details on this feature in Ref. [13]).

For the stacking case we consider a category of 5 flaring sources (FSRQs). Each source contributes with a double-flare structure located in a different time window. Signal events are injected in each location and chosen time window following a Poisson distribution with mean 6 (30 in total) and an  $E^{-2}$  energy spectrum for  $10^5$  simulated trials. Figure 2 shows the resulting best fit parameters. The centroid of this 2D distribution is located approximately in  $\hat{n}_s = 30$  and  $\hat{\gamma}_s = 2$  showing that the multi-flare algorithm is able to recover on average the parameters of the injected signal. Figure 1 shows the improvement in the discovery potential for the stacking case (filled triangles showing discovery potential per source) compared to the single source case (dashed lines showing individual source discovery potentials). Each source has to contribute with less signal

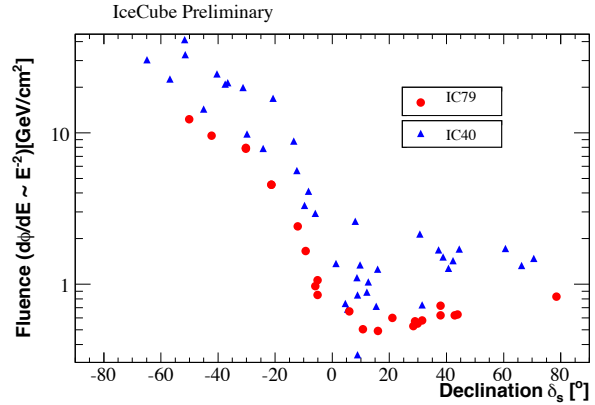


**Figure 4:** Fluence upper limit (assuming  $d\phi/dE \sim E^{-2}$ ) for the selected AGN obtained with the multi-flare analysis. For comparison the results of a time-clustering analysis applied to IceCube data in the 40-string configuration are also shown [8].

events on average to reach the  $5\sigma$  threshold in the stacking approach than if analyzed separately. Figure 3 shows the resulting discovery potential per source as a function of the total number of stacked sources for different flare activity times. Adding sources improves the discovery potential as is expected from a stacking analysis.

### 4 Source selection

A list of promising AGN candidates is selected in order to reduce the large trial factor that would be implied in an all-sky scan. There are several theoretical models predicting high energy neutrino emission from AGN. In Ref. [14] hard-spectrum BL-Lacs are selected as source candidates for IceCube whereas in Ref. [2] FSRQs bright in the GeV range are the promising objects without any assumption on the spectral index. The proton blazar model described in Ref. [3] predicts that the low synchrotron peaked BL-Lacs (LBL) are more likely to produce a significant neutrino emission than the high synchrotron peaked BL-Lacs (HBL). Data from the second Fermi Catalog has shown that LBLs have on average softer energy spectra than HBLs [7] and that FSRQs present a cutoff at a few GeV. In Ref. [15] a list of potential neutrino-loud AGNs is provided. In order to include these predictions in the selection of promising sources, data from the Fermi catalog was used to define the following criteria:

- **BL-Lacs:** Average flux [1 – 100 GeV]  $> 8 \times 10^{-8}$  photons  $\text{cm}^{-2}\text{s}^{-1}$  AND spectral index  $< 2.3$
- **FSRQs:** Average flux [0.1 – 1 GeV]  $> 1 \times 10^{-9}$  photons  $\text{cm}^{-2}\text{s}^{-1}$

With this selection we include most of the candidate sources listed in Refs. [2, 3, 14, 15]. In addition, for both source populations we require that the Fermi variability index is larger than 41.6 to select sources that are more likely to exhibit flaring periods [7]. The search time window for each AGN,  $\Delta T_{\text{Data}}$ , is defined by taking into account photon flare alerts in the IC79 period reported in astronomer telegrams (Atels) [16] or other relevant references. It is restricted to  $\Delta T_{\text{Data}} = T_m \pm 40$  days where  $T_m$  is the midpoint of the flare time interval reported in each alert [10].



**Table 1:** Results for the selected variable AGN using the multi-flare analysis. All the p-values are pre-trial. If  $\hat{n}_s = 0$  then no p-value or  $\hat{\gamma}_s$  are reported.

Source	Type	ra (°)	dec (°)	Atel ID	$T_m$ (MJD)	p-value	$\hat{n}_s$	$\hat{\gamma}_s$	$\Delta T(M_{opt})$ (days)	Fluence u.l. (GeV/cm <sup>2</sup> )
PKS 2326-502	FSRQ	352.317	-49.939	2783,3008	55415	-	0.0	-	15.974	12.15
PKS B1414-418	FSRQ	217.012	-42.104	3329,3337	55686	-	0.0	-	0.868	9.42
PKS 1830-211	FSRQ	278.413	-21.075	2943	55485	-	0.0	-	0.251	4.53
PKS 1830-211	FSRQ	278.413	-21.075	2950	55560	0.13	2.6	3.9	0.094	4.54
PKS 0727-11	FSRQ	112.572	-11.695	2895,2901	55460	-	0.0	-	6.409	2.38
PKS 1510-08	FSRQ	228.207	-9.103	3194,2385	55616	0.29	2.3	2.3	2.537	1.63
3C 279	FSRQ	194.042	-5.794	2886	55467	0.45	1.9	2.2	0.591	0.96
PKS 1329-049	FSRQ	203.015	-5.136	2728,2739	55384	-	0.0	-	8.334	1.04
PKS 1329-049	FSRQ	203.015	-5.136	2837	55450	-	0.0	-	0.192	0.84
3C 454.3	FSRQ	343.497	16.153	3064,3055	55520	-	0.0	-	0.107	0.49
4C+21.35	FSRQ	186.227	21.380	2684,2686	55364	-	0.0	-	7.441	0.59
Ton 599	FSRQ	179.877	29.247	2795	55423	-	0.0	-	0.672	0.56
B2 1520+31	FSRQ	230.542	31.744	3050	55519	0.39	1.8	2.0	0.418	0.57
4C +38.41	FSRQ	248.809	38.171	3238	55635	-	0.0	-	9.527	0.71
4C +38.41	FSRQ	248.809	38.171	3333	55689	-	0.0	-	1.377	0.61
PKS 2155-304	BL-Lac	329.714	-30.219	2944	55482	-	0.0	-	13.875	7.86
PKS 2155-304	BL-Lac	329.714	-30.219	2947	55600	-	0.0	-	13.851	7.82
PKS 0019+058	BL-Lac	5.643	6.124	2800	55387	0.40	1.6	2.2	0.432	0.66
MG1 J021114+1051	BL-Lac	32.806	10.836	3120,3129	55584	0.34	2.0	2.6	0.199	0.50
B2 2234+28A	BL-Lac	339.102	28.475	3056	55526	-	0.0	-	0.133	0.53
1ES 1215+303	BL-Lac	184.467	30.109	3100	55563	-	0.0	-	0.129	0.55
3C 66A	BL-Lac	35.661	43.036	3003	55503	-	0.0	-	0.152	0.62
MAGIC J2001+435	BL-Lac	300.288	43.879	2753	55393	-	0.0	-	0.374	0.63
5S5 1803+784	BL-Lac	270.147	78.483	3322,3323	55683	-	0.0	-	3.792	0.83

**Table 2:** Results of the multi-flare stacking search.

Category	p-value (post-trial)	$\hat{n}_s$	$\hat{\gamma}_s$	Fluence u.l. (GeV/cm <sup>2</sup> )
7 FSRQs (South)	0.16	7.4	3.6	1.00
5 FSRQs (North)	0.98	1.5	1.9	0.15
6 BL-Lacs (North)	0.91	3.7	2.4	0.24

## 5 Results

No significant set of events was found in the IC79 period. In Table 1 we list the results for each selected AGN: pre-trial p-values, best fit parameters  $\hat{n}_s$  and  $\hat{\gamma}_s$ , and flare activity time,  $\Delta T(M_{opt})$ . The fluence upper limit (u.l.) is calculated by integrating the differential energy spectrum ( $d\phi/dE \sim E^{-2}$ ) over the 90% energy range and over the  $\Delta T(M_{opt})$  time interval. Figure 4 shows the fluence upper limit as a function of the declination of the selected sources. It depends on declination since the IceCube sensitivity is different for different energy ranges accessible in each part of the sky [17]. The pre-trial p-value for the most significant AGN (PKS 1830-211) is 0.13 (0.93 post-trial) which is compatible with the expected background fluctuations.

The results for the multi-flare stacking search are shown in Table 2. The chosen categories also depend on the hemisphere in which the sources are located since IceCube is sensitive to higher energies in the southern sky [17]. The most significant category is the set of FSRQs located in the southern hemisphere ( $\delta_s < 0^\circ$ ) with a post-trial p-value of 0.16 which is compatible with the background-only hypothesis. The fluence upper limits shown in Table 2 are calculated for the sum of the most significant time windows extracted for each source in each category (Table 1) di-

vided by the number of contributing sources. We call this quantity the fluence upper-limit per source. These upper-limits are stronger than the ones extracted from the single-source analysis (Table 1) which again shows the advantage of the stacking procedure.

## References

- [1] A. Reimer, PoS(AGN2011) 006 (2006) 1.
- [2] A. Atoyan and C. Dermer, New Astron. Rev. 48(5) (2004) 381.
- [3] A. Mucke *et al.*, Astropart. Phys. 18(6) (2003) 593.
- [4] A. Achterberg *et al.*, Astropart. Phys. 26(3) (2006) 155.
- [5] R. Abbasi *et al.*, Astrophys. J. 732(1) (2011) 18.
- [6] IceCube Coll., paper 0550 these proceedings.
- [7] M. Ackermann *et al.*, Astrophys. J. 743(2) (2011) 171.
- [8] R. Abbasi *et al.*, Astrophys. J. 744(1) (2012) 1.
- [9] IceCube Coll., paper 0649 these proceedings.
- [10] D. Gora, E. Bernardini, A. Cruz, Astropart. Phys. 35(4) (2011) 201.
- [11] C. D. Dermer, E. Ramirez-Ruiz, T. Le, Astrophys. J. 664(2) (2007) L67.
- [12] B. Eichmann, R. Schlickeiser, W. Rhode, Astrophys. J. 749(2) (2012) 155.
- [13] D. Gora *et al.*, Proceedings 32nd ICRC, paper 0289 (2011).
- [14] A. Neronov *et al.*, Phys. Rev. D. 80 (2009) 083008.
- [15] A. Neronov, D. Semikoz, Phys. Rev. D. 66 (2002) 123003.
- [16] <http://www.astronomerstelegam.org/>
- [17] R. Abbasi *et al.*, Phys. Rev. Lett. 103 (2009) 221102.



## Calculating energy-dependent limits on neutrino point source fluxes with stacking and unfolding techniques in IceCube

THE ICECUBE COLLABORATION<sup>1</sup>,

<sup>1</sup>See special section in these proceedings

fabian.clevermann@udo.edu

**Abstract:** The stacking method is a standard technique to search for possible neutrino sources in which several sources of the same type are bundled into one catalogue so that the possible signal from their different positions can be superimposed for data analysis. Flux limits can be placed on models assuming specific neutrino energy spectra for the source class. To improve this result and obtain separate flux limits at different energies, this work uses a new approach that combines the stacking with an unfolding of the energy spectrum of the neutrino events at the source positions of the investigated catalogue. Because the unfolding algorithm is independent of an assumed model or spectrum, the results are model independent. No sources have been discovered yet, so the number of potential signal neutrinos contributing to the unfolded result will be very small. The novel software TRUEE is used to obtain unfolding results with few events, which can then be used to infer limits on additional astrophysical contributions to the detected atmospheric neutrino flux. We present the resulting sensitivity for a given source catalogue with this method using data collected by the IceCube detector when it was partially constructed in its 59-strings configuration.

**Corresponding authors:** F. Clevermann<sup>1</sup>

<sup>1</sup> TU Dortmund

**Keywords:** IceCube, neutrino, energy unfolding, point source, stacking

### 1 Introduction

IceCube is a cubic-kilometer neutrino detector installed in the ice at the geographic South Pole [1] between depths of 1 450 m and 2 450 m. Detector construction started in 2005 and finished in 2010. Neutrino reconstruction relies on the optical detection of Cherenkov radiation emitted by particles produced in neutrino interactions in the surrounding ice or the nearby bedrock.

Neutrino induced muons, traveling through the ice, produce Cherenkov radiation which can be detected by the Digital Optical Modules (DOMs). The light produced along the muon track provides directional and energy information [2] [3].

One of the main goals of IceCube is the detection of extra terrestrial neutrinos. Because single sources are too faint to be seen below the atmospheric background, the stacking method was introduced [4]. In this method several sources of the same type are bundled into one catalogue so that the possible signal from their different positions can be superimposed for data analysis. The observation time needed for measuring a signal is significantly reduced by this. The result is for the complete catalogue, and statements about individual sources can only be made after a *posteriori* analysis.

The standard stacking in IceCube [5] uses a log likelihood method with an assumed flux model to calculate a flux sensitivity. The flux model is usually chosen to be a power law  $\Phi \propto E^{-\gamma}$ . When analyzing data,  $\gamma$  is a free parameter which gets fitted. In order to provide more information about the energy distribution beyond a power-law fit, this work combines the stacking with an energy unfolding.

An energy unfolding is used to reconstruct the energy distribution of neutrinos. This method is needed, because

the energy of the primary neutrino is convoluted with the  $\nu$ - $N$  cross section, the finite detector resolution and the limited acceptance. The unfolding estimates the neutrinos' energy distribution from energy dependent observables of the muon.

### 2 Stacking analysis

The likelihood method for a single source is described in [6]. To include multiple sources, the signal term gets modified to include  $M$  sources with theoretical weights  $W(j)$ , relative source efficiencies  $R(j, \gamma)$  and the signal PDF's  $S_{i,j}$  for the  $i^{\text{th}}$  event w.r.t. the  $j^{\text{th}}$  source:

$$L(x_s, \gamma, n_s) = \prod_i \left[ \frac{\frac{n_s}{n_{\text{tot}}} \sum_{j=1}^M W(j) R(j, \gamma) S_{i,j}(x_i, E_i, \gamma)}{\sum_{k=1}^M W(k) R(k, \gamma)} + \left(1 - \frac{n_s}{n_{\text{tot}}}\right) B(x_i, E_i) \right] \quad (1)$$

For this work, 1 000 events with the highest  $S/B$  ratios for each catalogue are selected for the unfolding. The number of chosen events should be small to have fewest background events in the sample as possible, but still have enough statistics for a reliable result. After several tests and trials a number of events of 1 000 was found to be the best compromise for this analysis.

## 2.1 Source catalogues

A catalogue consists of several similar sources. This can be physical similarities, like the same accelerating process, as well as experimental similarities like being seen in a certain energy range from one experiment.

In these proceedings we describe, as an example, the analysis on the starburst galaxies catalogue.

- **Starburst galaxies:** This catalogue assembles galaxies with a high star formation rate (SFR). The high SFR results in a higher rate of super novae and supernova remnants (SNRs) which accelerate particles up to high energies (TeV). These particles are thought to create neutrinos in the interaction with dust clouds feeding the SFR. [7]

## 3 Unfolding analysis

For this analysis the ongoing events from the point source data sample of the 59-string configuration of IceCube was used [8]. It contains 43 339 events and has a 4.7% muon contamination according to Monte Carlo studies.

The unfolding is done by the software TRUEE [9]. To optimize the unfolding several configurations are evaluated on Monte Carlo data to determine the final settings.

### 3.1 Selection of observables

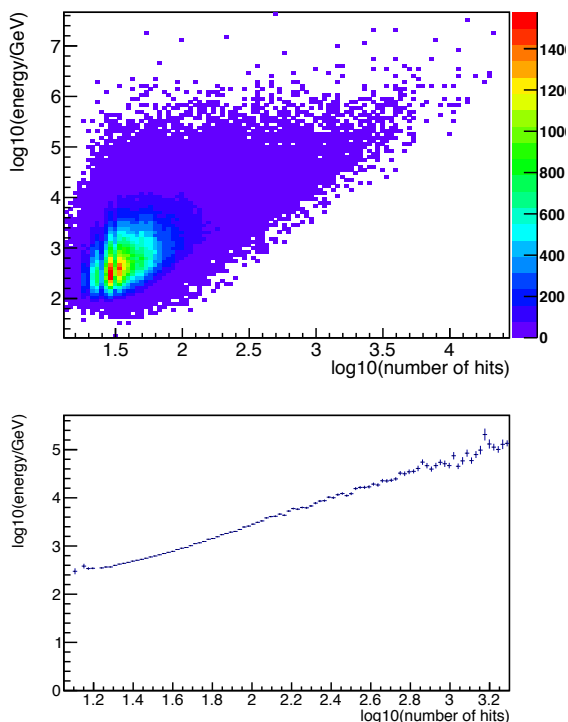


**Figure 1:** An example of the energy dependence of one of the observables used in the TRUEE unfolding. Top shows the distribution of energy and the number of total hits. Bottom plot shows the associated profile plot.

The first step is to select observables which are dependent on the neutrino energy. TRUEE yields scatter plots for all used observables showing its energy dependence. Out of many energy dependent variables a MRMR algorithm [10] implemented in the RapidMiner [11] selected 10

observables. Inspection of these 10 scatter plots produced by TRUEE resulted in the selection of the following three observables:

- Energy loss per unit track length
- Number of pulses observed in the DOMs
- Number of strings having a signal

Figure 1 shows the energy dependency of the total number of pulses observed in the DOMs.

### 3.2 Parameter selection

After the selection of the energy dependent observables to reconstruct the true energy distribution of the neutrinos, the parameters for the unfolding have to be found out.

The most important parameters are the degrees of freedom and the number of knots. The degrees of freedom are a measurement for the regularization, fewer degrees of freedom result in a stronger regularization. The number of knots determine the how many B-splines are used in the unfolding. With more splines more features can be reconstructed, but can also lead to oscillating results.

For this purpose TRUEE offers a validation mode, where Monte Carlo data is unfolded such that the unfolded result can be compared with the truth from the Monte Carlo. Figure 2 shows the resulting comparison plot for the starburst catalogue.

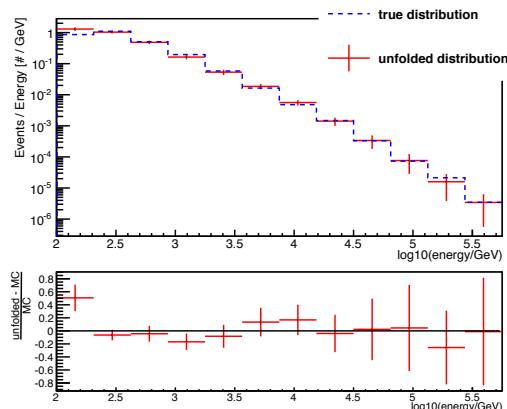


**Figure 2:** Verification of the unfolding comparing MC truth to pseudo data (top). Ratio plot (bottom) shows relative differences.

To make sure this good result is not an artifact from the randomly selected Monte Carlo events used for unfolding, this test is repeated several times on different event samples used as pseudo data, which is called pull mode. For each bin in each unfolding the difference between truth and unfolding result in units of standard deviation is plotted into a histogram. The Gaussian should be centered around zero. If the Gaussian is shifted to the right, TRUEE is overestimating the events in that energy bin. The plot in the top of figure 3 shows a resulting histogram. The bottom plot shows the mean distribution for each energy bin based on several experiments.

The overview plot shows a systematic deviation in the first and the last bin. This deviation is taken into account further on in the analysis. Instead of using the unfolded value for the limit calculation, the stat. error is added, respectively subtracted of the unfolded value.

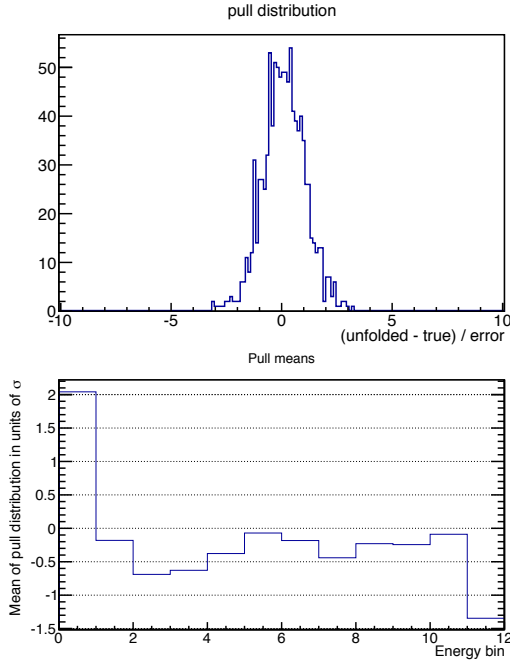


**Figure 3: top:** The plot shows the systematic deviation between the unfolded pseudo data and its truth for one bin. It is well centered around zero as expected. **bottom:** The plot shows an overview where all the means for each bin are shown. Only in the first and last bin the systematic uncertainty exceeds the statistical one.

### 3.3 Unfolding result

The unfolding technique gives as a result the energy distribution of the measured neutrinos. To verify the method on data, first we use a scrambled data set. By scrambling the events' right ascension in data it is possible to remove any influence of a signal in the sample. The result of this unfolding can be seen in figure 4. Although the last three bins have non-zero unfolded events which is used for limit calculations, the limit is compatible with zero to within one standard deviation.

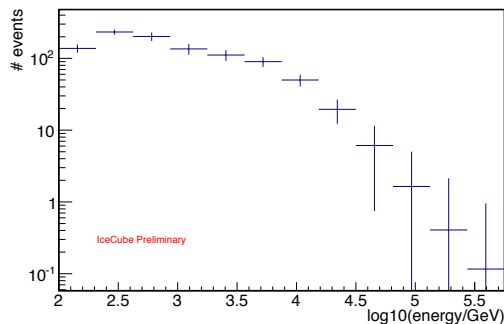


**Figure 4:** Unfolded result of the scrambled analyses. The x-axis shows the neutrino energy and on the y-axis the number of events are shown.

## 4 Sensitivity calculation

To calculate an upper limit for an excess above the expected background a profile likelihood method introduced by Rolke [12] is used. To get a robust background estimation, 2 000 different scrambled data sets were generated. The shape of these results for each bin follow a Gaussian distribution. Hence the model assuming the background  $Y$  is Gaussian distributed:

$$X \propto \text{Pois}(\mu + b), \quad (2)$$

$$Y \propto N(b, \sigma_b). \quad (3)$$

$X$  describes the signal as a Poisson distribution with the signal rate  $\mu$  and the background rate  $b$ .  $N$  is a Gaussian (or normal) distribution with the background rate  $b$  as mean and its standard deviation  $\sigma_b$ . The efficiency, which could also be included in this profile likelihood method, is assumed to be 100%, because it is taken into account in the effective area calculated from Monte Carlo simulations. With the  $X$  and  $Y$  chosen as mentioned above, the derivative of the likelihood is

$$\frac{\partial}{\partial b} \log l(\mu, b|x, y) = \frac{x}{\mu + b} - 1 + \frac{y - b}{\sigma_b} \stackrel{!}{=} 0, \quad (4)$$

with  $x$  and  $y$  being the realization, i. e. observation, of  $X$  and  $Y$  respectively.

The sensitivity is calculated by using these background values as expected background as well as observed events with a certain confidence level. The calculated sensitivities for a 90% confidence level for an excess on top of the expected background can be seen in figure 5. Any neutrino flux, and not those following a unbroken power-law spectrum, exceeding the sensitivities in each energy bin will be excluded with a 90% confidence level.

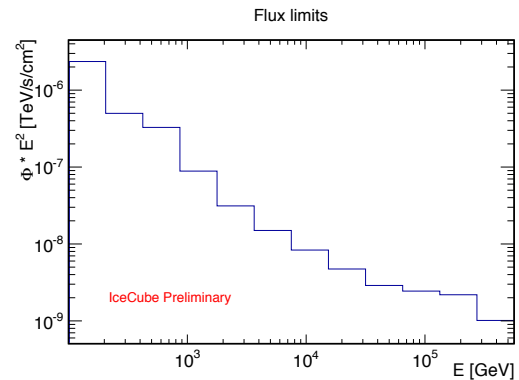


**Figure 5:** Unfolded sensitivities for the starburst catalogue. This result is calculated from the 90% upper limit for a pure background measurement, the effective area for the catalogue and the livetime of the detector.

It is also possible to calculate sensitivities depending on the spectral index  $\gamma$  for an unbroken power law. Figure 6 shows the  $\Phi_0$  for various  $\gamma$  between -1 and -4. The break at  $\approx 3.2$  is due to the constraint moving from the highest energy bin to other bins.

## 5 Conclusion and outlook

This new method, combining a stacked analysis with an energy unfolding, yields sensitivities for different energies.

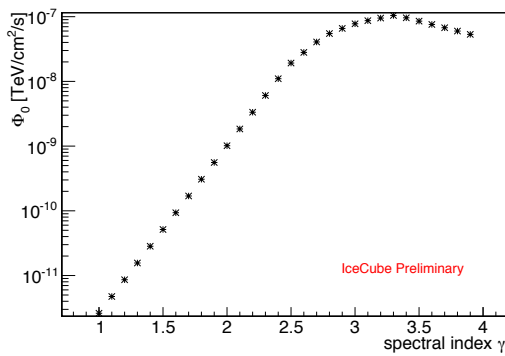


**Figure 6:** Different  $\Phi_0$  sensitivities for unbroken power laws with indices between -1 and -4 are shown. The entry at  $\gamma = -2$  corresponds to the y-axis intercept of the last bin in figure 5. The break at  $\gamma \approx 3.2$  originates from another bin being the limiting factor.

These sensitivities are completely independent of an assumed model, as well as Monte Carlo simulation.

The limiting factor for the unfolding is the low number of events. With larger configurations of IceCube it is possible to increase the number of events from the regions of interest and improve the energy resolution. A better energy resolution in the high energy region would increase the sensitivity, due to the higher detection probability and the lower background rates.

## 6 Acknowledgments

This work is supported by the German Research Foundation DFG (SFB 823/C4) and the Federal Ministry of Education and Research (BMBF).

## References

- [1] A. Achterberg *et al.*, *Astropart. Phys.* 26 (2006) 155
- [2] L. Gladstone, in *Proceedings of the XLVI Rencontres de Moriond* (2011) arXiv:1111.2969
- [3] R. Abbasi *et al.*, arXiv:1208.3430
- [4] A. Groß, *Astroparticle Physics* 26 (2006) 282 doi:10.1016/j.astropartphys.2006.06.012
- [5] R. Abbasi *et al.*, *The Astrophysical Journal* 732 (2011) 18 doi:10.1088/0004-637X/732/1/18
- [6] J. Braun, J. Dumm, F. De Palma *et al.*, *Astroparticle Physics* 29 (2008) 299 doi:10.1016/j.astropartphys.2008.02.007
- [7] J. Dreyer *et al.*, (2009) 27 pages, arXiv:0901.1775
- [8] IceCube Coll., paper 0550 these proceedings
- [9] N. Milke, M. Doert *et al.*, *Nuclear Instruments and Methods in Physics Research Section A* 697 (2013) 133 doi:10.1016/j.nima.2012.08.105
- [10] C. Ding, H. Peng, *Journal of bioinformatics and computational biology* 3 (2005) 185 PMID:15852500
- [11] I. Mierswa, M. Wurst, R. Klinkenberg *et al.*, *Proceedings of the 12th ACM SIGKDD international conference on Knowledge discovery and data mining - KDD '06* (2006) doi:10.1145/1150402.1150531
- [12] W. Rolke, A. M. López and J. Conrad, *Nuclear Instruments and Methods in Physics Research Section A* 551 (2005) 493 doi:10.1016/j.nima.2005.05.068

## IceCube : latest results on point and extended neutrino source searches

THE ICECUBE COLLABORATION<sup>1</sup>

<sup>1</sup>See special section in these proceedings

Juan.Aguilar@icecube.wisc.edu

**Abstract:** We present a variety of searches for time-independent neutrino emissions from astrophysical sources with the IceCube detector. The analyses use data collected between April 2008 and May 2011 by the partially-completed IceCube detector, as well as the first year of data from the completed 86-string detector. An unbinned maximum likelihood method is used to distinguish astrophysical signals from atmospheric backgrounds, utilizing both spatial and energy information. The analyses include searches for individual point sources, spatially extended sources, and targeted searches using stacked source catalogs. These analyses are sensitive to TeV - PeV energy neutrinos in the northern sky and PeV - EeV neutrinos in the southern sky. Limits on extraterrestrial neutrino fluxes are compared to model predictions. The expected performance with multiple years of data from the full IceCube detector is discussed.

**Corresponding authors:** J. A. Aguilar<sup>1</sup>, J. Feintzeig<sup>2</sup>, N. Kurahashi<sup>2</sup>, S. Odrowski<sup>3</sup>, M. Rameez<sup>1</sup>

<sup>1</sup> University of Geneva, Geneva, Switzerland

<sup>2</sup> Wisconsin IceCube Particle Astrophysics Center, University of Wisconsin, Madison, WI, USA

<sup>3</sup> Technische Universitat Munchen, Munich Germany

**Keywords:** neutrino telescope, astrophysical neutrino sources, time integrated searches

### 1 Introduction

IceCube is a cubic-kilometer neutrino detector installed in the ice at the geographic South Pole [1] between depths of 1450 m and 2450 m. Detector construction started in 2005 and finished in 2010. Neutrino event reconstruction relies on the optical detection of Cherenkov radiation emitted by secondary particles produced in neutrino interactions in the surrounding ice or the nearby bedrock. During its construction, the IceCube telescope ran in various configurations. From April 2008 to May 2009, 40 strings were operational and collecting data. The array increased to 59 strings in May 2009 and 79 strings in May 2010. Construction was completed on 18th December 2010, and data-taking with the 86 string detector began the following May.

Astrophysical neutrinos are excellent candidates for studying acceleration mechanisms of Cosmic Rays (CRs). Produced in the same environmental conditions as CRs and Gamma Rays, their neutral charge allows them to propagate directly from the source to Earth, preserving directional information. Their detection will shed light on sources of CRs and the acceleration mechanisms in extreme environments (Supernova Remnant Shocks, Active Galactic Nuclei jets, Gamma Ray Bursts etc).

Finding neutrino point sources in the sky requires locating an excess of events from a particular direction over the background, which consists of atmospheric neutrinos and muons. In addition to the spatial distribution, signal events are likely to have a different energy spectrum that allows us to distinguish them from the background. In this paper we will focus on the search for steady neutrino sources while optimized searches for time dependent emission are reported elsewhere [2]. The analysis carried out is on data from three years of operation in partial levels of completion and the first year of the completed 86 string detector.

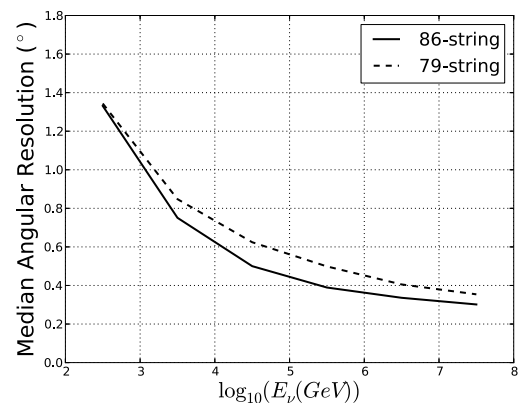


**Figure 1:** Median angular resolution (angle between reconstructed track and neutrino direction) as a function of neutrino energy for event samples from the 86-string (solid) and 79-string detectors (dashed). At 30 TeV, the 40 and 59 string event selections (not shown) give angular resolutions of  $\sim 0.8^\circ$  and  $\sim 0.75^\circ$ , respectively [4].

### 2 Data Selection and Detector Performance

The event selection for data from the 40, 59 and 79 string configurations is described in detail in [3] and [4] respectively. In the analysis of data from these configurations of IceCube, no significant excess over background fluctuations have been found and upper limits have been published [4].

Event selection for data from the first year of the 86-string detector closely follows strategies used in previous analyses [4]. The data stream is first reduced from a trigger rate of  $\sim 2500$  Hz to 2 Hz by a combination of real-time



filtering and subsequent offline, CPU-intensive processing. At these stages, the data is dominated by atmospheric muons from cosmic rays, either as direct down-going muons in the southern sky, or mis-reconstructed as up-going muons in the northern sky. These events are removed via quality cuts, first using simple reconstructions and event quality parameters, followed by advanced, likelihood-based muon reconstructions calculated offline.

From the 2 Hz of remaining data (still dominated by the atmospheric muon background), 4.8 mHz of events are selected for the final analysis sample. In the northern sky the mis-reconstructed muon background can be mostly eradicated so that a nearly pure sample of up-going atmospheric neutrinos remains. The event selection in this region of the sky is done using a classification algorithm, Boosted Decision Trees (BDTs). We trained four BDTs to separate astrophysical neutrino signal from the atmospheric muon background. We separate the northern hemisphere into two zenith bands, and in each band we train two BDTs for different neutrino signal spectra. Each BDT is trained using 11 event variables for signal/background discrimination, with detector data describing the background distributions. Of these eleven variables, four control for reconstruction stability, five can be considered event quality variables, and two describe the event topology. Cuts on the BDT output scores are optimized to achieve the best discovery potential for both  $E^{-2}$  and  $E^{-2.7}$  signal spectra. This event selection covers the entire northern hemisphere and extends  $5^\circ$  above the horizon, where the Earth and glacial ice still provide a shield from the cosmic ray background.

More than  $5^\circ$  above the horizon, we cannot isolate a pure neutrino sample. The data are dominated by high-energy atmospheric muon bundles, which closely mimic neutrinos. However, the background can be reduced via parameters that select neutrinos and reject muon bundles. One BDT is trained for the entire region, using data to describe the background and  $E^{-2}$  neutrino simulation for signal. Eleven variables are used in training the BDT. Five of these variables describe track quality, three describe event topology, and three exploit differences between single muons and bundles. These parameters rely on event topology and energy loss information. Large muon bundles consist of many low-energy muons that typically lose energy at a constant rate as they traverse the detector. Photons from these muons are detected within a wide time range. High-energy neutrino-induced muons instead have relatively stochastic energy loss profiles and narrower photon timing distributions. These properties are quantified by a likelihood technique and are used in the BDT. To obtain the final sample, a cut on BDT score is varied with zenith to select an equal event rate per solid angle. This technique avoids any hard energy threshold in the southern hemisphere, which previous analyses have used.

The final data sample for the 86-string detector has  $\sim 140,000$  events, including  $\sim 70,000$  atmospheric neutrino candidates in the northern hemisphere sample. The neutrino effective area for this selection is very similar to the 79-string analysis [4]. New to this event sample, a new muon reconstruction technique is used to improve the neutrino angular resolution. This likelihood-based reconstruction is similar to the reconstruction used in previous analyses [4], but uses more detailed information to describe the scattering and absorption of photons in the glacial ice. This leads to a 26% improvement in neutrino angular resolution at 30 TeV. The neutrino angular resolution for the 79 and 86 string event samples is shown in Figure 1. The expected sensitivity

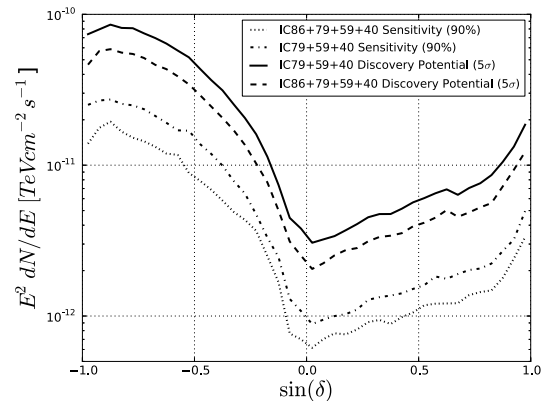


**Figure 2:** Flux required for  $5\sigma$  discovery of a point source emitting an  $E^{-2}$  flux at different declinations, for three years (solid, dotted) and four years (dashed) of data. The 90% sensitivity for four years is shown as a dashed-dotted line.

and discovery potential combining this event sample with the previous three years of data is shown in Figure 2.

### 3 Method

This analysis uses an unbinned maximum likelihood ratio test [5]. The significance of an excess of neutrinos above the background for a given direction can be calculated using this method. Both the reconstructed direction of the event and the reconstructed visible muon energy are used in order to discriminate between signal and background [3]. This method has been demonstrated to provide superior sensitivity over simple directional clustering based methods, as the signal events have a harder energy spectrum compared to the atmospheric neutrino and muon backgrounds. For each direction in the sky, the likelihood function is maximized with respect to the number of signal events  $n_s$  and the index of the power law neutrino spectrum,  $\gamma$ . The ratio of the likelihoods between the best fit hypothesis and the null hypothesis ( $n_s = 0$ ) forms the test statistic. To evaluate the background test statistic distribution, the analysis is performed repeatedly on scrambled data sets, wherein the right ascensions of the events are randomized but all other event properties are fixed. Uniform exposure in right ascension is ensured by the daily rotation of the detector with respect to the sky. Events close to the polar regions of the sky (declination  $< -85^\circ$  or  $> 85^\circ$ ) are excluded from the analysis as scrambling in right ascension does not work in these regions. The power of the method is expressed in terms of the flux required to produce a  $5\sigma$  discovery. Three different searches are performed:

#### 3.1 All Sky Scan

The maximum likelihood is evaluated for each direction in the sky on a grid of  $0.1^\circ \times 0.1^\circ$ , much finer than the angular resolution of the detector. The significance of any point on the grid is determined by the fraction of scrambled data sets containing at least one grid point with a likelihood ratio higher than the one observed in the data, and serves as the post-trial p-value for the all sky search. The search presented here is carried out with four years of data, including three years from partial detector configurations and one year of data from the full 86 string configuration.

### 3.2 *A Priori* Source list

Since the power of the all sky search is limited by the large number of effective trials, the second search is a scan over a restricted *a priori* selected set of 44 sources of interest (based on gamma ray observations and astrophysical modeling predicting neutrino emission [3]). The post-trial p-value is calculated by performing the same analysis on scrambled data sets. This search is carried out with data from the 40, 59 and 79 string configurations only.

### 3.3 Stacked Searches

The stacking method and its advantages are described in detail in [3] where it is explained how the signal and background are integrated over a set of sources using a uniform weighting for all stacked sources or a weighting scheme based on theoretical predictions. The fractional flux required for discovery for stacked sources scales inversely with the number of sources. The catalogs to stack are selected according to theoretical models or observational parameters connecting photon to neutrino emission. The stacking searches presented here are performed on a combination of the 40, 59 and 79 string samples only, with the exception of one catalog. We perform:

1. A stacking of 6 sources reported by Milagro with supernova remnant (SNR) associations, found *a posteriori* to have an excess in a stacking of 17 sources reported by Milagro carried out on data from the 40 string configuration [3], motivated by [6]. This search is hence confined to data from just the 59 and 79 string configurations to avoid bias.

2. A stacking search for 127 local ( $z < 0.03$ ) starburst galaxies [7]. Relative source luminosities are assumed to be proportional to their Far InfraRed (FIR) fluxes ( $60 \mu\text{m}$ ), due to models suggesting correlation between Radio, FIR and neutrino fluxes [7].

3. A stacking search for 5 nearby clusters of galaxies (GCs), consisting of Virgo, Centaurus, Perseus, Coma and Ophiuchus. Four different flux models are provided in [8] and described in detail in [3], differing in their assumption as to how the CRs are distributed within the cluster. Due to the very different extension of the sources as predicted by the different models [3], four different searches are carried out for this catalog. Relative source luminosities are taken from the norm of the predicted flux for each source, for each model.

4. A stacking search of 4 Supernova Remnants (SNRs) with Molecular Cloud associations detected in GeV and TeV photons by MAGIC, AGILE, Fermi, Veritas, HESS and HEGRA. Integrated Gamma Ray Fluxes above 1 TeV in Crab units are taken to be the relative source luminosities. Two of these sources, IC443 and W44 have been observed by the Fermi LAT to emit GeV photons that follow a typical neutral pion decay spectrum.[9].

5. A stacking of Black Hole Candidates within the GZK radius of 100 Mpc. A strong mass cut, motivated by [10] is applied on the catalog published in [11] to remove all but the most powerful emitters and the relative source luminosities are taken to be proportional to the Near InfraRed (NIR) flux ( $2 \mu\text{m}$ ) for the final 233 sources due to the high correlation shown between the NIR flux and the  $M/D^2$ .

## 4 Systematics

The background in the above searches is estimated from randomized data. Hence the p-values are unaffected by uncertainties in the theoretical estimate of atmospheric muon and neutrino fluxes which are influenced by hadronic

models of shower development in the atmosphere and the CR composition. They are also unaffected by uncertainties in prompt neutrino fluxes and in the detector simulation.

However, the upper limits are affected by the systematic errors on the simulation of the detector response to the flux of neutrinos. The detector efficiency and effective area are estimated from these simulations. Since the angular resolution is also affected by these systematic uncertainties, we propagate each of the detector simulations through the likelihood search and calculate the sensitivity of the search to a discrete set of simulated signal responses within the allowed range of uncertainties.

The two most relevant uncertainties concern the absolute efficiency of the optical modules and the uncertainties in modeling of the optical properties of the ice. Uncertainties in the relative sensitivity of the individual DOMs with respect to the detector average have been observed to have negligible impact. As a conservative estimate, we allow for a  $\pm 10\%$  uncertainty on both the absolute sensitivity of the optical modules, and in the absorption and scattering of the ice model, parameterized as in [12].

By summing in quadrature all the different contribution the expected uncertainty in the IC-79 sensitivity is about 18%. This is compatible with the 16% estimated for the IC-40 configuration [3].

The presented upper limits are for a pure muon neutrino signal, assuming contribution from no other flavors. With large mixing angles such as  $\Theta_{23} \sim 45^\circ$  and baselines of astrophysical scale, typical source flavor ratios of  $\nu_e : \nu_\mu : \nu_\tau = 1:2:0$  will translate to a 1:1:1 flavor ratio at Earth. Since the taus produced decay into muons with a branching ratio of about 17%,  $\nu_\tau$  can contribute to a possible signal flux in this analysis. In [3], this contribution has been estimated to be 10 - 16% of the  $\nu_\mu$  contribution.

## 5 Results

All observations are compatible with the background-only hypothesis. In the all sky scan with four years of data, the most significant deviation in the northern sky has a pre-trial p-value of  $9.15 \times 10^{-6}$  and is located at  $11.45^\circ$  r.a. and  $31.35^\circ$  dec. while in the southern sky it is at  $296.95^\circ$  r.a. and  $-75.75^\circ$  dec. and has a pre-trial p-value of  $1.10 \times 10^{-6}$ . The post-trial probabilities (the fraction of scrambled sky maps with at least one spot with an equal or higher significance for each region of the sky) corresponds to 38% and 9% respectively and are well compatible with the background hypothesis.

The *a priori* sources list search with three years of data found HESS J0632+057 as the most significant source in the northern sky with a probability of 5.8% while for the southern sky it was PKS 1454-354 with 23%. Their post-trial probabilities were 65% and 70% respectively and are also compatible with the background hypothesis. Table 1 lists a few of the most interesting sources from an astrophysical point of view and also the sources that produced the strongest deviations. Fig 3 shows upper limits for the Crab Nebula. Similar illustrations of flux limits for other interesting sources can be found in [4].

None of the stacking searches found a significant excess, with the smallest p-value (i.e. highest significance) found for the Milagro 6 catalog with a probability of 20.4%. Fig 4 shows the 90% C.L upper limits for some of the flux models motivating the stacking searches. The 90% C.L. upper limit on  $\Phi_{\nu_\mu + \bar{\nu}_\mu}^{90\%}$  was found to be 1.84 times the total flux predicted by the model of Halzen et al [6] for Milagro

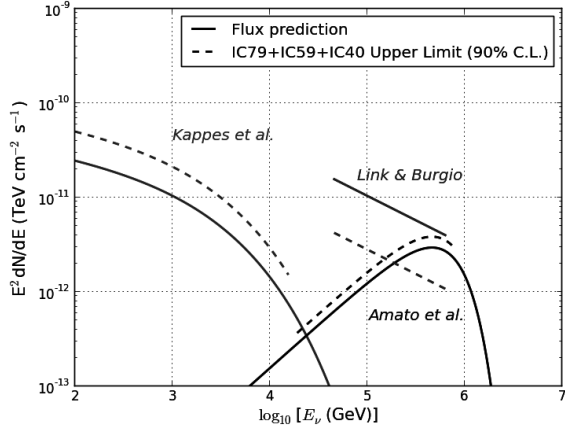


**Figure 3:** Predicted muon neutrino fluxes for several hadronic models about the Crab steady emission and upper limits based on 3 years of IceCube data. Solid lines indicate the flux prediction and the dashed lines the corresponding upper limit flux for a 90% C.L. for an energy range that contains 90% of the signal. Neutrino oscillations are accounted for.

Source	$\Phi_{\nu_{\mu}+\bar{\nu}_{\mu}}^{90\%}$	p-value	$\hat{n}_s$
PKS 1502 +106	2.40	0.076	8.4
HESS J0632+057	2.23	0.058	15.6
IC443	1.63	0.43	2.8
Mrk 421	3.45	0.18	3.7
Mrk 501	2.84	0.34	4.8
Cyg X-3	2.35	0.43	2.4

**Table 1:** A few sources from the *a priori* source list search and their pre-trial p-values calculated from 3 years of IceCube data.  $\Phi_{\nu_{\mu}+\bar{\nu}_{\mu}}^{90\%}$  is the normalization for an  $E^{-2}$  flux in units of  $10^{-12} \text{ TeV}^{-1} \text{ cm}^{-2} \text{ s}^{-1}$  denoting the 90% C.L. upper limit in the Neyman frequentist method and  $\hat{n}_s$  is the fitted number of signal events in the likelihood maximization.

6. For the Galaxy Clusters A, B, Isobaric and Central AGN Models, this upper limit was found to be 2 – 6 times the total predicted flux, depending on the assumed model of CR density.

## 6 Conclusion

The search for point sources of neutrinos with four years of data from the IceCube Neutrino Observatory has found no evidence of point source neutrino emissions in both the northern and southern hemisphere. The post-trial probabilities of the most significant coordinate in each hemisphere are compatible with the background hypothesis. More specific searches such as the *a priori* source list search and the catalog stacking searches, carried out with 3 years of data from the 40, 59 and 79 string configurations also have not found any significant fluctuations. 90% C.L. upper limits on the muon neutrino fluxes were calculated and compared to predictions. The most optimistic predictions can be ruled out while other limits are a factor of 2-6 worse than the predictions.

The muon neutrino upper limits presented are a factor of 3.5 better than the previous published by IceCube [3],

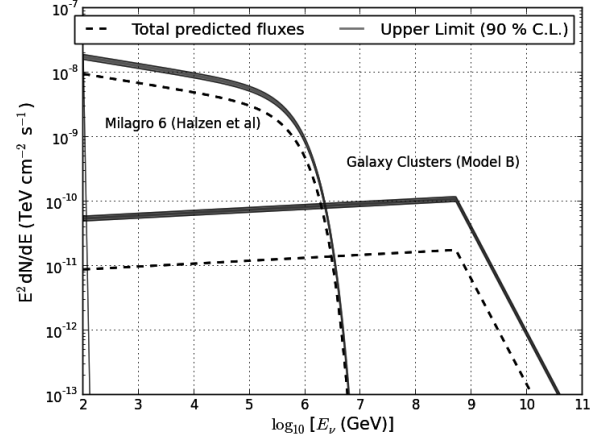


**Figure 4:** Upper limits (with bands denoting systematic uncertainties) for some of the models motivating the stacking searches. The fluxes are for muon neutrino fluxes at earth after oscillations.

and are the strictest limits to date in the TeV-PeV energy range in the northern sky and the PeV-EeV energy range in the southern sky. Some of these have reached the level of  $10^{-12} \text{ TeV cm}^{-2} \text{ s}^{-1}$  necessary to test current models of neutrino emission expected from galactic sources such as SNRs. With an additional four years of data from the full configuration of the detector, these limits are expected to further improve by a factor of  $\sim 2$ .

## References

- [1] R. Abbasi et al, Nucl. Inst. Meth. A 618 (2010) 139.
- [2] IceCube Collaboration, paper 649, these proceedings.
- [3] R. Abbasi et al, Astrophys. J. 732 (2011) 18.
- [4] M.G. Aartsen et al, *Search for time-independent neutrino emission from astrophysical sources with 3 years of IceCube*. Paper in preparation (2013).
- [5] J. Braun et al., Astropart. Phys. 33 (2010) 175.
- [6] F. Halzen, A. Kappes and A. O’Murchadha, Phys. Rev. D 78 (2008) 063004.
- [7] J. Becker et al., arXiv:0901.1775v1 [astro-ph.HE].
- [8] K. Murase, S. Inoue and S. Nagataki, Astrophys. J. Letters 689 (2008) L105.
- [9] M. Ackermann et al, Science 339 (2013) 6121.
- [10] P. Biermann and L. Caramete, arXiv:0908.2764 [astro-ph.CO].
- [11] P. Biermann and L. Caramete, arXiv:1107.2244 [astro-ph.GA].
- [12] M.G. Aartsen et al, Nucl. Inst. Meth. A 711 (2013) 73.



## Probing cosmic ray production in massive open star clusters with three years of IceCube data

THE ICECUBE COLLABORATION<sup>1</sup>.

<sup>1</sup> See special section in these proceedings

Yolanda.Sestayo@icecube.wisc.edu

**Abstract:** The ejecta of supernovae are the leading candidate sources of Galactic cosmic rays (CRs). Most Galactic supernovae are formed by the core-collapse of young massive stars that are clustered in regions of massive star formation. The combination of strong winds of the progenitors and the supernova ejecta leads to the formation of shocks where charged particles can be accelerated via diffusive shock acceleration. Neutrinos are a by-product of CR interactions in these clusters or their environment and can help to identify the sources of CRs. In this paper we study the sensitivity of IceCube to identify this spatially extended neutrino emission from massive open star clusters.

**Corresponding authors:** S. Odrowski<sup>1</sup>, Y. Sestayo<sup>2</sup>,

<sup>1</sup> Dept. of Physics, University of Alberta, Edmonton, Alberta, Canada T6G 2E1

<sup>2</sup> T.U. Munich, D-85748 Garching, Germany

**Keywords:** IceCube, cosmic rays, massive open clusters

### 1 Introduction

Massive stars are the major contributors to the chemical enrichment of the interstellar medium (ISM), restoring most of their total mass to the ISM through stellar winds and supernova explosions, after processing a fraction of it in the stellar interior [1]. They also inject large amounts of radiation and mechanical energy into the ISM, and their deaths as core-collapse supernova are recognized as the principal sources of energy for cosmic ray acceleration.

At Galactic scales, star formation is connected with the spiral structure as a result of the large scale dynamics of the interstellar medium. Star formation also occurs on the small scale of individual star forming events within a molecular cloud complex, with open clusters as the smallest groups in the hierarchy of star formation [2]. All this results in a structured distribution of massive stars in the Milky Way: from open clusters to open cluster complexes which are associated to giant molecular clouds following the underlying spiral pattern of the Milky Way. Massive stars are short lived, meaning that they not only form within an open cluster or association, but they also die in it, with only a small fraction of stars, 2% to 6%, not traceable to an origin in a cluster or association [3]. The spatial distribution of the main candidate sources of cosmic rays should then follow that of massive open clusters in an "accelerator-dominated" phase, that is, when their energetics are governed by the strong winds of dying massive stars and supernova explosions [4].

We present here a selection of massive open clusters to be studied with the IceCube neutrino detector. This selection is specifically made for IceCube and exploits its capability to continuously monitor the whole sky without the need for pointing. We customize both IceCube's target selection and data analysis by taking into account the spatial scales involved (from both the phenomenology and the detectors field of view and angular resolution) and the

sensitivity of the detector. IceCube achieves the highest sensitivity to TeV-PeV neutrino sources in the northern hemisphere, a feature which is advantageous to study local sources of neutrinos. The Sun is located in what is called the Local arm, a minor spiral feature of the Milky Way between the Perseus and Sagittarius arms, which can be accessed in its majority from the northern hemisphere. The Perseus arm runs at a distance between 2-3 kpc from the Sun at the Galactic longitudes accessible from the northern sky, our closest approach to one of the main spiral arms of the Milky Way. Cosmic-ray acceleration in nearby complexes with a high density of massive stars can therefore be studied with IceCube, and we propose to test this scenario by searching for a neutrino event pattern that would arise if cosmic rays produced in "accelerator-dominated" star clusters interact with ambient gas and radiation fields. With a proper selection of open clusters based on their total stellar mass and evolutionary status, we aim to target those in an accelerator-dominated phase as a proxy for local Galactic cosmic ray factories. Identification and distance estimation to young stars clusters can currently be determined with precision only for those that are within 3-4 kpc from the Sun. Therefore, we only investigate sources in the Solar neighborhood. In the following, we study neutrino production under two hypothesis: (1) cosmic ray confinement and neutrino production inside the cluster area, and (2) cosmic ray escape and neutrino production in the surrounding cluster environment by interactions of cosmic rays with dense gas clouds.

Our goal here is to shed some light to the problem of production, confinement and escape of cosmic rays using new data from the IceCube neutrino observatory. Our two hypotheses require two different search strategies. In our first approach, the search is carried out within open cluster complexes targeting the production of neutrinos close to the cosmic ray sources. Our second approach investigates neutrino emission in high-density gas clouds in close prox-



imity to the potential accelerators within the cluster. The status of the analysis are presented.

## 2 Data and modelling

This work uses the catalogue of open cluster data (COCD) from [5, 6], with the radii and masses compiled in [7]. The sample contains 641 open clusters and 9 compact associations for which a homogeneous set of cluster parameters is available. The COCD is thought to be complete up to distances of 850 pc from the Sun and contains optically selected open clusters, where all stars are already formed.

To select high density regions around the clusters environment, we use CO data from the composite survey of [8] as a tracer of molecular hydrogen. Due to the larger abundance of atomic hydrogen in the Milky Way, in particular in the outer Galaxy, we also use data from the 21-cm line of HI from the LAB survey [9] to study the kinematics of the gas in order to assign distances to molecular clouds from their observed velocity spectra along a given line of sight. Although the kinematical distance method can be rendered quite inaccurate by localized perturbations due to spiral shocks, expanding shells or other type of explosive phenomena, it is the most efficient method to derive distances to molecular clouds.

We model the gas component in the Milky Way as an exponential warped disk [10] with a grand-design four-armed spiral pattern originated from the spiral density wave perturbations of the disk [11]. The velocity of the gas at each line of sight ( $V_{los}$ ) is thus a combination of the rotational velocity of the material around the Galactic Center plus the streaming motions from the Galactic spiral potential, which are particularly large within the Perseus arm region of the Galaxy. We assume a Schmidt rotation curve and the standard density wave theory of [12] to calculate the  $V_{los}$  at each direction. The model parameters are then adjusted to best match the data in order to obtain the association between the velocity and the distance of the material responsible of the emission at each line of sight [13].

### 2.1 Selection of "accelerator-dominated" open clusters

Starting from the COCD sample we want to select those clusters having massive stars in their last stages of evolution, or that have recently exploded as core-collapse supernovae. The number of such stars in a cluster depends on both the cluster age and the cluster's stellar mass distribution at birth, i.e., the initial mass function (IMF). Given the uncertainties in both the age determination of the clusters and the theoretical stellar lifetimes (specially post-MS lifetimes), we will simplify the scenario by requiring only that the turn-off mass of the stars in the clusters is above  $9M_{\odot}$ . Stellar evolution models predict that only stars with initial mass above  $9M_{\odot}$  can lead to supernova explosions by the collapse of their nuclei. The lifetime of a star with a main sequence mass of  $\sim 9M_{\odot}$  is around 40 My. Clusters older than  $\sim 40$  My are not considered in our study, because we assume that they are scarce in potential accelerators, with all possible core-collapse supernova that have occurred in the past gone since long, and their remnants already dissipated into the ISM.

For the remaining clusters with  $t < 40$  My, we account for the large uncertainties in the open clusters' age [5] by allowing a safety margin in the ages of the clusters selected, using only those clusters in which the time in-

Gould's Belt	Local Arm	Perseus Arm	
NGC 2264	Berkeley 14A	NGC 146	NGC 7380
IC 1396	NGC 2244	Berkeley 4	King 12
ASCC 18	Collinder 106	NGC 457	NGC 7788
ASCC 20	NGC 6871	NGC 663	ASCC 7
ASCC 21	Biurakan 1	IC1805	ASCC8
ASCC 122	IC 4996	NGC 957	ASCC9
ASCC 126	Cyg OB2	IC 1448	ASCC17
	ASCC 111	NGC 1893	ASCC120
	ASCC 117	NGC 6823	ASCC130
	ASCC 125	Roslund 2	

Table 1: Final open cluster sample

terval  $t_{cluster} \pm 1\sigma_{cluster}$  allows for *at least* one star with  $M > 9M_{\odot}$  leaving off the main sequence. For the young and massive clusters, this would imply that a relatively high number of massive stars are in their last stages of evolution.

The stellar lifetimes are available from the stellar evolutionary codes developed by different groups. We observe no difference in our final selection by using different stellar grids (Padova grid vs. Geneva grid), due to the large uncertainties in the cluster ages.

Assuming that all the stars in the cluster were created in the same burst episode, and that stellar mass loss is negligible in young clusters, we obtain the stellar mass distribution of each cluster normalizing a the IMF [14] to the total stellar mass of the cluster. The IMF we use is the one from [15, 16], a Salpeter slope with correction from unresolved components and a fundamental mass upper limit .

#### 2.1.1 Final open cluster sample

Our final sample comprises 36 open clusters with masses between  $\sim 400M_{\odot}$  and  $3 \times 10^4M_{\odot}$ , and ages lower than 40 My . Fig. 1 shows the distribution in the Galactic Plane ( $-5^{\circ} < b < 5^{\circ}$ ) of the open clusters that passed our selection criteria together with their spatial extent. The appearance in the Galactic Plane is a combination of both the natural clustering of open clusters in cluster complexes and projection effects. According to their heliocentric distance, the cluster complexes we find are: in the Gould's belt (part of our Local arm up to  $\sim 800$  pc), in the Local arm, and in the Perseus arm.

The most nearby massive open clusters in the Gould's belt are: IC 1396, NGC 2264, ASCC 18, ASCC 20, ASCC 21, where the last three are part of the Orion complex at very low galactic latitudes (not shown in the Galactic Plane distribution of fig. 1).

#### 2.2 Cluster molecular environment

Our selection of northern sky open clusters in the "accelerator-dominated" stage span a range in Galactic longitude between  $l=59^{\circ}$  and  $l=210^{\circ}$ . We perform our distance determination from observed velocities in order to select molecular clouds in the vicinity of our target open clusters. Fig.2 shows the example case in the direction of NGC 6821 and Roslund 2, two open clusters that passed our selection criteria and that are both located in the Vul OB1 association at  $l=60^{\circ}$ ,  $b=0^{\circ}$ , with a distance of  $\sim 2$  kpc. The continuous line is data from the LAB survey [9], and the dotted line is our model. The observed velocities are a combination between different galactocentric distances

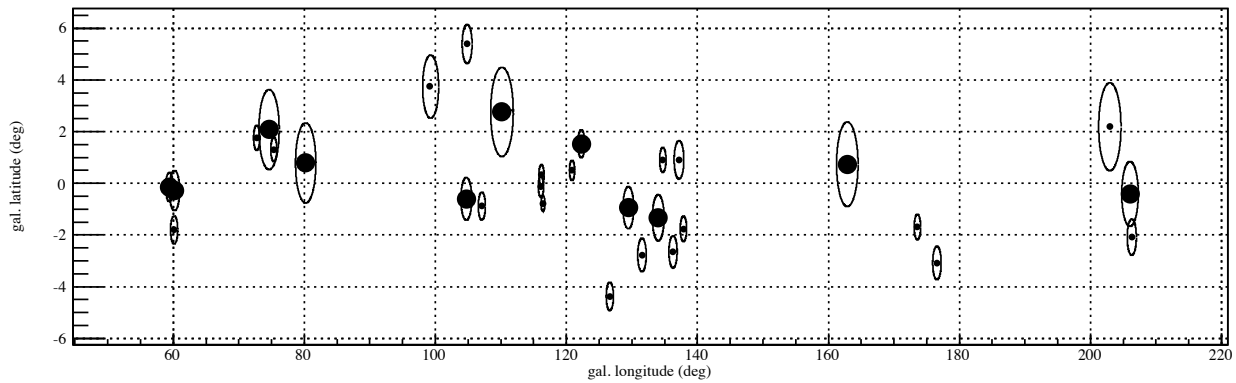


**Figure 1:** Final open cluster sample. The circles represent the clusters area

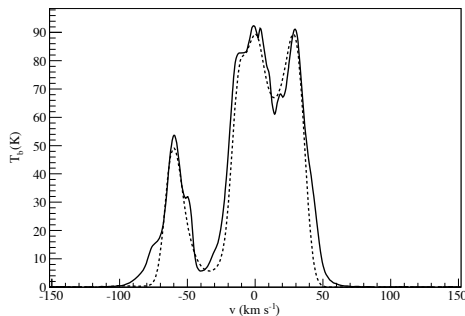


**Figure 2:** HI velocity profile along  $l=60^\circ$ ,  $b=0^\circ$  from the LAB survey (solid data) and from our model of the Milky Way (dotted line). This is the direction of our line of sight towards the Vul OB1 association, which harbors the massive open clusters NGC 6821 and Roslund 2.

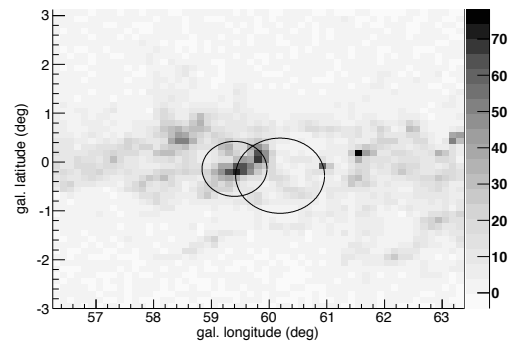


**Figure 3:** CO integrated emission (in units of K km/s) in the environment of the massive open clusters NGC 6821 and Roslund 2 ( $22\text{km/s} < v < 32\text{ km/s}$ ). The circles represent the spatial extent of the open clusters

resulting in a spectrum of projected velocities, streaming motions induced by the spiral density wave, and random cloud to cloud motions, which we model introducing a velocity dispersion of 5 km/s. Our model represents reasonably well the data and places our line of sight along the Local arm up to  $\sim 3$  kpc from the Sun. According to this model, NGC 6821 and Roslund 2 are located in the Local arm, together with molecular gas moving with  $V_{los} = 28$  km/s. Fig. 3 shows the CO integrated intensity over the velocity interval  $22\text{km/s} < v < 32\text{ km/s}$ , which corresponds to 1500 pc - 2500 pc in kinematic distance.

Another interesting region worth studying is the Cygnus region. Here, the observed CO distribution is found to be within the Local Arm, at distances  $< 2$  kpc from the Sun [17]. Part of the CO emission in this area belongs to the Gould's Belt and the rest to the famous Cygnus complex, rich in TeV gamma-ray sources [18, 20, 19]. Fig.4 shows that all CO emission is encompassed between -20 and +20 km/s. We want to focus only on the molecular gas nearby the accelerators; Perseus' gas is all at velocities around -42 km/s and does not pose a problem, and Gould's Belt clouds are at velocities higher than 7 km/s. Therefore, we select CO material in the velocity range  $-20 < v < 7\text{km/s}$ , as shown in Fig. 5.

The kinematical distance method is similarly applied to molecular gas around the remaining open clusters from our

sample. For each cluster, we select molecular material with velocities corresponding to a distance of  $\sim 500$  pc around the cluster.

### 3 Search method and IceCube sensitivities

Our two hypothesis are designed in order to search for neutrinos either from the interior of massive open clusters, or from molecular clouds in the proximity of the open clusters. If any of our two scenarios is correct, the location of the brightest spots in the IceCube maps should be correlated either with the cluster areas, or with our selected distribution of molecular gas. In order to search for such correlation, the analysis of IceCube data will make use of the Multi-Point Source (MPS) method, developed in [21] for the search of neutrino emission beyond the single and spherically symmetric source approach. By measuring the 2-point correlation function of events, using only those events inside the target area as primaries in the correlation, the method can account for the type of correlation information we are looking for (i.e., neutrino events emitted at any point inside the clusters area) and efficiently exploit it for the discovery of extraterrestrial neutrino signal.

In the case of the open cluster search, the target area is precisely the cluster area, represented in Fig. 1 with circles. MPS will also profit from the agglomeration of

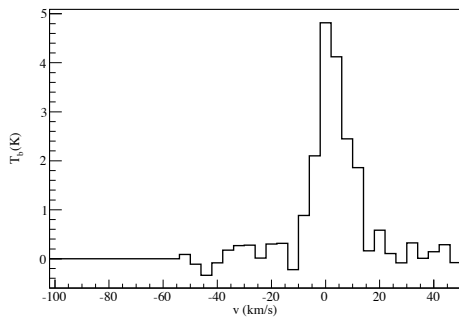


**Figure 4:** CO velocity profile along  $l=80^\circ$ ,  $b=0^\circ$ .

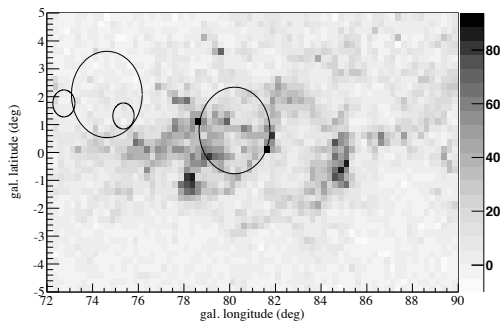


**Figure 5:** CO integrated emission ( $v < 7$  km/s) in the Cygnus region (in units of K km/s). The circles represent the spatial extent of the open clusters.

open clusters into open cluster complexes, making this method more advantageous than a stacking search.

For our second approach, a region around the open clusters of half the scale-height of the disk ( $\sim 144$ pc) is considered. At the typical distances of the clusters from our sample, this corresponds to an average angular scale of  $4^\circ$ . Within this area we apply a weighted MPS analysis in the velocity range considered, where higher weights are given to those regions with higher column densities. IceCube's angular resolution limits the minimum spatial structure we can distinguish to  $\sim 1^\circ$ , and selecting larger regions will cause source confusion. Then, the value of 144pc will define the maximum length at which we study the interactions of escaping cosmic rays.

### 3.1 Sensitivities

We report the sensitivities of three years of data collected by the IceCube detector in its 79, 59, and 40-strings configurations, for the analysis of the massive open clusters. The analysis of the molecular clouds in the cluster's neighborhood is on-going, and results will be presented in a future work.

The MPS analysis is applied to both background-only sky maps generated from the data (randomizing in right ascension), and to simulated sky maps where a source field is generated on top of the uniform background distribution. In the scenario considered here, one point source is simulated for each cluster. The finite angular resolution of the detector is taken into account in the simulation of the neutrino signal by applying a Gaussian smoothening.

The results are reported for the open clusters in our selection and according to their location in the Milky Way

Sensitivities ( $10^{-12} \text{ TeV}^{-1} \text{ cm}^{-2} \text{ s}^{-1}$ )

Gould's Belt	Local Arm	Perseus Arm
1.1	0.55	0.27

**Table 2:** Sensitivities per source for a  $E^{-2}$  spectrum.

spiral pattern. Table 2 shows the sensitivities per source, defined as the maximum flux that produces in 90% of the cases a higher value of the test statistics than the average background case. The sensitivity to neutrino sources in the northern hemisphere is at the level of  $(1 - 5) \times 10^{-12} \text{ TeV}^{-1} \text{ cm}^{-2} \text{ s}^{-1}$  with the same event sample [22]. The results of table 2 indicate that IceCube can lower this threshold taking into account the spatial distribution of potential accelerators in the solar neighborhood. The proximity of the targets selected here is also advantageous to achieve the minimum detectable flux from sources with a modest neutrino luminosity.

### References

- [1] Meynet, G. 2008, EAS Publication Series, 32, 187
- [2] de la Fuente Marcos, R., & de la Fuente Marcos, C. 2008, ApJ, 672, 342
- [3] de Wit, W. J., Testi, L., Palla, F., & Zinnecker, H. 2005, A&A, 437, 247
- [4] Higdon, J. C., & Lingenfelter, R. E. 2005, ApJ, 628, 738
- [5] Kharchenko, N. V., Piskunov, A. E., Röser, S., Schilbach, E., & Scholz, R.-D. 2005, A&A, 438, 1163
- [6] Kharchenko, N. V., Piskunov, A. E., Röser, S., Schilbach, E., & Scholz, R.-D. 2005, A&A, 440, 403
- [7] Piskunov, A. E., Schilbach, E., Kharchenko, N. V., Röser, S., & Scholz, R.-D. 2008, A&A, 447, 165
- [8] Dame, T. M., Hartmann, D., & Thaddeus, P. 2001, ApJ, 547, 792
- [9] Kalberla, P. M. W., Burton, W. B., Hartmann, D., et al. 2005, A&A, 440, 775
- [10] Binney, J., & Merrifield, M. 1998, Galactic astronomy, Princeton University Press, 1998
- [11] Efremov, Y. N. 2011, Astronomy Reports, 55, 108
- [12] Lin, C. C., Yuan, C., & Shu, F. H. 1969, ApJ, 155, 721
- [13] Foster, T., & MacWilliams, J. 2006, ApJ, 644, 214
- [14] Salpeter, E. E. 1955, ApJ, 121, 161
- [15] Weidner, C., Kroupa, P., & Bonell, I. A. D. 2010, MNRAS, 401, 275
- [16] Kroupa, P. 2002, Science, 295, 82
- [17] Schneider, N., Bontemps, S., Simon, R., et al. 2006, A&A, 458, 855
- [18] Bartoli, B., Bernardini, P., Bi, X. J., et al. 2012, ApJ, 745, L22
- [19] Abdo, A. A., Allen, B., Berley, D., et al. 2007, ApJ, 658, L33
- [20] Aliu, E. 2011, AAS/High Energy Astrophysics Division, 12, #34.13
- [21] Sestayo, Y., Resconi, E., 2013, Astroparticle Physics, 44, 15
- [22] IceCube Coll., paper 0550 these proceedings

## Searches for flaring and periodic neutrino emission with three years of IceCube data

THE ICECUBE COLLABORATION<sup>1</sup>

<sup>1</sup>See special section in these proceedings

Juan.Aguilar@icecube.wisc.edu

**Abstract:** Neutrinos provide a unique opportunity to study cosmic-ray acceleration processes, and their arrival times may provide additional insight about their sources. We present the results of searches for time-dependent neutrino emissions using three years of data (between April 2008 and May 2011) collected by the IceCube detector. The neutrino arrival time is used to enhance the discovery potential for sources with non-steady emission compared to that achieved by time-integrated searches for the same sources. Three different analyses are presented. An untriggered scan over one year of IceCube data has been performed using a maximum likelihood method that seeks to identify the point in the sky with the most significantly clustered events both in space and time. In the second search, a selection of flaring gamma-ray sources observed by the Fermi experiment and TeV telescopes were considered as promising sources. The gamma-ray lightcurves for each source were used to search for a coincident neutrino flux, under the assumption that neutrinos and gammas are produced at the same time in pp or p-gamma interactions. Finally, we searched for periodic neutrino emission coming from a selected catalog of binary systems and microquasars with known periodicities established from X-ray, gamma-ray and radio spectrum observations. The results of all the searches are compatible with fluctuations of the background.

### Corresponding authors:

J. A. Aguilar<sup>1</sup>,  
A. Christov<sup>1</sup>, T. Montaruli<sup>1</sup>, M. Rameez<sup>1</sup>

<sup>1</sup> University of Geneva, Geneva, Switzerland

**Keywords:** neutrino telescope, astrophysical neutrino sources, time dependent searches

## 1 Introduction

IceCube is a cubic-kilometer neutrino detector installed in the ice at the South Pole [1] between depths of 1450 m and 2450 m. The detector construction started in 2005 and finished in 2010. Neutrino event reconstruction relies on the optical detection of Cherenkov radiation emitted by secondary particles produced in neutrino interactions in the surrounding ice or the nearby bedrock. The completed detector has 86 vertical strings of optical modules.

In this paper we present three searches for flaring astrophysical neutrino sources with the IceCube neutrino telescope data, enhancing the sensitivity by using timing information. In contrast to time integrated searches [2], the analyses presented here aim for further reducing the background of atmospheric neutrinos and muons by adopting the idea of correlations in the neutrino arrival times.

One of the searches presented here is untriggered as the considered time correlations are among the neutrinos themselves. This untriggered “All Sky Time Scan” looks for any possible neutrino flare in the entire sky and no information from independent observations is used. Similar triggered analysis, the “Search for Periodic Neutrino Emission From Binary Systems”, assumes the period is fixed by photometric observations and the search is performed in the phase domain of the binary system. The two approaches are conceptually akin, one scanning in time and the second (equivalently) in phase; one considering the whole sky while the second only the direction of the selected binary systems.

The remaining triggered searches make use of the in-

formation obtained from gamma-ray observations. In this case we followed two approaches triggered by multi-wavelength measurements. They differ by what kind of multi-wavelength information is available. Namely “Time Dependent Searches for Flares with Extensive Coverage” uses the Fermi-LAT lightcurves which provide continuous monitoring. In contrast, the “Time Dependent Searches for Flares with Sporadic Coverage” are driven by flares reported by TeV range experiments where the data is available only for short time windows.

For searches which do not benefit from the addition of several data samples we use the 79 string configuration only. This is the case of the “All Sky Time Scan” and the “Time Dependent Searches for Flares with Sporadic Coverage”. For the other searches we combine the data taken between April 2008 and May 2011, spanning across the 79-String, 59-String and 40-String configurations of IceCube.

## 2 Data Selection

The event selection for data from the 40, 59 and 79 string configurations is described in detail in [4] and [5].

- IceCube took data in the partially completed IceCube 40-string configuration from April 2008 until May 2009. The final sample of events obtained contained a total of 36,000 events: 14,121 from the northern sky (dominated by atmospheric muon neutrino events) and 22,779 from the southern sky where very tight



selection cuts have been applied to deal with the huge atmospheric muon rate.

- From May 2009 until May 2010 59 strings were operational. The final data sample for the 59-string configuration has a total number of 107,569 events, among which almost 2/3 come from the southern sky. The rest are neutrino candidates in the northern sky.
- From May 2010 until May 2011 IceCube took data with 79 strings. The final sample contains 109,866 events where 50,857 are coming from the northern sky and 59,009 are located in the southern sky.

The detector performance was evaluated within the scope of the time integrated searches, a brief description of it and the related references are included in [2].

### 3 Method

This analysis uses an unbinned maximum likelihood ratio test [3]. The significance of an excess of neutrinos above the background for a given direction can be calculated using this method. Both the reconstructed direction of the event and the reconstructed visible muon energy are used in order to discriminate between signal and background [4]. This method has been demonstrated to provide superior sensitivity over simple directional clustering based methods, as the signal events have a harder energy spectrum compared to the atmospheric neutrino and muon backgrounds. The method is identical to the time integrated searches up to the point where the arrival time of the events is used to discriminate against background. To make use of the timing information in the likelihood a time “Probability Density Function” (PDF) is introduced. Depending on the search this PDF can have different forms, Gaussian, box or following the shape of an lightcurve.

#### 3.1 All Sky Time Scan

For each direction in the sky, the likelihood function is maximized with respect to the number of signal events  $n_s$ , the power law index  $\gamma$  and in addition specifically for this search the mean  $t_0$  and the width  $\sigma_w$  of a Gaussian function in time. The Gaussian function is a possible parametrization of a sudden increase in the emission of a source. This term is designed to identify events which are signal-like (i.e. clustered in the time). The ratio of the likelihoods between the best fit hypothesis and the null hypothesis ( $n_s = 0$ ) forms the test statistic. The maximum likelihood is evaluated for each direction in the sky on a grid of  $0.1^\circ \times 0.1^\circ$ , much finer than the angular resolution of the detector. To evaluate the background test statistic distribution, the analysis is performed repeatedly on scrambled data sets, wherein the arrival time of the events is randomized but all other event properties are fixed (i.e. the null hypothesis). The post-trial p-value is the fraction of scrambled data sets containing at least one grid point with a likelihood ratio higher than the one observed in the data. During a fixed period of time, larger number of narrower flares are possible than wider flares. This introduces an effective trial factor that makes this search method more sensitive to narrower flares than wider ones. To avoid being biased towards narrow flares, we introduce a marginalization term  $\sqrt{2\pi}\hat{\sigma}_w/T$  to penalize very narrow flares. The test statistic is defined as:

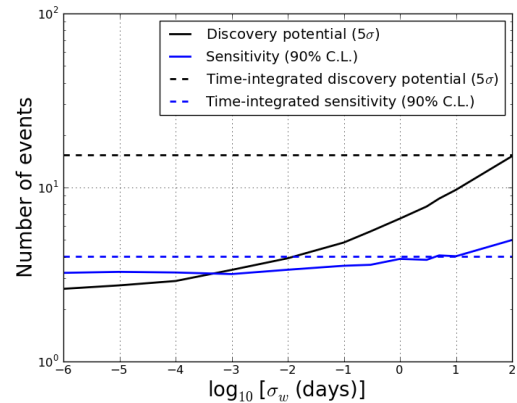


**Figure 1:** Discovery potential (for  $5\sigma$  discovery) and sensitivity (90% confidence level) for the “All Sky Time Scan” in terms of the number of signal events needed as a function of the width  $\sigma_w$  of the Gaussian flare. For comparison the time integrated results are shown.

$$\log \lambda = \log \left( \left( \frac{\sqrt{2\pi}\hat{\sigma}_w}{T} \right) \frac{\mathcal{L}(\hat{\gamma}, \hat{n}_s, \hat{t}_0, \hat{\sigma}_w)}{\mathcal{L}(n_s = 0)} \right)$$

where the parameters with hats denote the fitted values,  $T$  is the total livetime of the detector.

The expected performance of this search is illustrated in Fig. 1 which shows that on scales below one day this approach is more powerful than the time integrated search. For this search the most significant deviation from background is at  $343.45^\circ$  r.a. and  $-31.65^\circ$  dec. The best-fit parameters for this deviation are  $\hat{\sigma}_w = 1.8$  days and  $\hat{t}_0$  corresponding to the 27<sup>th</sup> of September 2010. The pre-trial p-value for this point is  $1.07 \times 10^{-5}$ . The post-trial p-value was determined to be 66% and therefore it is compatible with background fluctuations.

#### 3.2 Search for Periodic Neutrino Emission from Binary Systems

For certain binary systems such as microquasars, the time period is known from X-Ray, Gamma Ray and Radio spectrum observations. Microquasars are binary systems in which one of the bodies is either a compact black hole or a neutron star. Neutrinos could be produced in these systems in relativistic jets [8]. These jets are narrow and precess with the same time period as the binary system. The neutrino flux at earth from these sources depends upon the orientation of these jets with respect to the atmosphere of the massive star and our line of sight, and is hence expected to be high only during a narrow window during the orbit. We can use the knowledge of the period to enhance the discovery potential. The phase is calculated for each IceCube event from the period start  $T_0$  as defined by Fermi LAT [9] and the known period of the system.

This search also uses the marginalization. We then search for events clustered together in this phase space, rather than time. The width and the phase are fitted. The list of sources and their periods can be found in Table 1.

Figure 2 indicates the discovery potential and sensitivity of this search in terms of number of signal events. The search is very powerful for flares of width of  $1/100^{\text{th}}$  of

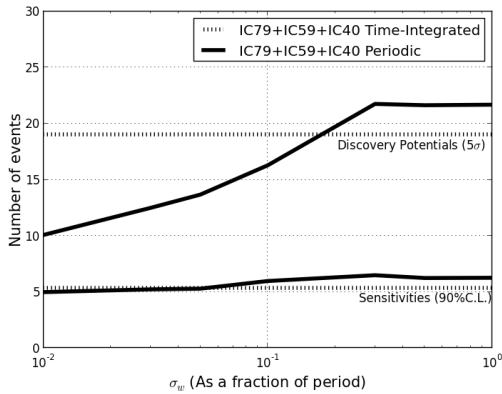


**Figure 2:** Discovery potential and sensitivity versus the duration of the flare divided by the period for the search for periodic neutrino emission from binary systems in terms of the number of signal events for the source GRO J0422+32

a period while for much wider flares, the time integrated search is preferable due to the penalty introduced by additional degrees of freedom in the fit.

Source	Period(days)	p-value
Cygnus X-1	$5.599829 \pm 0.000016$	0.45
Cygnus X-3	$0.199679 \text{ d} \pm 0.000003$	0.22
GRO J0422+32	$0.212140 \pm 0.000003$	-
GRS 1915+105	$30.8 \pm 0.2$	0.49
LSI + 61 303	$26.496 \pm 0.0028$	-
SS 433	$13.08227 \pm 0.00008$	-
XTE J1118+480	$0.1699339 \pm 0.0000002$	-
HESS J0632+057	$320 \pm 5$	-

**Table 1:** Candidate sources for the Periodic Neutrino emission search. The p-values are pre trial, “-” means under-fluctuation.

In the search for periodic neutrino emission, the most significant observation was from the source Cygnus X-3. This Gaussian fitted flare was observed at a phase of 0.79 with a width of  $\sigma_w = 0.042$  in terms of the fraction of the period, close to the peak of the gamma-ray flare as reported by Fermi around 0.8 [9]. The post-trial p-value of the Cygnus X-3 was found to be 80.5%, well compatible with the background hypothesis.

### 3.3 Time Dependent Searches for Flares with Extensive Coverage

This search targets a set of astronomical objects (FSRQs, blazars, etc.) which were observed in flaring state during the period of interest by the Fermi-LAT [6]. The tested hypothesis is that the neutrino emission follows the intensity of the photon emission. The Fermi-LAT provides continuous monitoring which allows for direct use of the lightcurves. We use the lightcurves to select flaring states following the selection criterium that the flux is above  $10^{-6}$  photons  $\text{cm}^{-2}\text{s}^{-1}$  for energies above 100 MeV. Then the lightcurves are used as input for building a time PDF.

In order to use the Fermi-LAT lightcurve as time PDF we apply a denoising procedure, the so called Bayesian Blocks method, implemented as described in [7]. The method takes

a parameter  $F_B$  which affects how sensitive the method is to fluctuations in the lightcurve. Small values cause the resulting PDF to follow almost every point in the lightcurve while for big values the method will ignore important structures in the lightcurve. To determine the optimal value for the parameter  $F_B$  a series of tests were done, using real Fermi-LAT exposure data to simulate realistic background noise and injecting Gaussian shaped flares. The width, the height and the multiplicity of the flares was varied and for these different configurations the performance was evaluated in terms of the rate of finding a fake flare and the rate of finding the injected flare. The criterium for “finding a flare” was the denoised lightcurve to exceed three times the standard deviation of the background noise. In Fig. 3 an example of the performance of the Bayesian Blocks method is shown as function of the parameter  $F_B$ . After evaluating the performance for various flare scenarios the value of the parameter  $F_B$  was fixed at 5.0 for this analysis. At this value the fake flare rate drops significantly while the success rate for the injected flares stays high. Example of the resulting denoised lightcurve together with the original data is shown in Fig. 4.

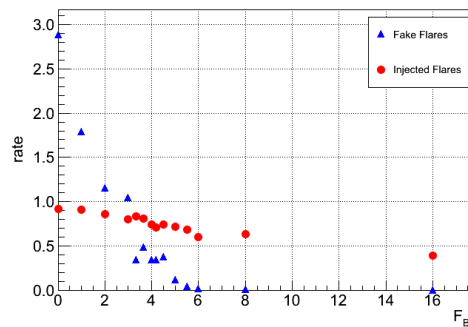


**Figure 3:** Example of the performance Bayesian Blocks method as function of the parameter  $F_B$ . In this example one Gaussian shaped flare was injected with width of two days and height of  $10^{-6}$  photons  $\text{cm}^{-2}\text{s}^{-1}$ . On the vertical axis is the rate of finding a flare, i.e. the number of flares found divided by the number of lightcurves simulated. The blue triangles indicate the rate at which fake flares are found. In red circles we show the rate for finding the injected flare. The value of  $F_B$  chosen to be used for the analysis is 5.0

For each candidate source the likelihood function is maximized with respect to the number of signal events  $n_s$ , the power law index  $\gamma$ , the time lag and time PDF threshold. The time lag parameter allows for a time offset between the flare time and the event arrival time up to  $\pm 0.5$  days. The last fit parameter, the time PDF threshold, makes it possible to modify the tested hypothesis, stating that only above this threshold the neutrino flux follows the photons. As the threshold is varied, the time PDF is redefined, setting it equal to zero below the threshold and normalizing to one what is left above the threshold. Time scrambled data sets are used to obtain the post-trial p-value. This search uses up to three years of IceCube data depending on the activity of the flaring sources.

There were 26 sources selected as flaring during the 79 string measurement period, 6 flaring in both the 59 and the 79 string measurement period and 2 with flares occurring throughout all three, 40, 59 and 79 string measurement pe-

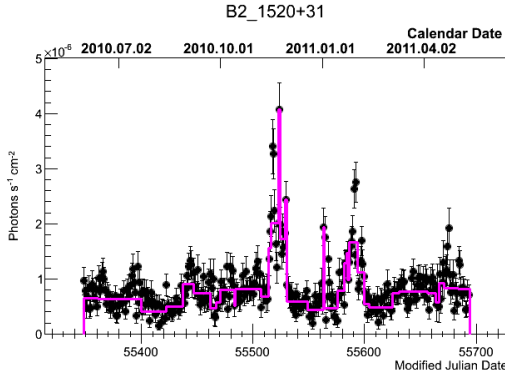


**Figure 4:** Example of a denoised lightcurve (solid line) together with the original data (black data points) for the blazar B2 1520+31.

riods. The source with the most significant deviation from background was the Seyfert 2 galaxy NGC 1275 at  $49.95^\circ$  r.a. and  $41.51^\circ$  dec. Fig. 5 shows the time PDF threshold resulting from the likelihood function maximization together with the time PDF and the IceCube event weights considering only the spatial and energy contribution to the likelihood, as function of time.

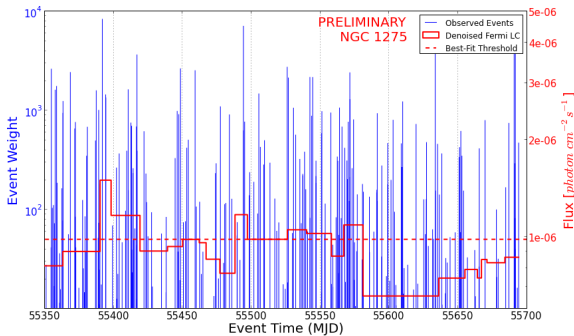


**Figure 5:** In red solid line and using the red scale on the right is drawn the time PDF for NGC 1275 obtained from Fermi-LAT data. Again using the red scale on the right, the red dashed horizontal line indicates the threshold resulting from the likelihood function maximization. The blue vertical lines are drawn at the times of measured IceCube events and the height indicates the event weights on the blue left scale. Events in the periods when the PDF is above the threshold are contributing to the significance.

The pre-trial p-value for this source was 0.058 which was translated using the scrambled datasets into post-trial p-value of 95% and therefore well compatible with background fluctuations.

### 3.4 Time Dependent Searches for Flares with Sporadic Coverage

There is yet another interesting set of sources, which show no distinct activity structure in the Fermi-LAT lightcurves but were reported to The Astronomer’s Telegram to be flaring by higher energy experiments like H.E.S.S., MAGIC or VERITAS. For these sources the Fermi-LAT lightcurve did not pass the criterium of flux is above  $10^{-6}$  photons  $\text{cm}^{-2}\text{s}^{-1}$  and therefore the time PDF is just a

box function in time with duration defined as the reported flare time plus one day margin before and after. The selected sources and the corresponding limits for the time PDF are listed in Table 2. Here only the number of signal events  $n_s$  and the index of the power law  $\gamma$  are free parameters in the maximization of the likelihood function. This search is carried out with data from the 79 string configuration since the flares reported previously were already analyzed with the corresponding data samples.

Source	ATel num.	Period in MJD
IES 0806+524	3192	55615-55617
HESS J0632+057	3153, 3161	55598-55602
IES 1215+303	3100	55562-55564

**Table 2:** Source candidates selected for the “Time Dependent Searches for Flares with Sporadic Coverage”.

Only one out of the three sources, namely IES 0806+524 at  $122.46^\circ$  r.a. and  $52.32^\circ$  dec, does not under-fluctuate. The pre-trial p-value for this source is 0.24 which using repeated analyses on time scrambled data translates into post-trial p value of 0.73 .

## 4 Conclusions

We presented the results of different time-dependent searches of neutrinos in IceCube. The test hypothesis differs from the time-integrated searches where a steady neutrino emission is assumed. The triggered searches use gamma-ray and optical information to drive the search of neutrinos in a multi-messenger fashion. The “All-Sky Time Scan” on the other hand, is the most general time-dependent search where the only assumption taken is that a neutrino flare can be well described by a Gaussian-profile in time. None of the searches presented in this contribution had shown a significant deviation from a background only hypothesis. The IceCube telescope is now taking data with its final configuration and high stability in the data is expected. Some of the searches described here will be applied in almost real-time, releasing on-line information on neutrino fluxes observed during ares, or, in the lack of a discovery, providing limits useful to constrain models together with photon observations.

## References

- [1] R. Abbasi et al., Nucl. Inst. Meth. A, 2010, 618 : 139.
- [2] IceCube Collaboration: latest results on point and extended neutrino source searches, these proceedings.
- [3] J. Braun et al., Astropart. Phys., 2010, 33 : 175.
- [4] R. Abbasi et al., ApJ., 2011, 732 : 18.
- [5] M.G. Aartsen et al., Search for time-independent neutrino emission from astrophysical sources with 3 years of IceCube. In preparation (2013).
- [6] <http://www-glast.stanford.edu/>
- [7] J. D. Scargle, J. P. Norris, B. Jackson, J. Chiang, arXiv:1207.5578
- [8] M. Reynoso et al, Mon.Not.Roy.Astron.Soc. 387 (2008) 1745-1754
- [9] A. Abdo et al., SCIENCE 326 1512F (2009)

## Optical and X-ray follow-up programs of IceCube

THE ICECUBE COLLABORATION<sup>1</sup>,

<sup>1</sup>See special section in these proceedings

voge@physik.uni-bonn.de

**Abstract:** IceCube is currently the world's most sensitive instrument for high-energy neutrinos in the TeV and PeV range. The detection of high-energy astrophysical neutrinos will provide invaluable information about their sources, e.g. SNe and GRBs, especially when combined with other observations. We perform analyses running in realtime that enable us to trigger electromagnetic (or other) follow-up observations. A neutrino trigger can result in observations of a source that would have been missed otherwise and that could help to identify and study the source of a multi-messenger signal. Furthermore, the coincident observation of a neutrino event and a signal from a different detection channel can increase the statistical significance. The status of these online IceCube analyses, in collaboration with the ROTSE network of optical telescopes, the optical PTF survey at Palomar Observatory and the Swift satellite in X-rays, is presented. A first limit has been derived on the fraction of SNe hosting a jet, and a first SN has been found in optical follow-up data which is discussed in the paper.

**Corresponding authors:** Markus Voge<sup>1</sup>, Andreas Homeier<sup>1</sup>,

<sup>1</sup> *Physikalisches Institut, University of Bonn, Nußallee 12, 53115 Bonn, Germany*

**Keywords:** supernova, GRB, neutrino, IceCube, multi-messenger, target of opportunity.

### 1 Introduction

IceCube is a cubic-kilometer neutrino detector installed in the ice at the geographic South Pole [1] between depths of 1450 m and 2450 m. Detector construction started in 2005 and finished in December 2010. Neutrino reconstruction relies on the optical detection of Cherenkov radiation emitted by secondary particles produced in neutrino interactions in the surrounding ice or the nearby bedrock.

Complementary to offline neutrino analyses—performed after a certain amount of data has been taken—an analysis running online, in realtime, has several advantages. With a short latency neutrino analysis, multi-wavelength follow-up observations can be triggered by neutrino events. These follow-up data have the potential to reveal the electromagnetic counterpart of a transient neutrino source, that might otherwise be missed and thus be unavailable for further observations. The coincident detection of neutrino and electromagnetic emission can be statistically more significant and provide more information about the physics of the source than just the neutrino detection alone. Another advantage of an online analysis is the prompt availability of the reconstructed neutrino dataset and thus the possibility of fast response analyses. This work has thus also enabled fast gamma-ray burst (GRB) searches like the one following GRB 130427A, published in a GCN Circular recently [2].

The online search for transient neutrino sources is mostly motivated by models of neutrinos from GRBs [3] and from choked jet supernovae (SNe) [4] that are SNe hosting a mildly relativistic jet. However, the choked jet is less energetic and thus cannot penetrate the stellar envelope, making it invisible in gamma-rays. In contrast, the produced high-energy neutrinos can escape and trigger a discovery of a SN in the follow-up channels. Both sources are expected to emit a short burst of neutrinos within seconds of the explosion time, setting the natural timescale of the neutrino

search. A GRB can be found by detection of the GRB afterglow, in optical or in X-ray data. A very fast response within minutes to hours is required for this. A choked jet SN is found by detecting a shock breakout or a SN light curve in the follow-up images, slowly rising and then decaying within weeks after the neutrino burst.

### 2 The optical and X-ray follow-up system

In late 2008, an online neutrino event selection has been set up at IceCube. The analysis is running in realtime within the limited computing resources at the South Pole, capable of reconstructing and filtering the neutrinos and sending alerts to follow-up instruments with a latency of only a few minutes [5, 6]. The overwhelming background of cosmic-ray induced muons from the atmosphere above the detector ( $\approx 10^6$  muon events vs. one neutrino event) is reduced by limiting the sample to the northern hemisphere, using the Earth as a muon shield, selecting only tracks that are reconstructed as up-going in the detector. Additional cuts on track quality are done to veto mis-reconstructed muons and select well reconstructed muon events induced by neutrinos from the northern hemisphere. In order to reject the remaining background of atmospheric neutrinos and to identify an extra-terrestrial neutrino signal, a multiplet of at least two neutrinos within 100 seconds and angular separation of  $3.5^\circ$  is required to trigger an alert. In addition, since mid-September 2011, a likelihood function is used, representing a single parameter for selection of the most significant alerts:<sup>1</sup>

1. Note that this likelihood function is strictly speaking only defined for doublets, which does not pose a problem since the expected background triplet rate is so low ( $\approx 0.06$  per year) that each observation of a triplet is significant by itself and is passed directly to all the follow-up instruments.



Instrument name	ROTSE	PTF	Swift
Follow-up since	Dec 2008	Aug 2010	Feb 2011
Alerts per year	$\approx 25$	$\approx 10$	$\approx 7$
FoV in ( $^\circ$ ) <sup>2</sup>	3.42	7.26	0.79

**Table 1:** Overview of the follow-up instruments participating in this work.

$$\lambda = -2 \ln \mathcal{L} = \frac{\Delta\Psi^2}{\sigma_q^2} + 2 \ln(2\pi\sigma_q^2) - 2 \ln \left( 1 - e^{-\frac{\theta_A^2}{2\sigma_w^2}} \right) + 2 \ln \left( \frac{\Delta T}{100 \text{ s}} \right) \quad (1)$$

where the time between the neutrinos in the multiplet is denoted as  $\Delta T$ , their angular separation as  $\Delta\Psi$ ,  $\sigma_q^2 = \sigma_1^2 + \sigma_2^2$  and  $\sigma_w^2 = (1/\sigma_1^2 + 1/\sigma_2^2)^{-1}$  with  $\sigma_1$  and  $\sigma_2$  being the uncertainties on the directional reconstruction of the two neutrino events, typically  $\sim 1^\circ$ , depending on neutrino energy.  $\theta_A$  corresponds to the (circularized) angular radius of the field of view (FoV) of the follow-up telescope (set to  $0.5^\circ$  for Swift and  $0.9^\circ$  for ROTSE and PTF).  $\lambda$  is smaller for more signal-like alerts that have small separation  $\Delta\Psi$ , small time difference  $\Delta T$  and a high chance to lie in the FoV of the telescope. Thus,  $\lambda$  is a powerful parameter to separate signal and background alerts. For each follow-up program, a specific cut on  $\lambda$  is applied in order to send the most significant alerts to the follow-up instruments.

The optical (OFU) and X-ray (XFU) follow-up programs currently encompass three follow-up instruments: the Robotic Optical Transient Search Experiment (ROTSE) [7], the Palomar Transient Factory (PTF) [8, 9] and the Swift satellite [10]. See Table 1 for the follow-up start times, rate of alerts sent by IceCube, and FoV of the instruments. In addition, there is a gamma-ray follow-up program targeting flaring AGNs, sending alerts to the gamma-ray telescopes MAGIC and VERITAS (see [11]).

**ROTSE** is a network of four optical telescopes with 0.45 m aperture and  $1.85^\circ \times 1.85^\circ$  FoV, located in Australia, Texas, Namibia and Turkey. Since late 2012, only the two northern hemisphere telescopes continue operation. ROTSE is a completely automatic and autonomous follow-up system.

**PTF** is located at the Palomar Observatory in California, USA. It uses a 1.2 m telescope with camera field dimensions of  $3.5^\circ \times 2.3^\circ$ . PTF achieves limiting AB magnitudes of up to 21 and pursues a number of science goals, most notably the discovery and observation of SNe.

**Swift** is a satellite operated by NASA and boarding various instruments: a 170 – 600 nm ultraviolet/optical telescope (UVOT), a 0.3 – 10 keV X-ray telescope (XRT) and a 15 – 150 keV hard X-ray Burst Alert Telescope (BAT). IceCube’s X-ray follow-up program triggers Swift’s XRT that can provide valuable information by observing a GRB afterglow in X-rays. The XRT has a FoV of only  $0.4^\circ$  in diameter, hence Swift performs seven pointings for each IceCube follow-up, resulting in an effective FoV of about  $1^\circ$  in diameter.

The follow-up images taken between 18 Dec 2008 and 31 Dec 2009 with the ROTSE telescope system were carefully analyzed and no detectable SN or similar transient source

in coincidence with a neutrino alert could be found [5], while one would expect to find 0.074 SNe coincident by chance with one of the neutrino alerts. This result can be compared to the predicted neutrino flux from the choked jet SN model in [4] and constraints on the abundance and properties of these sources can be set within this model. The most important parameters of the model are the bulk Lorentz factor  $\Gamma$  of the jet, and the jet kinetic energy  $E_{\text{jet}}$ . As a function of these two parameters, an upper limit on the rate of SNe hosting a jet with these properties has been derived. E.g. for a typical value of  $E_{\text{jet}} = 3 \times 10^{51}$  erg, it can be excluded at 90% confidence level that more than  $\approx 10^{-5}$  CCSNe per  $\text{Mpc}^3$  and year ( $\approx 6\%$  of all predicted CCSNe) host a soft relativistic jet with a Lorentz factor of 10 or more [5].

Soft astrophysical neutrino spectra, as expected from SNe, are very similar to the spectrum of atmospheric neutrinos. Thus, one has to depend on neutrino multiplets to select source neutrinos and suppress atmospheric neutrinos. Looking for hard spectra sources like GRBs, it is additionally possible to select single well-reconstructed high-energy neutrinos. A second stream containing these events is currently being studied and expected to be implemented this year.

### 3 Results of the IceCube neutrino multiplet search

Table 2 shows the number of found neutrino multiplets so far, together with the expected number of background alerts for comparison. Doublets are here defined as those being sent at least to ROTSE, i.e. having passed the ROTSE cut on the likelihood  $\lambda$ . Background multiplets arise from random accumulation of isotropic atmospheric muon neutrinos. The expected number of alerts is obtained by randomizing or *scrambling* the experimental data, which is achieved by randomly shuffling the times of the neutrino events and calculating equatorial coordinates (right ascension, declination) with the new times. That way, all detector effects like the reconstructed direction in local detector coordinates as well as the time distribution of the events, and seasonal variations, are entirely preserved. At the same time, all potential correlations of the events in time and space, and thus a potential signal, are destroyed.

The total number of observed doublets from all seasons is 94, against an expectation of 85.59, which corresponds to an over-fluctuation with p-value of 19.5% or  $1.3\sigma$ . No triplet has been found yet.

### 4 Detection of a II<sub>n</sub> supernova in PTF optical follow-up

On 30 Mar 2012 (MJD 56016), the most significant alert since initiation of the follow-up program was recorded and sent to ROTSE, PTF and Swift simultaneously. In the PTF images, a supernova, named PTF12csy, was discovered only  $0.14^\circ$  away from the average neutrino direction at right ascension  $104.636^\circ$  and declination  $+17.262^\circ$  (see Figure 1) at an AB magnitude of  $\approx 18.6$  (Mould R-band). Spectra were subsequently taken with Gemini North on 17 Apr 2012 (MJD 56034) and with Keck I on 9 Feb 2013 (MJD 56332) that allowed for redshift extraction and the identification of the supernova as a type II<sub>n</sub> (narrow emission lines). It was determined to be at a redshift of 0.067, corresponding

IceCube Season	Observed doublets	Expected doublets	Observed triplets	Expected triplets
IC40	15	8.55	0	0.003
IC59a	19	15.66	0	0.004
IC59b	10	10.32	0	0.004
IC79	22	32.20	0	0.008
IC86-1	28	18.86	0	0.037
Sum	94	85.59	0	0.056

**Table 2:** Neutrino multiplets found in IceCube’s OFU and XFU program and expected number of multiplets from background only. The season labels in the first column include the number of installed strings. The calendar periods are IC40: Dec 2008 – May 2009, IC59a: May 2009 – Dec 2009, IC59b: Dec 2009 – May 2010, IC79: May 2010 – May 2011, IC86-1: Sep 2011 – May 2012. Note that the periods of operation of the OFU system do not always correspond to IceCube operation. Also note that due to loosening the cuts, more triplets are expected for IC86 compared to previous configurations.

to a luminosity distance of about 300 Mpc. The limiting magnitude of ROTSE ( $\approx 16 - 17$  mag) was insufficient for a detection of the SN in ROTSE follow-up observations. Swift performed observations, but did not detect a source with XRT, though the source was seen with UVOT, close to the detection threshold.

The spectrum and photometry showed that the SN was several months old at the time of discovery, which was confirmed using archival Pan-STARRS [12] data. Pan-STARRS1 is a 1.8 m telescope located on Maui in the Hawaiian islands, equipped with a  $3.3^\circ$  FOV. In the course of its  $3\pi$  steradian survey it observes each part of the sky typically 8-10 times per year [13]. Earliest detection of PTF12csy in the Pan-STARRS1 data dates back to 13 Oct 2011 (MJD 55847), 169 days prior to the neutrino alert. We can therefore conclude that the explosion time of the SN was earlier than that.

The SN was already a few months old at the time of the neutrino alert. Therefore, the neutrinos are not consistent with the hypothesis of an up to 100 seconds long burst of high-energy neutrinos from a choked jet, shortly after the core-collapse. Also the large distance of 300 Mpc makes the detection of a neutrino doublet from the SN unlikely.

#### 4.1 The neutrino doublet

The two neutrino events causing the alert happened on 30 Mar 2012 at 01:06:58 UTC and 1.79 seconds later, with a directional separation of  $1.32^\circ$ . The (neutrino-induced) muons passing through IceCube have reconstructed energies of  $\approx 1$  and  $\approx 3$  TeV, which are lower limits on the neutrino energy. The value of the likelihood classifier  $\lambda$  for the doublet amounts to  $-18.1$ . See Figure 2 for a distribution of  $\lambda$  of alerts generated by background events, mostly isotropic atmospheric neutrinos.

The probability of an alert as signal-like or more signal-like than this to happen by chance from an isotropic background sample is calculated via integration of the  $\lambda$  distribution and is  $\approx 13.9\%$  over the 242.4 days of OFU livetime in IC86-1. Considering that the OFU system was already

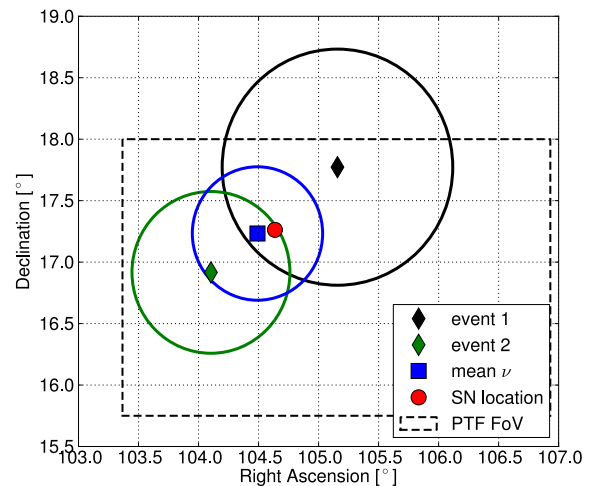


**Figure 1:** Map of the sky with the two neutrino event directions, the average neutrino direction and the location of SN PTF12csy. Estimated reconstruction errors are indicated with circles, the PTF FoV is shown as dashed box.

in operation for  $\approx 1000$  days at the time of the alert (and the OFU livetime in IC86-1 was 242.4 days), one can scale the number of expected alerts with  $\lambda \leq -18.1$  up and calculate a prob. of  $\approx 46\%$  over 1000 days, which is an over-estimation, since the detector in its first stages (esp. 40 and 59 strings) could not deliver such high quality alerts at the same frequency as the completed detector.

#### 4.2 Significance of the SN detection

The number of core-collapse supernova detections of any type, at any time after explosion, and within a distance of 300 Mpc or less, randomly coincident with one neutrino alert, is:

$$\bar{N}_{\text{det}} = \Omega_{\text{search}} \cdot \int_0^{300\text{Mpc}} \frac{dN_{\text{SN}}}{dt dV} \cdot T(m_{\text{lim}}, \hat{M}, r) \cdot r^2 dr \quad (2)$$

where  $\Omega_{\text{search}}$  is the solid angle in which a SN is searched for (set to the solid angle of the doublet error, which is  $\approx 0.93$  ( $^\circ$ ) $^2$ ),  $\frac{dN_{\text{SN}}}{dt dV}$  is the volumetric CCSN rate ( $7.8 \times 10^{-5} \text{ yr}^{-1} \text{ Mpc}^{-3}$  is used, see [14]), and  $T(m_{\text{lim}}, \hat{M}, r)$  is the average time window in which a SN is detectable, i.e. brighter than the limiting magnitude. The average detection time window depends on the distance to the source  $r$ , the peak absolute magnitude  $\hat{M}$  of the SNe (assumed to be a normal distribution with mean  $-17.5$  mag and width  $\sigma = 1$  mag), the limiting magnitude  $m_{\text{lim}}$  of the telescope ( $19.5 \pm 1$  mag is assumed for PTF), and the shape of the light curve (taken from the II n SN on P. Nugent’s template webpage [15]).

The resulting expectation value for random SN detections is  $\bar{N}_{\text{det}} \approx 0.016$ , which results in a Poissonian probability of  $\approx 1.6\%$  to detect a CCSN like PTF12csy. Combining this probability with the probability of 13.9% for the neutrino alert, Fisher’s method delivers a combined p-value of 1.6%, corresponding to a significance of  $2.4\sigma$ . Combining it with the up-scaled probability of 46% during 1000 days of livetime, one gets 4.3% or  $2\sigma$  significance.

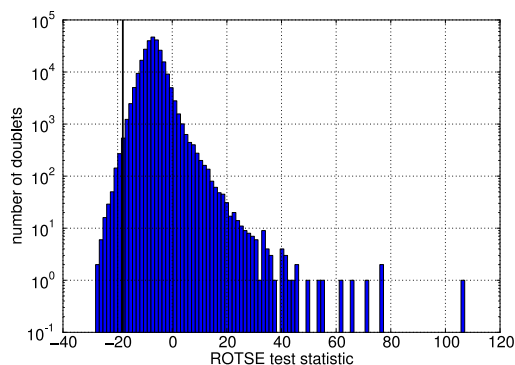


**Figure 2:** Distribution of likelihood classifier  $\lambda$  (see Eq. 1) for random coincidence doublets generated by scrambling the  $\approx 8$  months of experimental data (mostly atmospheric neutrinos) 6000 times, as explained in Section 3. The found value of  $\lambda$  for the reported alert from 30 Mar 2012 is indicated as vertical line. Signal-like doublets tend to smaller values.

### 4.3 Discussion and next steps

Type II<sub>n</sub> supernovae, such as PTF12csy, are a promising class of high-energy transients (see [16]). The supernova ejecta are crashing into the massive circumstellar shells, producing a forward and reverse shock. Cosmic rays could be accelerated and multi-TeV neutrinos produced, potentially detectable with IceCube. The collisionless shocks generating the neutrinos are expected to generate X-rays as well at late times (see e.g. [17, 18, 19]), but no X-rays were detected for PTF12csy, likely because of the long distance to the SN.

The expected duration of neutrino emission from II<sub>n</sub> SNe is 1 – 10 months [16], hence it seems unlikely that two neutrinos arrive within less than 2 s of each other, so late after the SN explosion. To test the possibility of a long-term emission, a search for neutrinos from PTF12csy within a search window of several months is being prepared, even though the large distance to the source makes a large neutrino flux unlikely. Assuming a typical total kinetic energy of  $\approx 10^{51}$  erg, that optimistically is entirely emitted in TeV neutrinos, one can expect to receive  $\approx 1$  event on an area of 1 m<sup>2</sup>, about the effective area of IceCube at 1 TeV. The possibility of neutrino emission from Type II<sub>n</sub> SNe is further being tested by a dedicated (offline) stacking analysis, where a catalog of nearby SNe is cross-correlated with the neutrino signal from IceCube.

## 5 Conclusions

The IceCube OFU and XFU program has been running stably since December 2008 and is taking high-quality data from both IceCube and the follow-up instruments. Multiple neutrino events within 100 seconds and 3.5° are reconstructed within minutes and alerts are sent to follow-up telescopes. So far, no significant deviation from the hypothesis of pure background was observed. First limits on the choked jet SN model [4] could be set (see [5]).

An interesting coincidence of the most significant neutrino alert to date with the direction of a type II<sub>n</sub> supernova has been found, however it is statistically not significant and both the distance to the source and the long time be-

tween explosion and neutrino alert speak against a correlation. But type II<sub>n</sub> SNe are indeed promising neutrino source candidates and it is planned to do a complementary offline analysis to search for neutrinos from this and other type II<sub>n</sub> SNe over a longer period of several months.

**Acknowledgment:** IceCube gratefully acknowledges collaboration with PTF, Swift, ROTSE, and Pan-STARRS on automated follow-up and data sharing.

## References

- [1] A. Achterberg et al., *Astropart. Phys.* 26 (2006) 155.
- [2] E. Blaufuss, GCN Circular 14520 (2013) 13/05/01, <http://gcn.gsfc.nasa.gov/gcn3/14520.gcn3>.
- [3] P. Meszaros and M.J. Rees, *Mon. Not. Roy. Astron. Soc.* 257 (1992) 29-31.
- [4] S. Ando and J.F. Beacom, *Phys. Rev. Lett.* 95 (2005) 061103.
- [5] R. Abbasi et al., *Astron. Astrophys.* 539 (2012) A60.
- [6] M. Kowalski and A. Mohr, *Astroparticle Physics* 27 (2007) 533-538.
- [7] C.W. Akerlof et al., *Pub. o. t. Astron. Soc. o. t. Pacific* 115 (2003) 132-140.
- [8] N.M. Law et al., *Pub. o. t. Astron. Soc. o. t. Pacific* 121 (2009) 1395-1408.
- [9] A. Rau et al., *Pub. o. t. Astron. Soc. o. t. Pacific* 121 (2009) 1334-1351.
- [10] N. Gehrels et al., *The Astrophysical Journal* 611 (2004) 1005.
- [11] IceCube Coll., paper 0537 these proceedings
- [12] N. Kaiser, *Proc. SPIE* 5489, *Ground-based Telescopes* (2004) 11-22, doi:10.1117/12.552472.
- [13] C. Inserra, S.J. Smartt, A. Jerkstrand et al. (2013), arXiv:1304.3320
- [14] S. Horiuchi et al., *The Astrophysical Journal* 769 (2013) 113.
- [15] P. Nugent, Peter Nugent's Spectral Templates, [http://supernova.lbl.gov/~nugent/nugent\\_templates.html](http://supernova.lbl.gov/~nugent/nugent_templates.html).
- [16] K. Murase et al., *Phys. Rev. D* 84 (2011) 043003.
- [17] B. Katz et al., *Proc. of the Int. Astron. Union* 7 (2011) 274-281.
- [18] G. Svirski et al., *The Astrophysical Journal* 759 (2012) 108.
- [19] E.O. Ofek et al., *The Astrophysical Journal* 763 (2013) 42.

## Stacked searches for high-energy neutrinos from blazars with IceCube

THE ICECUBE COLLABORATION<sup>1</sup>,

<sup>1</sup>See special section in these proceedings

*schattok@uni-mainz.de*

**Abstract:** Blazars, Active Galactic Nuclei whose relativistic jets are aligned with our line of sight, are promising candidates for sources of high-energy cosmic rays. As a result, they are also theorized to emit high-energy neutrinos from photo meson production or pp-interactions, in addition to emitting gamma rays that have already been detected. To search for this high-energy neutrino emission, three classes of blazars were selected from gamma ray measurements by the Fermi Large Area Telescope that have high potential to be neutrino sources: flat spectrum radio quasars, low synchrotron-peaked BL Lac objects, and hard spectrum BL Lac objects. The analysis presented here is based on three years of data collected by the IceCube detector when it was partially instrumented with 40, 59 and 79 strings, and tests these catalogues of sources for high-energy neutrino emission with an unbinned likelihood stacking method.

**Corresponding authors:**

Kai Schatto<sup>1</sup>

<sup>1</sup> *Institute of Physics, Johannes Gutenberg-Universität Mainz, Germany*

**Keywords:** IceCube, neutrino, blazar, AGN, stacking

### 1 Introduction

IceCube is a cubic-kilometer neutrino detector installed in the ice at the geographic South Pole [1] between depths of 1450 m and 2450 m. Detector construction started in 2005 and finished in 2010. The neutrino reconstruction relies on the optical detection of Cherenkov radiation emitted by secondary particles produced in neutrino interactions in the surrounding ice or the nearby bedrock.

The detection of neutrino point sources would not only shed light on the origin of high-energy cosmic rays, but can also reveal intrinsic physical processes in detected astrophysical objects. In the case of blazars, the lower energy hump in the electromagnetic spectral energy distribution (SED), as shown in figure 1, is believed to be created by synchrotron radiation of ultra-relativistic electrons, while the high-energy feature is still under discussion.

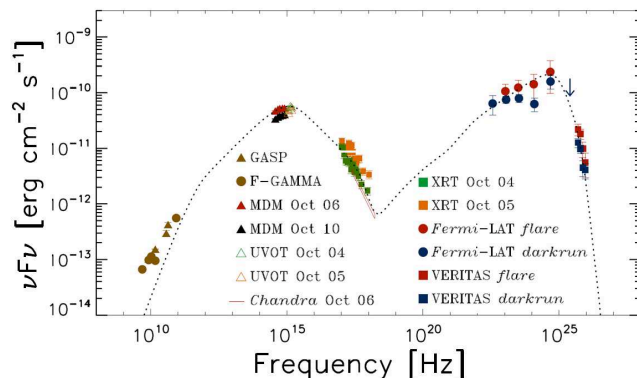


**Figure 1:** Broadband spectral energy distribution of 3C 66A during the Oct. 2008 multiwavelength campaign from [2]. As an example, the EBL-absorbed EC+SSC model [2] for  $z = 0.3$  is plotted as the dashed line for reference.

Current models for the observed  $\gamma$  flux assume that either hadrons, leptons or a mixture of both are accelerated (see [3] for a blazar emission model overview). The detection of a neutrino flux from blazars would directly point to hadronic processes like photo meson production or pp-interactions with subsequent  $\pi^\pm$  decays into neutrinos:

$$p\gamma \longrightarrow \Delta^+ \longrightarrow n\pi^+ \quad (1)$$

$$pp \longrightarrow \pi^\pm + N \quad (2)$$

$$\pi^- \longrightarrow \mu^- \bar{\nu}_\mu \longrightarrow e^- \bar{\nu}_e \nu_\mu \bar{\nu}_\mu. \quad (3)$$

Blazars are classified by emission features in the SED. Flat spectrum radio quasars (FSRQs) show broad emission lines in the optical spectrum while these lines are lacking for BL Lac objects. Further specification includes the peak frequency of the low energy hump in the SED, dividing blazars into low- ( $\nu_{peak} < 10^{14}$  Hz), intermediate- ( $10^{14}$  Hz  $< \nu_{peak} < 10^{15}$  Hz) and high- ( $\nu_{peak} > 10^{15}$  Hz) synchrotron peaked objects referred to as LSP, ISP and HSP [4]. In this work, three blazar catalogs (FSRQs, LSP BL Lac objects, and BL Lac objects with hard gamma spectra) are used to search for a possible high-energy neutrino flux. While all FSRQ objects and per definition also the objects in our second catalogue are LSP, our third catalogue is composed by mainly HSP with a few ISP and LSP objects.

Stacking multiple sources in neutrino astronomy can enhance the discovery potential and further constrain astrophysical models for uniform populations of sources. The stacking method is described in detail in [5], where an explanation is provided on how signal and background can be integrated over a set of sources using the same weight for all sources or a model dependent weighting scheme for specific tests. As shown in [5], the fractional flux needed for discovery for stacked sources compared to single sources at  $5\sigma$  confidence level (C.L.) is close to the inverse of the number of stacked sources.



## 2 Analysis method and data samples

A recent search for astrophysical neutrinos originating from galactic and extragalactic sources using a likelihood (LH) method [5, 6] is reported in [7]. This method uses energy and directional information to distinguish the relatively soft backgrounds of atmospheric muons and neutrinos from the harder astrophysical neutrinos. Such astrophysical neutrinos, still to be associated to specific sources[8], could originate from shocks (in jets) via Fermi acceleration. The background is estimated by uniformly scrambling real events in their arrival times (or right ascensions) in the LH method. In this way, the p-value (the fraction of observations from background with a test statistic value of at least the observed value) can be derived solely from data and does not depend on the accuracy of the simulation [5].

While [7] is focused on the LH search for steady emissions from point sources across the whole sky and from selected sources of interest, the work reported in [9] is focused on extending the likelihood method by utilizing the time dependence of emission (GRBs and AGN flares). The work presented here extends the LH method to the stacking of sources belonging to one of three blazar classes. The sensitivity and upper limits at a 90% C.L. are calculated according to the classical (frequentist) construction of upper limits by Neyman [10]. The median discovery potential is the flux required for 50% of trials with simulated signal to yield a p-value less than  $2.87 \cdot 10^{-7}$  (i.e.  $5\sigma$  significance if expressed as the one-sided tail of a Gaussian distribution).

We combine the data samples collected for 375.5 days in the 40-string configuration of IceCube during the period from April 5, 2008 to May 20, 2009 [5], with 348.1 days in the 59-string configuration collected from May 20, 2009 to May 30, 2010 [11] and for 316 days in the 79-string (IC79) configuration collected from May 31, 2010 to May 13, 2011 [12]. The IC79 data was later reprocessed to introduce an improved angular reconstruction described in section 2.1. Different data samples can be combined in the LH approach as every single track carries its individual angular uncertainty estimation. The total data sample consists of 48904 (46499) events for 79 strings in the upgoing (downgoing) hemisphere, 43,339 (64,230) events with 59 strings and 14,121 (22,779) for 40 strings. Hence the total number of events on which this search is performed in the whole sky is 239,932.

It is to be noted that the search for astrophysical sources in IceCube extends to the entire sky but the sensitivity is different in the upgoing (Northern sky) and in the downgoing (Southern sky) regions. As explained in more detail in [5], the upgoing region is dominated by atmospheric neutrinos since muons are filtered by the Earth. Astrophysical neutrinos are characterized by an energy spectrum that is harder than that of atmospheric muons and neutrinos. By requiring an energy threshold of  $\mathcal{O}(1 \text{ PeV})$ , also the downgoing region can be searched for a clustering of astrophysical events amongst a relatively low atmospheric background.

In this report, we present preliminary sensitivities for the blazar stacking. Only after addition of the data of the first year from the completed IceCube detector [7] (May 2011 - May 2012), the searches will be unblinded and p-values and corresponding fluxes will be provided.

### 2.1 Improved angular reconstruction

The angular reconstruction of neutrino induced muons in IceCube is based on the distribution of detected Cherenkov photons in space and time. Photon propagation is influenced by scattering and absorption, which causes the photons to arrive later at a photomultiplier (PMT) compared to the straight geometrical path along the Cherenkov cone. The probability density function (pdf) for the time delay (time residual  $t_{res}$ ) of the first photon for a given muon track is crucial for maximizing the track hypothesis likelihood

$$L = \prod n \cdot \text{pdf}(\vec{\theta}, t_{res}) \cdot \left(1 - \text{cdf}(\vec{\theta}, t_{res})\right)^{n-1}. \quad (4)$$

Here  $\vec{\theta} = (x_0, y_0, z_0, \theta, \phi)$  describes the track parameters of an infinite track,  $n$  the number of photons detected in a particular PMT and  $\text{cdf} = \int_0^{t_{res}} dt' \text{pdf}(\vec{\theta}, t')$  is the cumulated probability density function.

The pdf used in IceCube up to the IC79 configuration is based on a parametrization assuming homogeneous ice. However, the deep antarctic ice consists of a layered structure of scattering centers leading to a range of scattering and absorption lengths. To include these layer effects into the reconstruction, muons were simulated in the IceCube simulation framework using a precise ice model [13] and their light emission was propagated photon by photon on graphical processing units (GPU's) and recorded with respect to muon declination, PMT-track distance, depth, PMT-track orientation and time residual. Afterwards, the resulting fine-binned 5 dimensional table with in total two billion entries was fitted by a multidimensional spline surface as shown in figure 2, providing a smooth, continuous representation where pdf and cdf are connected analytically by the gradient.

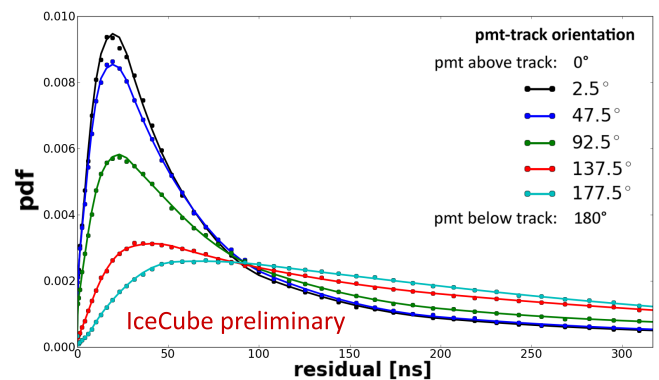


**Figure 2:** PDF of time residual distributions for a muon with a zenith angle of  $55^\circ$  passing a PMT located at 2310 m depth at a distance of 45 m. Circles represent the simulated data while the lines display the fitted spline surfaces. PMT-track configurations for 5 angles in a cylindrical coordinate system around the muon track are shown. An angle of  $0^\circ$  identifies a PMT exactly above the track and  $180^\circ$  a PMT below the muon track. As the PMTs in IceCube head to the earth's center, a PMT above the track can collect direct, unscattered light with small time residuals while the light has to be scattered around the PMT if it is located below the track. Other parameters influencing these distributions are distance, zenith angle and depth.

Using this layered ice pdf representation results in a significantly improved angular resolution, which leads to a better discovery potential for the IC79 data as shown in figure 3. This reconstruction method is also used for later IceCube data [7]. The layered ice IC79 data will be used in the stacking analysis shown in this work.

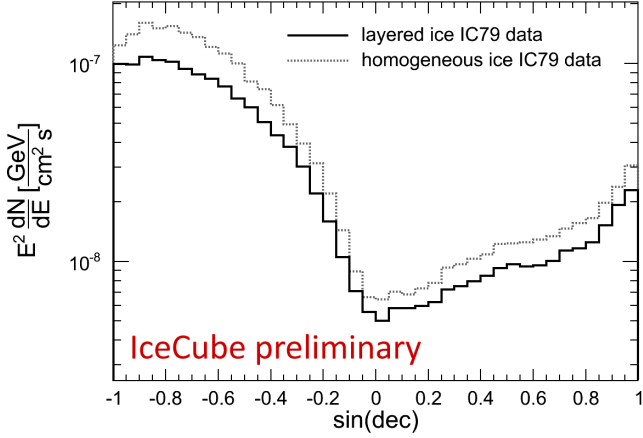


**Figure 3:**  $5\sigma$ -discovery potential relative to an injected  $E^{-2}$  spectrum as function of declination for the IC79 configuration of IceCube. The data sample based on the improved layered ice reconstruction provides an improvement of 20% to 35% in the northern sky and 15% to 25% in the southern hemisphere.

### 3 Blazar stacking

We perform a stacking search for three different blazar selections, composed from the 2 year Fermi LAT AGN catalogue [4]:

1. **Flat spectrum radio quasars (FSRQ):** Luminous FSRQs are thought to accelerate protons to ultra high energies, while their strong broad emission lines indicate the presence of the radiation field needed for photo meson production. These conditions could lead to a detectable neutrino flux. See [14].
2. **LSP BL Lac objects:** The spectrum of high-energy neutrinos from BL Lac objects has been calculated in [15] by applying the Synchrotron Proton blazar Model [16]. It is stated that the high-energy contribution of pion photoproduction is higher for the brighter LSP BL Lac objects than for HSP BL Lac objects, where the high energetic hump is dominated by proton synchrotron radiation. Therefore neutrino production is assumed to be more efficient in LSP BL Lacs.
3. **BL Lac objects with hard gamma spectra:** These objects are less luminous, lacking background light radiation and thus do not provide ideal neutrino production conditions. However, the assumption of a connection between the spectral shape of  $\gamma$ -rays and neutrinos could allow IceCube, being most sensitive above 1 TeV, to detect few but high energetic neutrinos [17]. Additionally, the high variability of some TeV-blazars indicates a very small emission region, where the intrinsic synchrotron radiation could provide a target for pion production itself [18].

### 3.1 Source weights

In this work, we use a  $\gamma$ -ray driven approach for source selection and weighting. Under the assumption of hadronic processes, the blazar neutrino flux should be directly connected to the observed  $\gamma$ -emission. If the high-energy hump in the blazar SEDs is mainly caused by  $\pi^0$  decays, the neutrinos created in the accompanying charged pion decays will exhibit a similar spectral shape. As described in [5], one can associate a weight with every stacked source. This value is the medium expected number of neutrinos ( $N_V$ , see equation 5) for a certain neutrino flux. This incorporates the detector response at the source declination to the assumed flux depending on the effective area shown in figure 4 as well as a theoretical flux weight, which in this work is chosen to be the integrated Fermi LAT  $\gamma$  flux between 1 GeV and 100 GeV.

For each blazar catalogue we apply two weighting models by making different assumptions about the power law spectrum index  $\Gamma$  for each source:

- **variable  $\Gamma$  model:** Here we consider the shape of the neutrino spectrum of the sources to be unknown, but equal. One overall spectral index  $\Gamma$ , will be fitted in the likelihood optimization process and the source's weights will be based on the same spectral index at a time. Besides on source declination, the relative weights will therefore mainly depend on the measured integral  $\gamma$  flux.
- **fixed  $\Gamma$  model:** As the experiment response heavily depends on energy, sources with hard spectra are more visible to IceCube. In this weighting method, we assume the same spectral shape for the  $\gamma$  and neutrino flux. In the likelihood optimization and source weight calculation the power law index  $\Gamma$  will be fixed to the individual value measured by Fermi Lat for every source. Besides the source declination, the relative weights will depend on the  $\gamma$  flux and now heavily on the  $\gamma$  power law index measured by Fermi LAT. As a result, sources with harder spectra will enter with a higher weight.

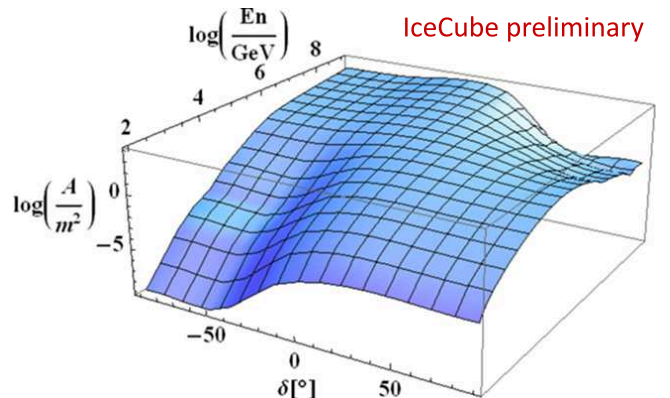


**Figure 4:** Effective area  $A$  of the IC79 configuration of IceCube as a function of declination  $\delta$  and neutrino energy  $En$ . The plot shows IceCube's higher sensitivity to lower energies in the northern (upgoing) sky compared to the southern hemisphere (downgoing), while the sensitivity worsens for very high energies due to  $\nu$  absorption in the earth [12].

### 3.2 Blazar selection

Starting with the two-year Fermi LAT AGN catalogue, we first require a minimum integrated  $\gamma$  flux between 1 and 100 GeV of  $1.5 \cdot 10^{-9}$  photons  $\cdot$  cm $^{-2}$  s $^{-1}$  to avoid faint sources with large uncertainties on the power law index. A source is then selected if either its  $\gamma$  flux or the expected number of neutrinos  $N_\nu$  exceeds a certain limit. We calculate  $N_\nu$  under the assumption that the neutrino flux has the same spectral shape as the  $\gamma$  flux measured by Fermi. Compared to the  $\gamma$ -flux selected sources, this adds sources with a slightly lower flux but a hard  $\gamma$ -spectrum:

$$dN_\nu = k \cdot \frac{d\Phi_\gamma}{dE} \cdot A_{\text{eff}}(\delta, E) \cdot T \cdot dE. \quad (5)$$

Here  $k$  is a proportionality constant,  $\Phi_\gamma$  is the  $\gamma$  flux,  $A_{\text{eff}}$  is the effective area shown in figure 4 for IC79,  $\delta$  is the declination,  $E$  is the energy and  $T$  is the livetime. As  $N_\nu$  is only used as a relative weight in the source selection, we can set arbitrary values for  $k = 1$  and  $T = 1$ y. The differential  $\gamma$  flux can then be written as:

$$\frac{d\Phi_\gamma}{dE} = F_\gamma(1 \text{ GeV}-100 \text{ GeV}) \cdot \frac{E^{-\Gamma}}{\int_{1 \text{ GeV}}^{100 \text{ GeV}} E^{-\Gamma} dE}. \quad (6)$$

$F_\gamma$  is the integral gamma flux by Fermi and  $\Gamma$  represents the power law spectral index. Hard spectrum BL Lac objects additionally require an index  $\Gamma < 2.3$  while FSRQs should have a minimal luminosity between 100 MeV and 100 GeV of  $> 1 \cdot 10^{46}$  erg s $^{-1}$ . Table 1 lists the criteria selecting 33 FSRQs, 27 LSP BL Lacs objects and 37 hard spectrum BL Lac objects.

type	$N_\nu$	$\gamma$ flux	$\Gamma$
FSRQ	$> 1$	$> 8 \cdot 10^{-9}$	-
LSP BL Lac	$> 1$	$> 3 \cdot 10^{-9}$	-
hard spectr. BL Lac	$> 50$	$> 5 \cdot 10^{-9}$	$< 2.3$

**Table 1:** Selection criteria for the three blazar catalogues depending on the number of expected neutrinos  $N_\nu$ , the Fermi LAT integrated  $\gamma$  flux in the unit of [photons cm $^{-2}$ s $^{-1}$ ] between 1 GeV and 100 GeV and the power law index  $\Gamma$ .

### 3.3 Performance

The derived sensitivities and discovery potentials apply to the overall flux sum from all sources of a given catalog.

For the variable  $\Gamma$  weighting, we inject an  $E^{-2}$  power law spectrum for every source to calculate the performance shown in table 2. Fit parameters are the spectral index  $\Gamma$  and the summed number of signal events  $n_s$ .

Type	Sensitivity	Discovery Pot.
FSRQ	$3.6 \cdot 10^{-9} \times E2$	$1.3 \cdot 10^{-8} \times E2$
LSP BL Lac	$5.9 \cdot 10^{-9} \times E2$	$2.1 \cdot 10^{-8} \times E2$
hard spectr. BL Lac	$4.3 \cdot 10^{-9} \times E2$	$2.0 \cdot 10^{-8} \times E2$

**Table 2:** Median discovery potential (p-value  $< 2.87 \cdot 10^{-7}$ ) and sensitivity (90% CL) for the three stackings using the variable  $\Gamma$  weighting.  $E2$  represents the unit of  $E^2 dN/dE$  [GeV cm $^{-2}$  s $^{-1}$ ] valid from 1.5 TeV to 4 PeV.

For the fixed  $\Gamma$  weighting, we inject a neutrino flux with the individual  $\gamma$  flux power law index of each source. The sensitivities in table 3 are then given relative to the weighted

Type	Sensitivity	Discovery Pot.
FSRQ	$3.0 \cdot 10^{-8} \times F$	$1.2 \cdot 10^{-7} \times F$
LSP BL Lac	$9.5 \cdot 10^{-9} \times F$	$3.6 \cdot 10^{-8} \times F$
hard spectr. BL Lac	$2.1 \cdot 10^{-10} \times F$	$8.3 \cdot 10^{-10} \times F$

**Table 3:** Median discovery potential (p-value  $< 2.87 \cdot 10^{-7}$ ) and sensitivity (90% CL) for the three stackings using the fixed  $\Gamma$  weighting.  $F$  represents the scaling factor to the predicted flux profile in units of [GeV $^{-1}$ cm $^{-2}$ s $^{-1}$ ].

sum of individual spectra, referred to as  $F$ . The fit parameter is the total number of signal events  $n_s$ .

With two weighting schemes for each of the three blazar catalogues, the upcoming unblinding will then provide 6 p-values for the null hypotheses and the discovery probability.

### 3.4 Summary

An improved likelihood prescription for a track fit in ice with depth dependent scattering and absorption was developed. Depending on declination, the median discovery potential could be improved by 15-35%. Three blazar catalogues, selected on basis of theoretical arguments to potentially yield large neutrino fluxes, were prepared and will be compared to the data. The discovery potential ranges between  $(1.3 - 2.1) \times 10^{-8}$  GeV cm $^{-2}$ s $^{-1}$  if an  $E^{-2}$  spectrum is assumed for all sources. After adding data taken from May 2011- May 2012, the searches will be unblinded and corresponding fluxes and the detailed catalogue composition will be reported.

### References

- [1] A. Achterberg et al., *Astropart. Phys.* 26 (2006) 155.
- [2] A. A. Abdo et al. and V. A. Acciari et al. and multi-wavelength partners, arXiv:1011.1053, 2010.
- [3] M. Boettcher, *Astrophys. SpaceSci.* 309 (2007) 95.
- [4] M. Ackermann et al., *Astrophys. J.* 743 (2011) 171
- [5] R. Abbasi et al., *Astrophys. J.* 732 (2011) 18.
- [6] J. Braun, J. Dumm, F. de Palma, C. Finley, A. Karle, and T. Montaruli, *Astropart. Phys.* 29 (2008) 299.
- [7] IceCube Coll., paper 0550, these proceedings.
- [8] IceCube Coll., paper 0650, these proceedings.
- [9] IceCube Coll., paper 0649, these proceedings.
- [10] J. Neyman, *Philosophical Transactions of the Royal Society of London A*, 236, 333-380. (1937)
- [11] J. A. Aguilar, M. Baker, J. Dumm, T. Montaruli and N. Kurahashi, Contribution 909 to session OG2.3, Proceeding of the 32nd International Cosmic Ray Conference, Beijing, China, 11-18 August 2011
- [12] M.G. Aartsen et al. Search for time-independent neutrino emission from astrophysical sources with 3 years of IceCube. Paper in preparation (2013).
- [13] M. G. Aartsen et al. *Nucl. Instrum. Meth.* A711 (2013) 73.
- [14] A. Atayan and C. D. Dermer, *Phys.Rev.Lett.* 87 (2001) 221102.
- [15] A. Muecke, R. J. Protheroe, R. Engel, J. P. Rachen and, T. Stanev, *Astropart. Phys.* 18 (2003) 593.
- [16] A. Mücke and R.J. Protheroe, *Astropart. Phys* 15 (2001), 121.
- [17] M. Ribordy and A. Neronov, *Phys. Rev. D* 80 (2009) 083008.
- [18] C. D. Dermer (pers. communication, July 24, 2012).



## Search for Prompt Neutrino Emission from Gamma Ray Bursts with IceCube

THE ICECUBE COLLABORATION<sup>1</sup>,

<sup>1</sup>See special section in these proceedings

richman@umd.edu

**Abstract:** IceCube is the first neutrino telescope with TeV-PeV sensitivity sufficient to constrain the prompt neutrino flux from Gamma Ray Bursts (GRBs). Limits based on data from the 40- and 59-string partially completed detector configurations have been published previously. Much of the parameter space for the previous generation of neutrino fluence models was excluded, which has encouraged continued theoretical work on more precise GRB fireball particle physics calculations. With data from the first year of the completed 86-string detector, plus one year of the 79-string partial detector, our analysis is now more sensitive to prompt neutrino emission from GRBs by more than a factor of 2. We present results from analysis of the latest data set as well as combined results including data from the 40- and 59-string partial detector configurations.

**Corresponding authors:** Mike Richman<sup>1</sup>

<sup>1</sup> University of Maryland

**Keywords:** GRB, gamma ray burst, neutrinos

### 1 Introduction

Very energetic astrophysical events are required to accelerate cosmic rays to above  $10^{18}$  eV. Gamma Ray Bursts (GRBs) have been proposed as source candidates because of the enormous energy these events release in very little time in gamma rays:  $\sim 10^{51} - 10^{54} \text{ erg} \times \Omega/4\pi$ , where  $\Omega$  is the solid angle of a possible beamed emission [1]. If nucleons are present in the acceleration engine, and if they are accelerated with similar efficiency to electrons, then GRBs could account for the observed ultra high energy cosmic rays. It is very difficult to correlate cosmic rays directly to GRBs (or other sources). Because they are charged, and they therefore travel in curved paths through galactic and intergalactic magnetic fields, information about the source location and time is lost. However, if high energy protons are present in the acceleration engine, then interactions such as  $p + \gamma \rightarrow \Delta^+ \rightarrow n + \pi^+$  would take place. Cosmic rays could escape the acceleration region as neutrons or possibly protons, and high-energy muon and electron neutrinos would be produced by the decay of charged pions. An observation of neutrinos coincident with GRBs in time and direction would confirm the presence of high energy protons in the source, thereby lending support to the hypothesis that GRBs produce high energy cosmic rays.

IceCube has previously published limits [2] which constrain models that normalize the GRB neutrino fluence<sup>1</sup> with the assumption that the entire cosmic ray flux at the highest energies is due to neutrons accelerated in GRBs. IceCube has also published limits which constrain models [3] that derive a neutrino fluence prediction from the observed gamma ray fluence, but using some approximations which break down at next-to-leading order [4]. In this contribution, we update these limits using four years of IceCube data. For models based on the gamma ray fluence, we also update the model prediction, using numerical simulation of the GRB fireball particle physics to account for all relevant standard model processes.

### 2 IceCube

IceCube is a  $\text{km}^3$ -scale neutrino detector deployed deep in the South Polar ice cap. Construction of the detector was completed in December, 2010. IceCube detects Cherenkov light emitted by energetic charged particles produced in neutrino-nucleon interactions in the ice. The finished detector consists of 5160 optical modules (DOMs), with 60 optical modules placed on each of the 86 strings. Construction was performed during southern summers; each year during the construction process, a new set of strings was commissioned for data taking. The results presented here were obtained with three years of data with 40, 59, and 79 string partially completed detector configurations, as well as one year of data using the completed detector.

### 3 Event Reconstruction

IceCube's astrophysical neutrino sensitivity varies with neutrino flavor, energy, and declination due to event topology and relevant backgrounds. For this analysis we focus on the promising upgoing  $\nu_\mu$  channel, which allows us to use both time and space correlation with GRBs. Product muons can travel long distances through the ice, providing high detection efficiency and good angular resolution which both improve with increasing neutrino energy. The energy of a muon neutrino may also be estimated, although resolution worsens with neutrino energy because an increasing fraction of product muon energy is deposited outside of the instrumented volume. A high purity sample (consisting of muons which really are produced by neutrinos interacting in the ice) may be obtained for upgoing events because an upgoing muon can only be produced by an upgoing neutrino interacting in the ice after passing through the Earth. For this analysis, we set the horizon at declination  $-5^\circ$ ;

1. We define *fluence* as the number of events arriving from a source per detection area. Fluence is the time integral of *flux*.



between 0 and  $-5^\circ$ , the ice cap itself provides sufficient overburden to attenuate the cosmic ray muon background.

Muon events in IceCube are reconstructed by using a maximum likelihood method [5] to fit the spatial and temporal Cherenkov light detection pattern observed by the DOMs. IceCube is sensitive to muons with sufficiently high energy that the interaction frame is highly boosted with respect to the detector frame, so that the muon is nearly collinear with the neutrino. The angular resolution is  $1^\circ$  for neutrino energy of 3 TeV; for energies above 1 PeV, the resolution is  $0.5^\circ$ . Muon energy is reconstructed by measuring the charge collected by the DOMs as the muon traverses the detector. For an  $E^{-2}$  spectrum, the median energy error is a factor of 4, with 90% of events having true energies between 800 GeV and 1.4 PeV. Much better resolution is possible for analyses requiring the interaction vertex to be within the instrumented volume. All resolution estimates are based on simulation.

#### 4 Event Selection

In this analysis, the primary background consists of down-going cosmic ray muons, which trigger the detector at a rate of 2 kHz. A large fraction of these events are correctly reconstructed as downgoing, and they are easily excluded from this analysis. The primary remaining backgrounds are (1) muons passing near the boundary of the instrumented volume and emitting light upwards, and (2) independent muons traversing the detector at the same time. These backgrounds may be separated from true upgoing muon events based on fit quality, fit stability and event topology parameters. The remaining sample consists primarily of atmospheric neutrino events from the northern hemisphere. For this analysis, atmospheric neutrinos constitute an irreducible background which can only be separated from astrophysical neutrinos probabilistically based on reconstructed energy and correlation with a GRB.

The results presented here were obtained by combining different event selections optimized separately for multiple detector configurations as the detector was constructed. For the 40 string configuration, a simple set of cuts was used to select events which performed well on several quality criteria. For the 59, 79 and 86 string configurations, Boosted Decision Tree forests (BDTs) were trained using well-reconstructed simulated neutrino events as signal and off-time data (not within  $\pm 2$  hours of a GRB) as background. For well-reconstructed events, the  $E^{-2}$  efficiency is  $> 80\%$  with respect to trigger level, with a data rate of  $< 4$  mHz.

#### 5 GRB Selection

Between 2008-04-05 and 2012-05-15, 543 GRBs were observed at declination greater than  $-5^\circ$  and reported via the GRB Coordinates Network (GCN) [6] and the Fermi GBM catalogs [7, 8]. 492 bursts which occurred during stable IceCube data taking are included in this analysis. The search window is determined by the time of gamma emission and the location in the sky for each burst. When multiple satellites observed a given burst, the time window is defined by the most inclusive start and end times reported by any satellite. The angular window is determined by the direction and angular error reported by whichever satellite reports the smallest angular error. For modeling neutrino fluence predictions, the gamma ray fluence and

spectral parameters are taken preferentially from Fermi GBM [7], Konus Wind [9], Suzaku [10], Swift/BAT [11], and INTEGRAL [12] in this order. When a parameter is unreported, average parameters are used. The average parameters are calculated separately for short bursts (shorter than 2 s) and long bursts (longer than 2 s). Burst information is cataloged in an online database called GRB-web [13].

#### 6 Analysis

While alternative GRB neutrino models are possible, the analysis presented here is designed to be sensitive to neutrinos arriving from the direction of GRBs at the same time as the observed gamma rays. We use an unbinned likelihood analysis [14] in which the likelihood that a given event is a signal event is quantified based on separately normalized time, direction, and energy probability distribution functions (PDFs):  $S/B = (S/B)_{\text{time}} \times (S/B)_{\text{direction}} \times (S/B)_{\text{energy}}$ .

For a given burst, the signal time PDF is flat during gamma emission, with Gaussian tails with a width equal to the duration of the burst but no less than 2 s and no more than 30 s. The burst time window is truncated at  $4\sigma$ , and the background time PDF is flat throughout the time window.

The signal direction PDF is a two-dimensional circular Gaussian:  $S_{\text{direction}}(\mathbf{v}, \text{GRB}) = 1/(2\pi\sigma^2) \exp[-\Delta\Psi^2/(2\sigma^2)]$ , where  $\sigma^2 = \sigma_{\text{GRB}}^2 + \sigma_{\text{v}}^2$  and  $\Delta\Psi$  is the opening angle between the burst and the reconstructed neutrino direction. For most satellites [15, 11, 12, 16, 17] the GRB localization error ( $\sigma_{\text{GRB}}$ ) is much more tightly constrained than the per-event estimated neutrino reconstruction error ( $\sigma_{\text{v}}$ ). However, for Fermi GBM, there is a systematic error of  $2.6^\circ$  with 72% weight plus  $10.4^\circ$  with 28% weight [7]. To include GBM bursts in the analysis chain, we set  $\sigma_{\text{GRB}}^2 = \sigma_{\text{stat}}^2 + \sigma_{\text{sys}}^2$ , with the conservative setting that  $\sigma_{\text{sys}} = 10.4^\circ$ . The background direction PDF is constructed from off-time data, taking into account the direction-dependent acceptance of the detector.

The signal energy PDF is computed from the reconstructed muon energy of simulated signal events with an  $E^{-2}$  spectrum. The background energy PDF is taken from off-time data in the regime where we have good statistics; at higher energies, this PDF is extended using the tail of the reconstructed muon energy distribution of simulated atmospheric neutrinos.

The signal and background PDFs provide a measure of the signalness of a single event. To calculate the signalness of an ensemble of events, we use the following test statistic:

$$T = -n_s + \sum_{i=1}^N \ln \left( \frac{n_s S_i}{\langle n_b \rangle B_i} + 1 \right),$$

which is the log of the ratio of the likelihood an ensemble consists of  $n_s + \langle n_b \rangle$  signal plus background events to the likelihood the ensemble consists of  $\langle n_b \rangle$  expected number of background events. Specifically, for a given ensemble, we take the value of  $T$  corresponding to the value of  $n_s$  which maximizes this likelihood ratio.

The significance of an observation is determined by calculating the probability  $p$  of finding an equal or greater  $T$  given background alone. To find this probability, pseudo-experiments are performed in which background-like events are generated by drawing from the energy, direction, and direction error distributions in off-time data. The resulting  $T$  distribution sets the significance of any single observation.

Given a particular observed test statistic  $T_{\text{obs}}$ , we can calculate upper limits on models. We use a Feldman-Cousins

	GRB100718B	IceCube $\nu$
time	T100 = 39s	15 s into burst
RA, Dec	298°, 41.4°	284°, 57°
$\Delta$ angle		16°
$\sigma_{\text{stat}}$	10.2°	1.3°
$\sigma_{\text{sys}}$	10.4°	$\sim 1^\circ$
energy	$2.5 \times 10^{-6} \text{ erg cm}^{-2}$	10TeV

**Table 1:** While the 79 string configuration was running, a single neutrino was associated with GRB100718B. The table above summarizes the burst and neutrino properties. This observation is fully consistent with background.

approach [18] to calculate 90% confidence upper limits. Signal simulation is used to determine the signal strength required to obtain a larger  $T$  in 90% of experiments. To find this signal strength, we perform pseudo-experiments as described above, but this time, in addition to a typical ensemble of background events, we inject in each pseudo-experiment a set of simulated signal events with a probability determined by the simulation weight of each event and the signal strength under consideration. For a given signal strength, a large enough number of pseudo-experiments is performed to constrain the fraction which yield  $T > T_{\text{obs}}$ ; then, the signal strength is adjusted until the 90% confidence upper limit is found. This procedure may be repeated for arbitrary models. Each model provides a spectral weighting and reference normalization.

## 7 Results

Before evaluating a combined four-year result, we obtain the results from each detector configuration individually. For the 40, 59, and 86 string configurations, no events were found to be on-time and on-source with any burst, so in each case, we obtain  $T = 0$  and  $p = 1$ . Analysis of data from the 79 string configuration yielded a single event which is potentially associated with GRB100718B; however, it is still very low significance. The test statistic evaluated to  $T = 0.054$ , which gives a single-year, pre-trials  $p = 0.11$  or  $1.2\sigma$ . The GRB and  $\nu$  properties are summarized in Table 1.

The significance of this single coincident neutrino is further reduced when we analyze the four year data sample in combination. The test statistic in this case is 0, which gives a final post-trials  $p = 1$ .

In the absence of a significant observation, we produce limits on some contemporary models. Previous model-dependent limits have been based on the treatment by Guetta et al. [3], which derives an expected neutrino fluence from the measured gamma fluence and assumptions about the GRB fireball properties such as the ratio of energy in protons vs. electrons, the bulk Lorentz factor  $\Gamma$  of the fireball, and the characteristic time scale  $t_{\text{var}}$  of variability in the fireball due to magnetic shocks. This treatment neglected physics details such as the energy distribution of fireball particles and interaction channels other than the  $\Delta^+$  resonance. Numerical simulation of these fireball details allows a next-to-leading order fluence prediction which is generally lower than the approximate result [4]. Here, we refer to this model generically as the fireball model. Zhang and Kumar [19] present an analytic model similar to Guetta et al. but with proton acceleration and

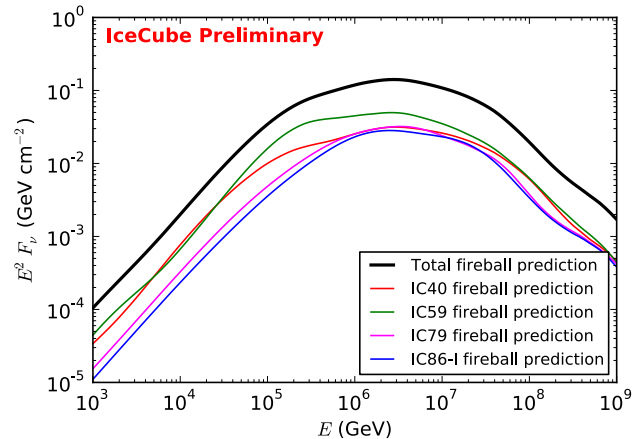


**Figure 1:** Fireball model predicted neutrino fluence for bursts occurring during each detector configuration included in this analysis. IC## indicates the number of strings in operation; IC86-I refers specifically to the first year of 86 string operation.

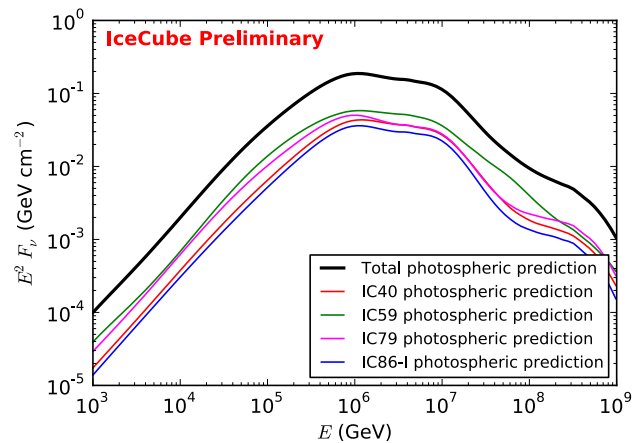


**Figure 2:** Photospheric model predicted neutrino fluence for bursts occurring during each detector configuration included in this analysis, labeled as in Figure 1.

neutrino production taking place at the photosphere, where the fireball transitions from optically thick to optically thin with respect to  $\gamma\gamma$  interactions. This production hypothesis, too, can be simulated numerically. Here, we refer to this model as the photospheric model.

Figures 1 and 2 summarize the photospheric and generic fireball model predicted fluence for the bursts occurring during each detector configuration. Each total fluence prediction may be recast as a quasi-diffuse flux, assuming that our burst sample is representative of some total number of bursts per year in the observable universe; we assume a conventional value of 667 bursts as has been done in past analyses [14]. Figure 3 shows the quasi-diffuse flux predictions for the photospheric and generic fireball models as well as the limits obtained with four years of IceCube data.

The above models are normalized by the gamma ray fluence and spectral parameters of each burst. An alternative approach is to assume that GRBs are the dominant progenitor of the cosmic ray flux observed at Earth. These models [20, 21, 22] assume an average double-broken power law emission from each burst with indices  $(-1, -2, -4)$ ;

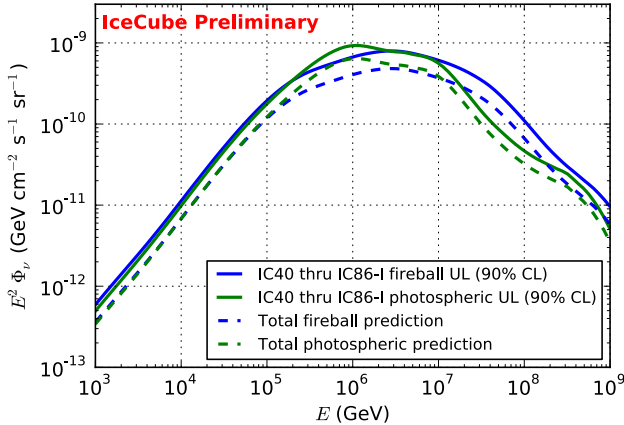


**Figure 3:** Fireball and photospheric model quasi-diffuse flux predictions and 90% CL upper limits from the combined analysis of four years of IceCube data. Full systematic treatment is deferred to a later publication, so these limits include an assumed 6% systematic uncertainty, which is the estimated uncertainty in the most recently published analysis. The fireball and photospheric model limits are 1.72 and 1.47 times the model predictions, respectively, so these models are not yet constrained by our results.

the models differ in spectral break energies and the method in which the normalization is fit to the observed cosmic ray fluence. For all realistic models, the fluence is low enough at the high-energy break that its presence has a negligible effect on the number of events observed by IceCube; therefore, it is sufficient for us to report, as a function of the first break energy  $\varepsilon_b$ , a limit on single-broken power law emission of the form  $\Phi_\nu \cdot \{E^{-1}/\varepsilon_b, E < \varepsilon_b; E^{-2}, \varepsilon_b \leq E\}$ . The limit from four years of IceCube data is shown along with the most recently published limit and three model predictions in Figure 4.

## 8 Conclusion

Previous results from IceCube have excluded models in which the entire cosmic ray flux at the highest energies results from neutrons escaping from GRBs and decaying later to protons [2]. Our updated limits based on four years of data tighten this constraint further still. Our previous results have also excluded models which normalize the neutrino fluence to the per-burst gamma ray fluence without properly simulating the particle physics interactions in the fireball [2]. The theory community has responded by delivering more complete calculations [4]. Since the updated model predictions give a smaller neutrino flux, we are not yet able to constrain them, but within  $\sim 3$  years we expect to have sufficient exposure to begin to do so or to observe the flux they predict. In addition, an updated analysis of southern hemisphere bursts and a new  $\nu_e$  analysis are planned, and results from a search for a correlation between GRB and high energy starting events (in which the interaction vertex is contained within the instrumented volume) will be available soon [23].

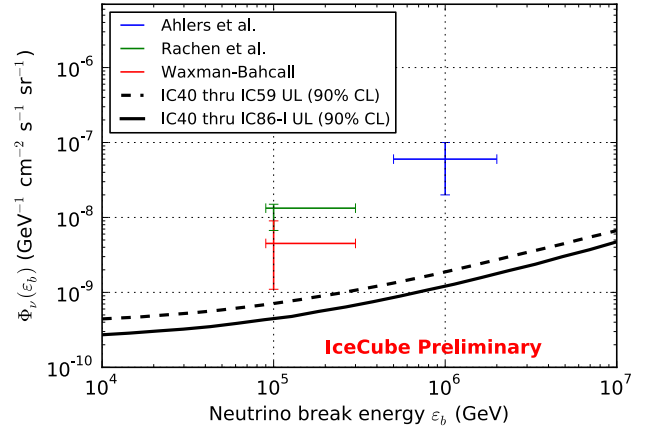


**Figure 4:** Compatibility of some models [20, 21, 22] of cosmic-ray-normalized neutrino fluxes with observations. The 90% CL upper limits from the published IC40+IC59 analysis [2] as well as the new four year analysis are shown in comparison with some model predictions indicated as points with error bars. Without modification, these models are excluded by our results.

## References

- [1] E. Waxman, Phys. Rev. Lett. 75 (1995) 386–389.
- [2] R. Abbasi, et al., Nature 484 (2012) 351–354.
- [3] D. Guetta, et al., Astroparticle Phys. 20 (2004) 429–455.
- [4] S. Hümmer, et al., Phys. Rev. Lett. 108 (2012) 231101.
- [5] J. Ahrens, et al., Nucl. Instrum. and Meth. A 524 (2004) 169–194.
- [6] GCN. <http://gcn.gsfc.nasa.gov>
- [7] W. Paciesas, et al., ApJS 199 (2012) 18.
- [8] A. Goldstein, et al., ApJS 199 (2012) 19.
- [9] R. Aptekar, et al., Space Sci. Rev. 71 (1995) 265.
- [10] K. Yamaoka, et al., Publ. Astron. Soc. Japan 61 (2009) 35.
- [11] N. Gehrels, et al., ApJ 611 (2004) 1005–1020.
- [12] C. Winkler, et al., Astron. Astrophys. 411 (2003) L1–L6.
- [13] GRB-web. <http://grbweb.icecube.wisc.edu>
- [14] R. Abbasi, et al., ApJ 710 (2010) 346–359.
- [15] W. Atwood, et al., ApJ 697 (2009) 1071–1102.
- [16] M. Feroci, et al., Nucl. Instrum. Meth. A 581 (2007) 728–754.
- [17] IPN. <http://www.ssl.berkeley.edu/ipn3/>
- [18] G. Feldman, R. Cousins, Phys. Rev. D. 57 (1998) 3873–3889.
- [19] B. Zhang, P. Kumar, Phys. Rev. Lett. 110 (2013) 121101.
- [20] M. Ahlers, et al., Astroparticle Physics 35 (2011) 87–94.
- [21] J. P. Rachen, P. Mészáros, in: C. A. Meegan, et al. (Eds.), Gamma-Ray Bursts, 4th Hunstville Symp., Vol. 428 of AIP Conf. Proc., 1998, pp. 776–780.
- [22] E. Waxman, J. Bahcall, Phys. Rev. Lett. 78 (1997) 2292–2295.
- [23] IceCube Coll., paper 367, these proceedings.